CHAPTER 1

Aerodynamics: Some Introductory Thoughts

The term "aerodynamics" is generally used for problems arising from flight and other topics involving the flow of air.

Ludwig Prandtl, 1949

Aerodynamics: The dynamics of gases, especially atmospheric interactions with moving objects.

The American Heritage Dictionary of the English Language, 1969

PREVIEW BOX

Why learn about aerodynamics? For an answer, just take a look at the following five photographs showing a progression of airplanes over the past 70 years. The Douglas DC-3 (Figure 1.1), one of the most famous aircraft of all time, is a low-speed subsonic transport designed during the 1930s. Without a knowledge of low-speed aerodynamics, this aircraft would have never existed. The Boeing 707 (Figure 1.2) opened high-speed subsonic flight to millions of passengers beginning in the late 1950s. Without a knowledge of high-speed subsonic aerodynamics, most of us would still be relegated to ground transportation.

Figure 1.1 Douglas DC-3 (*Courtesy of the American Aviation Historical Society*).

Figure 1.2 Boeing 707 (*Courtesy of the Harold Andrews Collection*).

Figure 1.3 Bell X-1 (*Courtesy of the National Air and Space Museum*).

Figure 1.4 Lockheed F-104 (*Courtesy of the Harold Andrews Collection*).

The Bell X-1 (Figure 1.3) became the first piloted airplane to fly faster than sound, a feat accomplished with Captain Chuck Yeager at the controls on October 14, 1947. Without a knowledge of transonic aerodynamics (near, at, and just above the speed of sound), neither the X-1, nor any other airplane, would have ever broken the sound barrier. The Lockheed F-104 (Figure 1.4) was the first supersonic airplane

Figure 1.5 Lockheed-Martin F-22 (*Courtesy of the Harold Andrews Collection*).

Figure 1.6 Blended wing body (NASA).

point-designed to fly at twice the speed of sound, accomplished in the 1950s. The Lockheed-Martin F-22 (Figure 1.5) is a modern fighter aircraft designed for sustained supersonic flight. Without a knowledge of supersonic aerodynamics, these supersonic airplanes would not exist. Finally, an example of an innovative new vehicle concept for high-speed subsonic flight is the blended wing body shown in Figure 1.6. At the time of writing, the blended-wing-body promises to carry from 400 to 800 passengers over long distances with almost 30 percent less fuel per seat-mile than a conventional jet transport. This would be a "renaissance" in long-haul transport. The salient design aspects of this exciting new concept are discussed in Section 11.10. The airplanes in Figures 1.1–1.6 are six good reasons to learn about aerodynamics. The major purpose of this book is to help you do this. As you continue to read this and subsequent chapters, you will progressively learn about low-speed aerodynamics, high-speed subsonic aerodynamics, transonic aerodynamics, supersonic aerodynamics, and more.

Airplanes are by no means the only application of aerodynamics. The air flow over an automobile, the gas flow through the internal combustion engine powering an automobile, weather and storm prediction, the flow through a windmill, the production of thrust by gas turbine jet engines and rocket engines, and the movement of air through building heater and air-conditioning systems are just a few other examples of the application of aerodynamics. The material in this book is powerful stuff—important stuff. Have fun reading and learning about aerodynamics.

To learn a new subject, you simply have to start at the beginning. This chapter is the beginning of our study of aerodynamics; it weaves together a series of introductory thoughts, definitions, and concepts essential to our discussions in subsequent chapters. For example, how does nature reach out and grab hold of an airplane in flight—or any other object emmersed in a flowing fluid—and exert an aerodynamic force on the object? We will find out here. The resultant aerodynamic force is frequently resolved into two components defined as lift and drag; but rather than dealing with the lift and drag forces themselves, aerodynamicists deal instead with lift and drag *coefficients*. What is so magic about lift and drag coefficients? We will see. What is a Reynolds number? Mach number? Inviscid flow? Viscous flow? These rather mysterious sounding terms will be demystified in the present chapter. They, and others constitute the language of aerodynamics, and as we all know, to do anything useful you have to know the language. Visualize this chapter as a beginning language lesson, necessary to go on to the exciting aerodynamic applications in later chapters. There is a certain enjoyment and satisfaction in learning a new language. Take this chapter in that spirit, and move on.

1.1 IMPORTANCE OF AERODYNAMICS: HISTORICAL EXAMPLES

On August 8, 1588, the waters of the English Channel churned with the gyrations of hundreds of warships. The great Spanish Armada had arrived to carry out an invasion of Elizabethan England and was met head-on by the English fleet under the command of Sir Francis Drake. The Spanish ships were large and heavy; they were packed with soldiers and carried formidable cannons that fired 50 lb round shot that could devastate any ship of that era. In contrast, the English ships were smaller and lighter; they carried no soldiers and were armed with lighter, shorter-range cannons. The balance of power in Europe hinged on the outcome of this naval encounter. King Philip II of Catholic Spain was attempting to squash Protestant England's rising influence in the political and religious affairs of Europe; in turn, Queen Elizabeth I was attempting to defend the very existence of England as a sovereign state. In fact, on that crucial day in 1588, when the English floated six fire ships into the Spanish formation and then drove headlong into the ensuing confusion, the future history of Europe was in the balance. In the final outcome, the heavier, sluggish, Spanish ships were no match for the faster, more maneuverable, English craft, and by that evening the Spanish Armada lay in disarray, no longer a threat to England. This naval battle is of particular importance because it was the first in history to be fought by ships on both sides powered completely by sail (in contrast to earlier combinations of oars and sail), and it taught the world that political power was going to be synonymous with naval power. In turn, naval power was going to depend greatly on the speed and

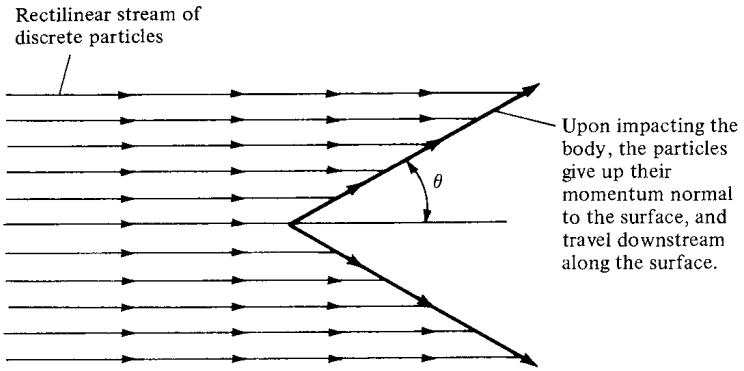

Figure 1.7 Isaac Newton's model of fluid flow in the year 1687. This model was widely adopted in the seventeenth and eighteenth centuries but was later found to be conceptually inaccurate for most fluid flows.

maneuverability of ships. To increase the speed of a ship, it is important to reduce the resistance created by the water flow around the ship's hull. Suddenly, the drag on ship hulls became an engineering problem of great interest, thus giving impetus to the study of fluid mechanics.

This impetus hit its stride almost a century later, when, in 1687, Isaac Newton (1642–1727) published his famous *Principia,* in which the entire second book was devoted to fluid mechanics. Newton encountered the same difficulty as others before him, namely, that the analysis of fluid flow is conceptually more difficult than the dynamics of solid bodies. A solid body is usually geometrically well defined, and its motion is therefore relatively easy to describe. On the other hand, a fluid is a "squishy" substance, and in Newton's time it was difficult to decide even how to qualitatively model its motion, let alone obtain quantitative relationships. Newton considered a fluid flow as a uniform, rectilinear stream of particles, much like a cloud of pellets from a shotgun blast. As sketched in Figure 1.7, Newton assumed that upon striking a surface inclined at an angle θ to the stream, the particles would transfer their normal momentum to the surface but their tangential momentum would be preserved. Hence, after collision with the surface, the particles would then move along the surface. This led to an expression for the hydrodynamic force on the surface which varies as $\sin^2 \theta$. This is Newton's famous sine-squared law (described in detail in Chapter 14). Although its accuracy left much to be desired, its simplicity led to wide application in naval architecture. Later, in 1777, a series of experiments was carried out by Jean LeRond d'Alembert (1717–1783), under the support of the French government, in order to measure the resistance of ships in canals. The results showed that "the rule that for oblique planes resistance varies with the sine square of the angle of incidence holds good only for angles between 50 and 90° and must be abandoned for lesser angles." Also, in 1781, Leonhard Euler (1707–1783) pointed out the physical inconsistency of Newton's model (Figure 1.7) consisting of a rectilinear stream of particles impacting without warning on a surface. In contrast to this

model, Euler noted that the fluid moving toward a body "*before* reaching the latter, bends its direction and its velocity so that when it reaches the body it flows past it along the surface, and exercises no other force on the body except the pressure corresponding to the single points of contact." Euler went on to present a formula for resistance that attempted to take into account the shear stress distribution along the surface, as well as the pressure distribution. This expression became proportional to $\sin^2 \theta$ for large incidence angles, whereas it was proportional to $\sin \theta$ at small incidence angles. Euler noted that such a variation was in reasonable agreement with the ship-hull experiments carried out by d'Alembert.

This early work in fluid dynamics has now been superseded by modern concepts and techniques. (However, amazingly enough, Newton's sine-squared law has found new application in very high-speed aerodynamics, to be discussed in Chapter 14.) The major point here is that the rapid rise in the importance of naval architecture after the sixteenth century made fluid dynamics an important science, occupying the minds of Newton, d'Alembert, and Euler, among many others. Today, the modern ideas of fluid dynamics, presented in this book, are still driven in part by the importance of reducing hull drag on ships.

Consider a second historical example. The scene shifts to Kill Devil Hills, 4 mi south of Kitty Hawk, North Carolina. It is summer of 1901, and Wilbur and Orville Wright are struggling with their second major glider design, the first being a stunning failure the previous year. The airfoil shape and wing design of their glider are based on aerodynamic data published in the 1890s by the great German aviation pioneer Otto Lilienthal (1848–1896) and by Samuel Pierpont Langley (1934–1906), secretary of the Smithsonian Institution—the most prestigious scientific position in the United States at that time. Because their first glider in 1900 produced no meaningful lift, the Wright brothers have increased the wing area from 165 to 290 ft^2 and have increased the wing camber (a measure of the airfoil curvature—the larger the camber, the more "arched" is the thin airfoil shape) by almost a factor of 2. But something is still wrong. In Wilbur's words, the glider's "lifting capacity seemed scarcely one-third of the calculated amount." Frustration sets in. The glider is not performing even close to their expectations, although it is designed on the basis of the best available aerodynamic data. On August 20, the Wright brothers despairingly pack themselves aboard a train going back to Dayton, Ohio. On the ride back, Wilbur mutters that "nobody will fly for a thousand years." However, one of the hallmarks of the Wrights is perseverance, and within weeks of returning to Dayton, they decide on a complete departure from their previous approach. Wilbur later wrote that "having set out with absolute faith in the existing scientific data, we were driven to doubt one thing after another, until finally after two years of experiment, we cast it all aside, and decided to rely entirely upon our own investigations." Since their 1901 glider was of poor aerodynamic design, the Wrights set about determining what constitutes good aerodynamic design. In the fall of 1901, they design and build a 6 ft long, 16 in square wind tunnel powered by a two-bladed fan connected to a gasoline engine. A replica of the Wrights' tunnel is shown in Figure 1.8*a*. In their wind tunnel they test over 200 different wing and airfoil shapes, including flat plates,

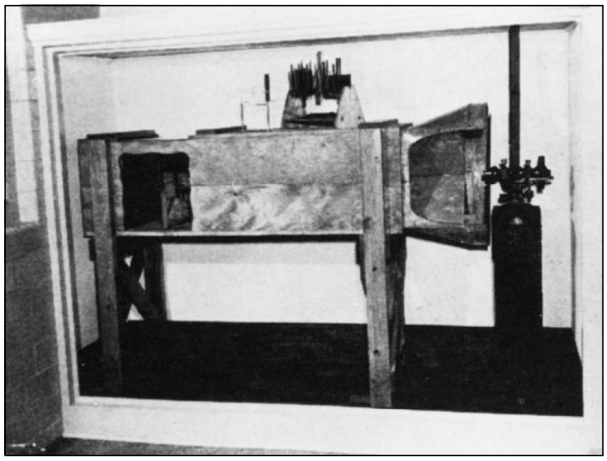

(*a*)

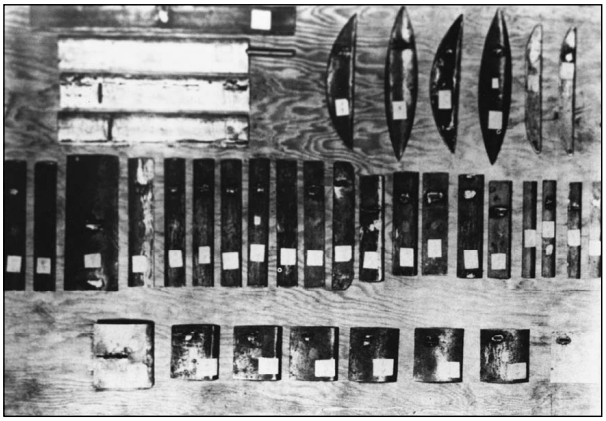

(*b*)

Figure 1.8 (*a*) Replica of the wind tunnel designed, built, and used by the Wright brothers in Dayton, Ohio, during 1901–1902. (*b*) Wing models tested by the Wright brothers in their wind tunnel during 1901–1902. *(Photos Courtesy of the John Anderson Collection)*

curved plates, rounded leading edges, rectangular and curved planforms, and various monoplane and multiplane configurations. A sample of their test models is shown in Figure 1.8*b*. The aerodynamic data are taken logically and carefully. Armed with their new aerodynamic information, the Wrights design a new glider in the spring of 1902. The airfoil is much more efficient; the camber is reduced considerably, and the location of the maximum rise of the airfoil is moved closer to the front of the wing. The most obvious change, however, is that the ratio of the length of the wing (wingspan) to the distance from the front to the rear of the airfoil (chord length) is increased from 3 to 6. The success of this glider during

the summer and fall of 1902 is astounding; Orville and Wilbur accumulate over a thousand flights during this period. In contrast to the previous year, the Wrights return to Dayton flushed with success and devote all their subsequent efforts to powered flight. The rest is history.

The major point here is that good aerodynamics was vital to the ultimate success of the Wright brothers and, of course, to all subsequent successful airplane designs up to the present day. The importance of aerodynamics to successful manned flight goes without saying, and a major thrust of this book is to present the aerodynamic fundamentals that govern such flight.

Consider a third historical example of the importance of aerodynamics, this time as it relates to rockets and space flight. High-speed, supersonic flight had become a dominant feature of aerodynamics by the end of World War II. By this time, aerodynamicists appreciated the advantages of using slender, pointed body shapes to reduce the drag of supersonic vehicles. The more pointed and slender the body, the weaker the shock wave attached to the nose, and hence the smaller the wave drag. Consequently, the German V-2 rocket used during the last stages of World War II had a pointed nose, and all short-range rocket vehicles flown during the next decade followed suit. Then, in 1953, the first hydrogen bomb was exploded by the United States. This immediately spurred the development of long-range intercontinental ballistic missiles (ICBMs) to deliver such bombs. These vehicles were designed to fly outside the region of the earth's atmosphere for distances of 5000 mi or more and to reenter the atmosphere at suborbital speeds of from 20,000 to 22,000 ft/s. At such high velocities, the aerodynamic heating of the reentry vehicle becomes severe, and this heating problem dominated the minds of high-speed aerodynamicists. Their first thinking was conventional—a sharp-pointed, slender reentry body. Efforts to minimize aerodynamic heating centered on the maintenance of laminar boundary layer flow on the vehicle's surface; such laminar flow produces far less heating than turbulent flow (discussed in Chapters 15 and 19). However, nature much prefers turbulent flow, and reentry vehicles are no exception. Therefore, the pointed-nose reentry body was doomed to failure because it would burn up in the atmosphere before reaching the earth's surface.

However, in 1951, one of those major breakthroughs that come very infrequently in engineering was created by H. Julian Allen at the NACA (National Advisory Committee for Aeronautics) Ames Aeronautical Laboratory—he introduced the concept of the *blunt* reentry body. His thinking was paced by the following concepts. At the beginning of reentry, near the outer edge of the atmosphere, the vehicle has a large amount of kinetic energy due to its high velocity and a large amount of potential energy due to its high altitude. However, by the time the vehicle reaches the surface of the earth, its velocity is relatively small and its altitude is zero; hence, it has virtually no kinetic or potential energy. Where has all the energy gone? The answer is that it has gone into (1) heating the body and (2) heating the airflow around the body. This is illustrated in Figure 1.9. Here, the shock wave from the nose of the vehicle heats the airflow around the vehicle; at the same time, the vehicle is heated by the intense frictional dissipation within the boundary layer on the surface. Allen reasoned that if more of the total reentry

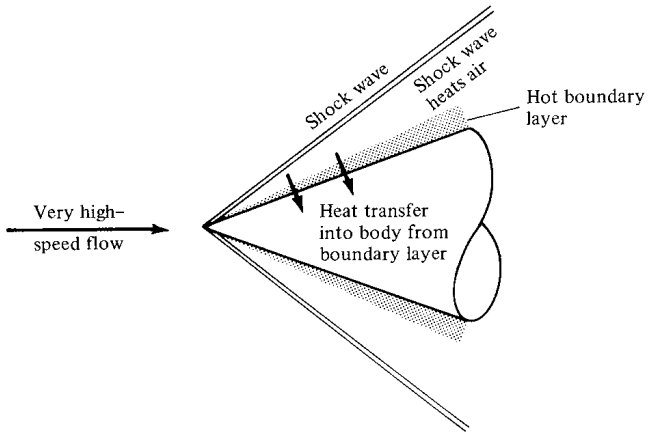

Figure 1.9 Energy of reentry goes into heating both the body and the air around the body.

energy could be dumped into the airflow, then less would be available to be transferred to the vehicle itself in the form of heating. In turn, the way to increase the heating of the airflow is to create a stronger shock wave at the nose (i.e., to use a blunt-nosed body). The contrast between slender and blunt reentry bodies is illustrated in Figure 1.10. This was a stunning conclusion—to minimize aerodynamic heating, you actually want a blunt rather than a slender body. The result was so important that it was bottled up in a secret government document. Moreover, because it was so foreign to contemporary intuition, the blunt-reentry-body concept was accepted only gradually by the technical community. Over the next few years, additional aerodynamic analyses and experiments confirmed the validity of blunt reentry bodies. By 1955, Allen was publicly recognized for his work, receiving the Sylvanus Albert Reed Award of the Institute of the Aeronautical Sciences (now the American Institute of Aeronautics and Astronautics). Finally, in 1958, his work was made available to the public in the pioneering document NACA Report 1381 entitled "A Study of the Motion and Aerodynamic Heating of Ballistic Missiles Entering the Earth's Atmosphere at High Supersonic Speeds." Since Harvey Allen's early work, all successful reentry bodies, from the first Atlas ICBM to the manned Apollo lunar capsule, have been blunt. Incidentally, Allen went on to distinguish himself in many other areas, becoming the director of the NASA Ames Research Center in 1965, and retiring in 1970. His work on the blunt reentry body is an excellent example of the importance of aerodynamics to space vehicle design.

In summary, the purpose of this section has been to underscore the importance of aerodynamics in historical context. The goal of this book is to introduce the fundamentals of aerodynamics and to give the reader a much deeper insight to many technical applications in addition to the few described above. Aerodynamics is also a subject of intellectual beauty, composed and drawn by many great minds over the centuries. If you are challenged and interested by these thoughts, or even the least bit curious, then read on.

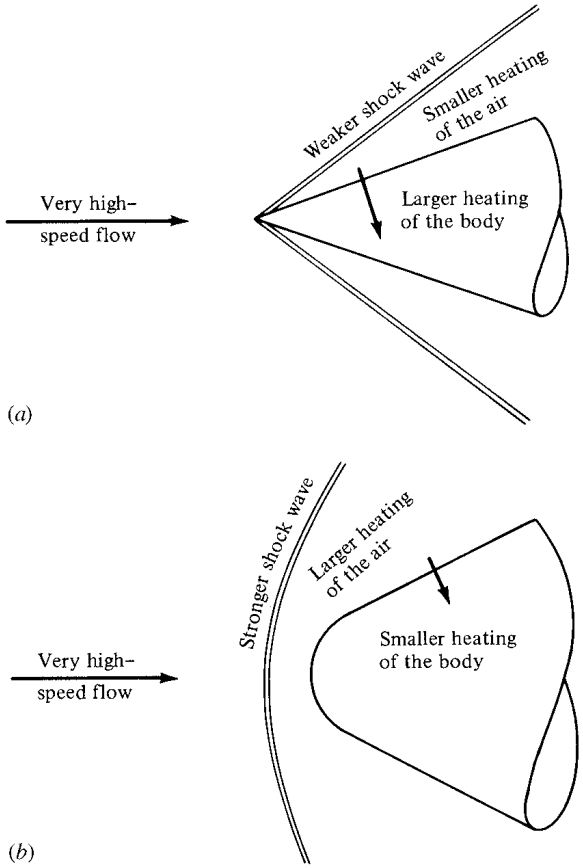

Figure 1.10 Contrast of aerodynamic heating for slender and blunt reentry vehicles. (*a*) Slender reentry body. (*b*) Blunt reentry body.

1.2 AERODYNAMICS: CLASSIFICATION AND PRACTICAL OBJECTIVES

A distinction between solids, liquids, and gases can be made in a simplistic sense as follows. Put a solid object inside a larger, closed container. The solid object will not change; its shape and boundaries will remain the same. Now put a liquid inside the container. The liquid will change its shape to conform to that of the container and will take on the same boundaries as the container up to the maximum depth of the liquid. Now put a gas inside the container. The gas will completely fill the container, taking on the same boundaries as the container.

The word *fluid* is used to denote either a liquid or a gas. A more technical distinction between a solid and a fluid can be made as follows. When a force is applied tangentially to the surface of a solid, the solid will experience a *finite* deformation, and the tangential force per unit area—the shear stress—will usually be proportional to the amount of deformation. In contrast, when a tangential shear

stress is applied to the surface of a fluid, the fluid will experience a *continuously increasing* deformation, and the shear stress usually will be proportional to the rate of change of the deformation.

The most fundamental distinction between solids, liquids, and gases is at the atomic and molecular level. In a solid, the molecules are packed so closely together that their nuclei and electrons form a rigid geometric structure, "glued" together by powerful intermolecular forces. In a liquid, the spacing between molecules is larger, and although intermolecular forces are still strong they allow enough movement of the molecules to give the liquid its "fluidity." In a gas, the spacing between molecules is much larger (for air at standard conditions, the spacing between molecules is, on the average, about 10 times the molecular diameter). Hence, the influence of intermolecular forces is much weaker, and the motion of the molecules occurs rather freely throughout the gas. This movement of molecules in both gases and liquids leads to similar physical characteristics, the characteristics of a fluid—quite different from those of a solid. Therefore, it makes sense to classify the study of the dynamics of both liquids and gases under the same general heading, called *fluid dynamics*. On the other hand, certain differences exist between the flow of liquids and the flow of gases; also, different species of gases (say, N_2, He, etc.) have different properties. Therefore, fluid dynamics is subdivided into three areas as follows:

Hydrodynamics—flow of liquids

Gas dynamics—flow of gases

Aerodynamics—flow of air

These areas are by no means mutually exclusive; there are many similarities and identical phenomena between them. Also, the word "aerodynamics" has taken on a popular usage that sometimes covers the other two areas. As a result, this author tends to interpret the word *aerodynamics* very liberally, and its use throughout this book does *not* always limit our discussions just to air.

Aerodynamics is an applied science with many practical applications in engineering. No matter how elegant an aerodynamic theory may be, or how mathematically complex a numerical solution may be, or how sophisticated an aerodynamic experiment may be, all such efforts are usually aimed at one or more of the following practical objectives:

1. The prediction of forces and moments on, and heat transfer to, bodies moving through a fluid (usually air). For example, we are concerned with the generation of lift, drag, and moments on airfoils, wings, fuselages, engine nacelles, and most importantly, whole airplane configurations. We want to estimate the wind force on buildings, ships, and other surface vehicles. We are concerned with the hydrodynamic forces on surface ships, submarines, and torpedoes. We need to be able to calculate the aerodynamic heating of flight vehicles ranging from the supersonic transport to a planetary probe entering the atmosphere of Jupiter. These are but a few examples.

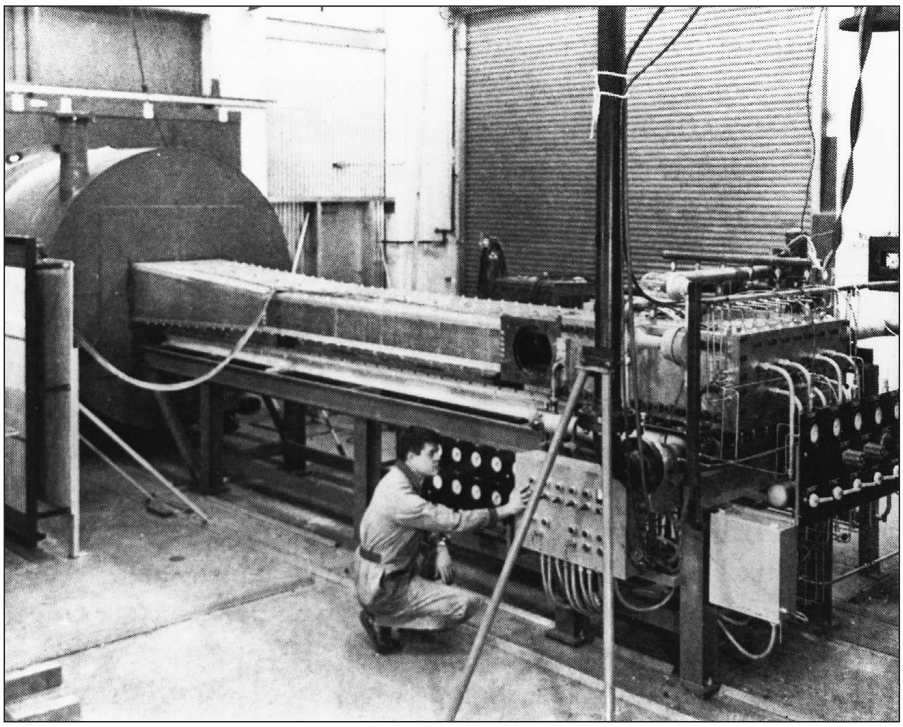

Figure 1.11 A CO_2-N_2 gas-dynamic laser, circa 1969. *(Photo Courtesy of the John Anderson Collection)*

2. Determination of flows moving internally through ducts. We wish to calculate and measure the flow properties inside rocket and air-breathing jet engines and to calculate the engine thrust. We need to know the flow conditions in the test section of a wind tunnel. We must know how much fluid can flow through pipes under various conditions. A recent, very interesting application of aerodynamics is high-energy chemical and gas-dynamic lasers (see Reference 1), which are nothing more than specialized wind tunnels that can produce extremely powerful laser beams. Figure 1.11 is a photograph of an early gas-dynamic laser designed in the late 1960s.

The applications in item 1 come under the heading of *external aerodynamics* since they deal with external flows over a body. In contrast, the applications in item 2 involve *internal aerodynamics* because they deal with flows internally within ducts. In external aerodynamics, in addition to forces, moments, and aerodynamic heating associated with a body, we are frequently interested in the details of the flow field away from the body. For example, the communication blackout experienced by the space shuttle during a portion of its reentry trajectory is due to a concentration of free electrons in the hot shock layer around the body. We need to calculate the variation of electron density throughout such flow fields. Another example is the propagation of shock waves in a supersonic flow; for instance, does

the shock wave from the wing of a supersonic airplane impinge upon and interfere with the tail surfaces? Yet another example is the flow associated with the strong vortices trailing downstream from the wing tips of large subsonic airplanes such as the Boeing 747. What are the properties of these vortices, and how do they affect smaller aircraft which happen to fly through them?

The above is just a sample of the myriad applications of aerodynamics. One purpose of this book is to provide the reader with the technical background necessary to fully understand the nature of such practical aerodynamic applications.

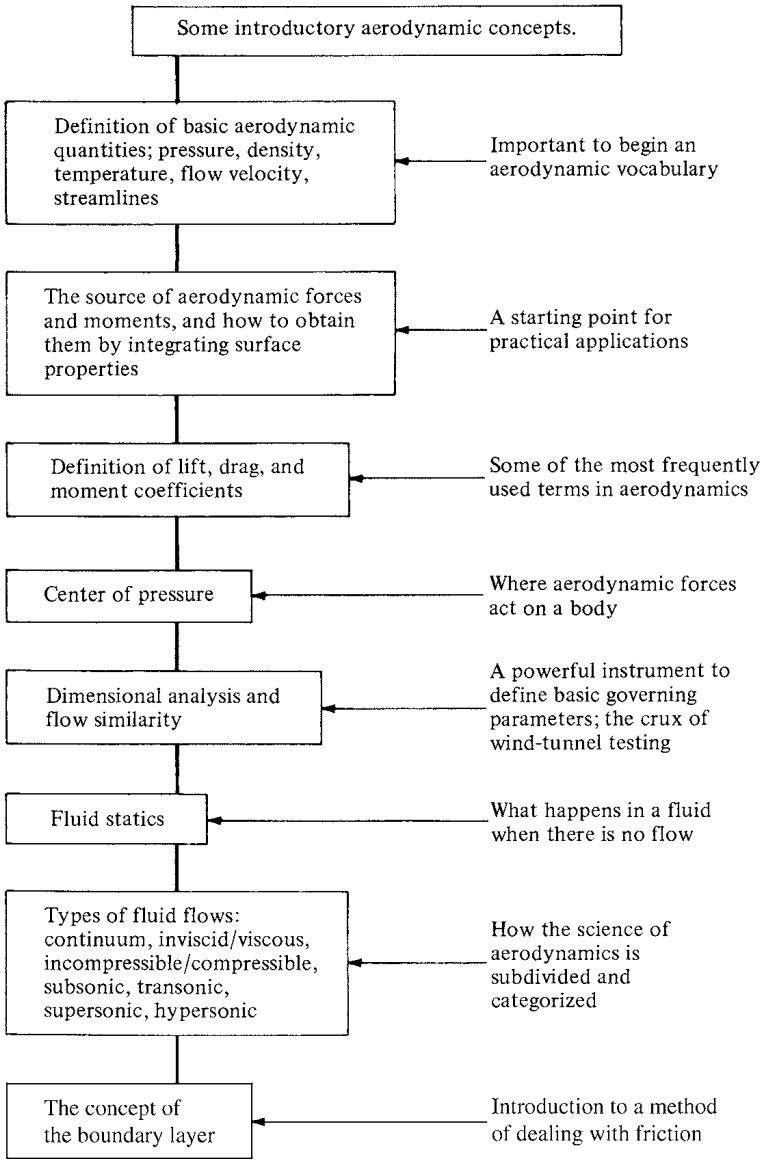

Figure 1.12 Road map for Chapter 1.

1.3 ROAD MAP FOR THIS CHAPTER

When learning a new subject, it is important for you to know where you are, where you are going, and how you can get there. Therefore, at the beginning of each chapter in this book, a road map will be given to help guide you through the material of that chapter and to help you obtain a perspective as to how the material fits within the general framework of aerodynamics. For example, a road map for Chapter 1 is given in Figure 1.12. You will want to frequently refer back to these road maps as you progress through the individual chapters. When you reach the end of each chapter, look back over the road map to see where you started, where you are now, and what you learned in between.

1.4 SOME FUNDAMENTAL AERODYNAMIC VARIABLES

A prerequisite to understanding physical science and engineering is simply learning the vocabulary used to describe concepts and phenomena. Aerodynamics is no exception. Throughout this book, and throughout your working career, you will be adding to your technical vocabulary list. Let us start by defining four of the most frequently used words in aerodynamics: *pressure, density, temperature,* and *flow velocity.*[1]

Consider a surface immersed in a fluid. The surface can be a real, solid surface such as the wall of a duct or the surface of a body; it can also be a free surface which we simply imagine drawn somewhere in the middle of a fluid. Also, keep in mind that the molecules of the fluid are constantly in motion. *Pressure* is the normal force per unit area exerted on a surface due to the time rate of change of momentum of the gas molecules impacting on (or crossing) that surface. It is important to note that even though pressure is defined as force "per unit area," you do not need a surface that is exactly 1 ft^2 or 1 m^2 to talk about pressure. In fact, pressure is usually defined at a *point* in the fluid or a *point* on a solid surface and can vary from one point to another. To see this more clearly, consider a point B in a volume of fluid. Let

dA = elemental area at B

dF = force on one side of dA due to pressure

Then, the pressure at point B in the fluid is defined as

$$p = \lim \left(\frac{dF}{dA} \right) \qquad dA \to 0$$

The pressure p is the limiting form of the force per unit area, where the area of interest has shrunk to nearly zero at the point B.[2] Clearly, you can see that pressure

[1] A basic introduction to these quantities is given on pages 56–61 of Reference 2.

[2] Strictly speaking, dA can never achieve the limit of zero, because there would be no molecules at point B in that case. The above limit should be interpreted as dA approaching a very small value, near zero in terms of our macroscopic thinking, but sufficiently larger than the average spacing between molecules on a microscopic basis.

is a *point property* and can have a different value from one point to another in the fluid.

Another important aerodynamic variable is *density,* defined as the mass per unit volume. Analogous to our discussion on pressure, the definition of density does not require an actual volume of 1 ft^3 or 1 m^3. Rather, it is a *point property* that can vary from point to point in the fluid. Again, consider a point B in the fluid. Let

$$dv = \text{elemental volume around } B$$
$$dm = \text{mass of fluid inside } dv$$

Then, the density at point B is

$$\rho = \lim \frac{dm}{dv} \qquad dv \to 0$$

Therefore, the density ρ is the limiting form of the mass per unit volume, where the volume of interest has shrunk to nearly zero around point B. (Note that dv cannot achieve the value of zero for the reason discussed in the footnote concerning dA in the definition of pressure.)

Temperature takes on an important role in high-speed aerodynamics (introduced in Chapter 7). The temperature T of a gas is directly proportional to the average kinetic energy of the molecules of the fluid. In fact, if KE is the mean molecular kinetic energy, then temperature is given by $\text{KE} = \frac{3}{2}kT$, where k is the Boltzmann constant. Hence, we can qualitatively visualize a high-temperature gas as one in which the molecules and atoms are randomly rattling about at high speeds, whereas in a low-temperature gas, the random motion of the molecules is relatively slow. Temperature is also a point property, which can vary from point to point in the gas.

The principal focus of aerodynamics is fluids in motion. Hence, flow velocity is an extremely important consideration. The concept of the velocity of a fluid is slightly more subtle than that of a solid body in motion. Consider a solid object in translational motion, say, moving at 30 m/s. Then all parts of the solid are simultaneously translating at the same 30 m/s velocity. In contrast, a fluid is a "squishy" substance, and for a fluid in motion, one part of the fluid may be traveling at a different velocity from another part. Hence, we have to adopt a certain perspective, as follows. Consider the flow of air over an airfoil, as shown in Figure 1.13. Lock your eyes on a specific, infinitesimally small element of mass

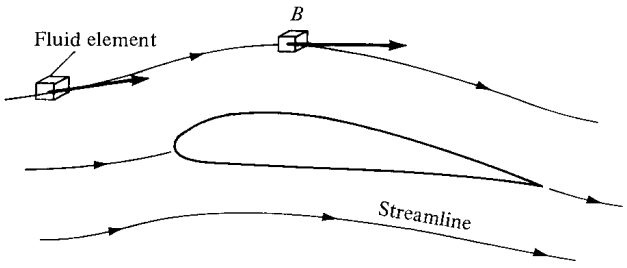

Figure 1.13 Illustration of flow velocity and streamlines.

in the gas, called a *fluid element,* and watch this element move with time. Both the speed and direction of this fluid element can vary as it moves from point to point in the gas. Now fix your eyes on a specific fixed point in space, say, point B in Figure 1.13. *Flow velocity* can now be defined as follows: The velocity of a flowing gas at any fixed point B in space is the velocity of an infinitesimally small fluid element as it sweeps through B. The flow velocity $\mathbf{V}$ has both magnitude and direction; hence, it is a vector quantity. This is in contrast to p, ρ, and T, which are scalar variables. The scalar magnitude of $\mathbf{V}$ is frequently used and is denoted by V. Again, we emphasize that velocity is a point property and can vary from point to point in the flow.

Referring again to Figure 1.13, a moving fluid element traces out a fixed path in space. As long as the flow is steady (i.e., as long as it does not fluctuate with time), this path is called a *streamline* of the flow. Drawing the streamlines of the flow field is an important way of visualizing the motion of the gas; we will frequently be sketching the streamlines of the flow about various objects. A more rigorous discussion of streamlines is given in Chapter 2.

Finally, we note that friction can play a role internally in a flow. Consider two adjacent streamlines a and b as sketched in Figure 1.14. The streamlines are an infinitesimal distance, dy, apart. At point 1 on streamline b the flow velocity is V; at point 2 on streamline a the flow velocity is slightly higher, $V + dV$. You can imagine that streamline a is rubbing against streamline b and, due to friction, exerts a force of magnitude dF_f on streamline b acting tangentially towards the right. Furthermore, imagine this force acting on an elemental area dA, where dA is perpendicular to the y axis and tangent to the streamline b at point 1. The local *shear* stress, τ, at point 1 is

$$\tau = \lim \left(\frac{dF_f}{dA} \right) \qquad dA \to 0$$

The shear stress τ is the limiting form of the magnitude of the frictional force per unit area, where the area of interest is perpendicular to the y axis and has shrunk

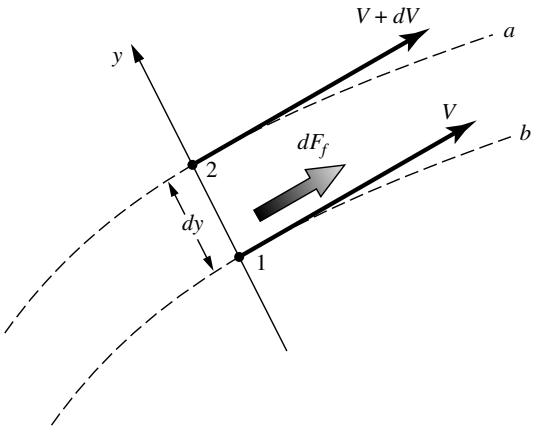

Figure 1.14 Generation of frictional force due to a velocity gradient in a flow.

to nearly zero at point 1. Shear stress acts tangentially along the streamline. For the type of gases and liquids of interest in aerodynamic applications, the value of the shear stress at a point on a streamline is proportional to the spatial rate of change of velocity normal to the streamline at that point (i.e., for the flow illustrated in Figure 1.14, $\tau \propto dV/dy$). The constant of proportionality is defined as the *viscosity coefficient*, μ. Hence,

$$\tau = \mu \frac{dV}{dy}$$

where dV/dy is the velocity gradient. In reality, μ is not really a constant; it is a function of the temperature of the fluid. We will discuss these matters in more detail in Section 1.11. From the above equation, we deduce that in regions of a flow field where the velocity gradients are small, τ is small and the influence of friction locally in the flow is small. On the other hand, in regions where the velocity gradients are large, τ is large and the influence of friction locally in the flow can be substantial.

1.4.1 Units

Two consistent sets of units will be used throughout this book, SI units (Systeme International d'Unites) and the English engineering system of units. The basic units of force, mass, length, time, and absolute temperature in these two systems are given in Table 1.1.

For example, units of pressure and shear stress are lb/ft^2 or N/m^2, units of density are slug/ft^3 or kg/m^3, and units of velocity are ft/s or m/s. When a consistent set of units is used, physical relationships are written without the need for conversion factors in the basic formulas; they are written in the pure form intended by nature. Consistent units will always be used in this book. For an extensive discussion on units and the significance of consistent units versus nonconsistent units, see pages 65–70 of Reference 2.

The SI system of units (metric units) is the standard system of units throughout most of the world today. In contrast, for more than two centuries the English engineering system (or some variant) was the primary system of units in the United States and England. This situation is changing rapidly, especially in the aerospace industry in the United States and England. Nevertheless, a familiarity with both systems of units is still important today. For example, even though most engineering work in the future will deal with the SI units, there exists a huge bulk of

Table 1.1

	Force	Mass	Length	Time	Temp.
SI Units	Newton (N)	kilogram (kg)	meter (m)	second (s)	Kelvin (K)
English Engineering Units	pounds (lb)	slug	feet (ft)	second (s)	deg. Rankine (°R)

present and past engineering literature written in the English engineering system, literature that will be used well into the future. The modern engineering student must be bilingual in these units, and must feel comfortable with both systems. For this reason, although many of the worked examples and end-of-the-chapter problems in this book are in the SI units, some are in the English engineering system of units. You are encouraged to join this bilingual spirit and to work to make yourself comfortable in both systems.

1.5 AERODYNAMIC FORCES AND MOMENTS

At first glance, the generation of the aerodynamic force on a giant Boeing 747 may seem complex, especially in light of the complicated three-dimensional flow field over the wings, fuselage, engine nacelles, tail, etc. Similarly, the aerodynamic resistance on an automobile traveling at 55 mi/h on the highway involves a complex interaction of the body, the air, and the ground. However, in these and all other cases, the aerodynamic forces and moments on the body are due to only two basic sources:

1. *Pressure distribution* over the body surface
2. *Shear stress distribution* over the body surface

No matter how complex the body shape may be, the aerodynamic forces and moments on the body are due entirely to the above two basic sources. The *only* mechanisms nature has for communicating a force to a body moving through a fluid are pressure and shear stress distributions on the body surface. Both pressure p and shear stress τ have dimensions of force per unit area (pounds per square foot or newtons per square meter). As sketched in Figure 1.15, p acts *normal* to the surface, and τ acts *tangential* to the surface. Shear stress is due to the "tugging action" on the surface, which is caused by friction between the body and the air (and is studied in great detail in Chapters 15 to 20).

The net effect of the p and τ distributions integrated over the complete body surface is a resultant aerodynamic force R and moment M on the body, as sketched in Figure 1.16. In turn, the resultant R can be split into components, two sets of

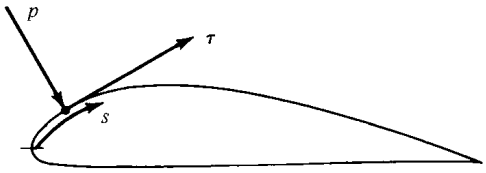

$p = p(s)$ = surface pressure distribution
$\tau = \tau(s)$ = surface shear stress distribution

Figure 1.15 Illustration of pressure and shear stress on an aerodynamic surface.

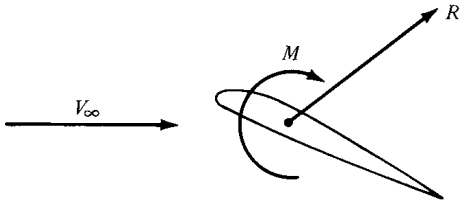

Figure 1.16 Resultant aerodynamic force and moment on the body.

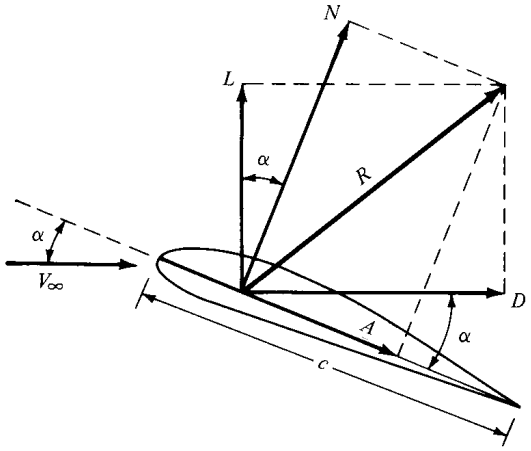

Figure 1.17 Resultant aerodynamic force and the components into which it splits.

which are shown in Figure 1.17. In Figure 1.17, V_∞ is the *relative wind,* defined as the flow velocity far ahead of the body. The flow far away from the body is called the *freestream,* and hence V_∞ is also called the freestream velocity. In Figure 1.17, by definition,

$$L \equiv \text{lift} \equiv \text{component of } R \text{ perpendicular to } V_\infty$$

$$D \equiv \text{drag} \equiv \text{component of } R \text{ parallel to } V_\infty$$

The chord c is the linear distance from the leading edge to the trailing edge of the body. Sometimes, R is split into components perpendicular and parallel to the chord, as also shown in Figure 1.17. By definition,

$$N \equiv \text{normal force} \equiv \text{component of } R \text{ perpendicular to } c$$

$$A \equiv \text{axial force} \equiv \text{component of } R \text{ parallel to } c$$

The angle of attack α is defined as the angle between c and V_∞. Hence, α is also the angle between L and N and between D and A. The geometrical relation between these two sets of components is, from Figure 1.17,

$$L = N \cos\alpha - A \sin\alpha \tag{1.1}$$

$$D = N \sin\alpha + A \cos\alpha \tag{1.2}$$

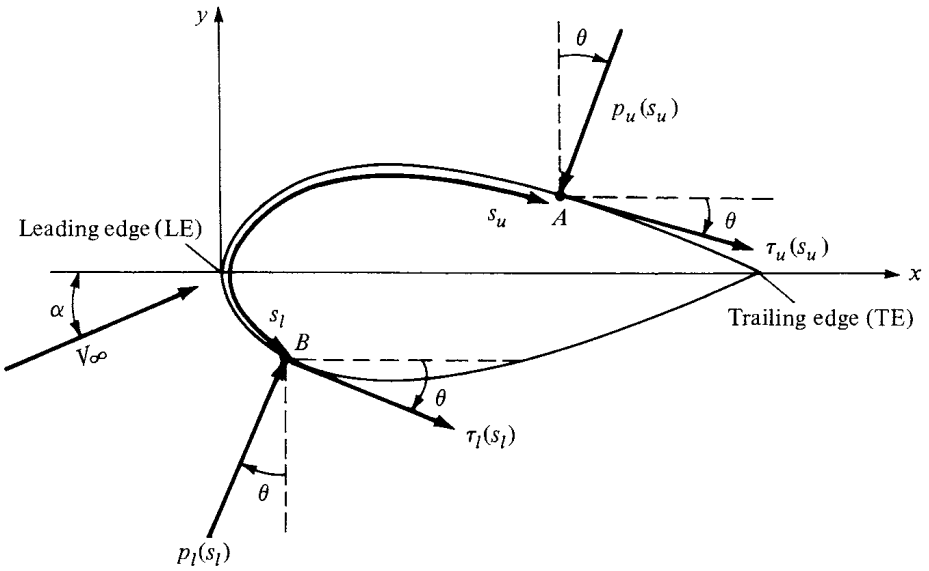

Figure 1.18 Nomenclature for the integration of pressure and shear stress distributions over a two-dimensional body surface.

Let us examine in more detail the integration of the pressure and shear stress distributions to obtain the aerodynamic forces and moments. Consider the two-dimensional body sketched in Figure 1.18. The chord line is drawn horizontally, and hence the relative wind is inclined relative to the horizontal by the angle of attack α. An xy coordinate system is oriented parallel and perpendicular, respectively, to the chord. The distance from the leading edge measured along the body surface to an arbitrary point A on the upper surface is s_u; similarly, the distance to an arbitrary point B on the lower surface is s_l. The pressure and shear stress on the upper surface are denoted by p_u and τ_u, both p_u and τ_u are functions of s_u. Similarly, p_l and τ_l are the corresponding quantities on the lower surface and are functions of s_l. At a given point, the pressure is normal to the surface and is oriented at an angle θ relative to the perpendicular; shear stress is tangential to the surface and is oriented at the same angle θ relative to the horizontal. In Figure 1.18, the sign convention for θ is positive when measured *clockwise* from the vertical line to the direction of p and from the horizontal line to the direction of τ. In Figure 1.18, all thetas are shown in their positive direction. Now consider the two-dimensional shape in Figure 1.18 as a cross section of an infinitely long cylinder of uniform section. A unit span of such a cylinder is shown in Figure 1.19. Consider an elemental surface area dS of this cylinder, where $dS = (ds)(1)$ as shown by the shaded area in Figure 1.19. We are interested in the contribution to the total normal force N' and the total axial force A' due to the pressure and shear stress on the elemental area dS. The primes on N' and A' denote force per unit span. Examining both Figures 1.18 and 1.19, we see that the elemental normal and axial forces acting on the elemental surface dS on the

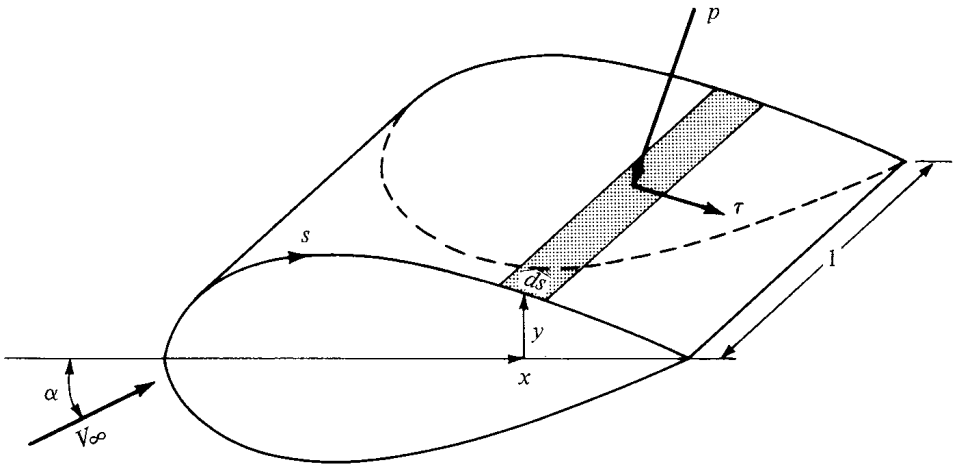

Figure 1.19 Aerodynamic force on an element of the body surface.

upper body surface are

$$dN'_u = -p_u ds_u \cos\theta - \tau_u ds_u \sin\theta \tag{1.3}$$

$$dA'_u = -p_u ds_u \sin\theta + \tau_u ds_u \cos\theta \tag{1.4}$$

On the *lower* body surface, we have

$$dN'_l = p_l ds_l \cos\theta - \tau_l ds_l \sin\theta \tag{1.5}$$

$$dA'_l = p_l ds_l \sin\theta + \tau_l ds_l \cos\theta \tag{1.6}$$

In Equations (1.3) to (1.6), the positive directions of N' and A' are those shown in Figure 1.17. In these equations, the positive clockwise convention for θ must be followed. For example, consider again Figure 1.18. Near the leading edge of the body, where the slope of the upper body surface is positive, τ is inclined upward, and hence it gives a positive contribution to N'. For an upward inclined τ, θ would be counterclockwise, hence negative. Therefore, in Equation (1.3), $\sin\theta$ would be negative, making the shear stress term (the last term) a positive value, as it should be in this instance. Hence, Equations (1.3) to (1.6) hold in general (for both the forward and rearward portions of the body) as long as the above sign convention for θ is consistently applied.

The total normal and axial forces *per unit span* are obtained by integrating Equations (1.3) to (1.6) from the leading edge (LE) to the trailing edge (TE):

$$N' = -\int_{\text{LE}}^{\text{TE}} (p_u \cos\theta + \tau_u \sin\theta)\, ds_u + \int_{\text{LE}}^{\text{TE}} (p_l \cos\theta - \tau_l \sin\theta)\, ds_l \tag{1.7}$$

$$A' = \int_{\text{LE}}^{\text{TE}} (-p_u \sin\theta + \tau_u \cos\theta)\, ds_u + \int_{\text{LE}}^{\text{TE}} (p_l \sin\theta + \tau_l \cos\theta)\, ds_l \tag{1.8}$$

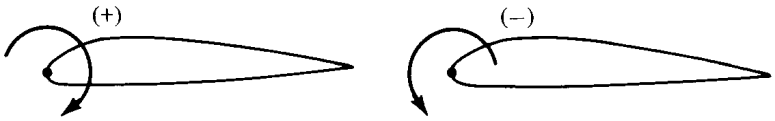

Figure 1.20 Sign convention for aerodynamic moments.

In turn, the total lift and drag per unit span can be obtained by inserting Equations (1.7) and (1.8) into (1.1) and (1.2); note that Equations (1.1) and (1.2) hold for forces on an arbitrarily shaped body (unprimed) and for the forces per unit span (primed).

The aerodynamic moment exerted on the body depends on the point about which moments are taken. Consider moments taken about the leading edge. By convention, moments that tend to increase α (pitch up) are positive, and moments that tend to decrease α (pitch down) are negative. This convention is illustrated in Figure 1.20. Returning again to Figures 1.18 and 1.19, the moment per unit span about the leading edge due to p and τ on the elemental area dS on the upper surface is

$$dM'_u = (p_u \cos\theta + \tau_u \sin\theta)x \, ds_u + (-p_u \sin\theta + \tau_u \cos\theta)y \, ds_u \tag{1.9}$$

On the bottom surface,

$$dM'_l = (-p_l \cos\theta + \tau_l \sin\theta)x \, ds_l + (p_l \sin\theta + \tau_l \cos\theta)y \, ds_l \tag{1.10}$$

In Equations (1.9) and (1.10), note that the same sign convention for θ applies as before and that y is a positive number above the chord and a negative number below the chord. Integrating Equations (1.9) and (1.10) from the leading to the trailing edges, we obtain for the moment about the leading edge per unit span

$$\begin{aligned} M'_{\text{LE}} = & \int_{\text{LE}}^{\text{TE}} [(p_u \cos\theta + \tau_u \sin\theta)x - (p_u \sin\theta - \tau_u \cos\theta)y] \, ds_u \\ & + \int_{\text{LE}}^{\text{TE}} [(-p_l \cos\theta + \tau_l \sin\theta)x + (p_l \sin\theta + \tau_l \cos\theta)y] \, ds_l \end{aligned} \tag{1.11}$$

In Equations (1.7), (1.8), and (1.11), θ, x, and y are known functions of s for a given body shape. Hence, if p_u, p_l, τ_u, and τ_l are known as functions of s (from theory or experiment), the integrals in these equations can be evaluated. Clearly, Equations (1.7), (1.8), and (1.11) demonstrate the principle stated earlier, namely, *the sources of the aerodynamic lift, drag, and moments on a body are the pressure and shear stress distributions integrated over the body.* A major goal of theoretical aerodynamics is to calculate $p(s)$ and $\tau(s)$ for a given body shape and freestream conditions, thus yielding the aerodynamic forces and moments via Equations (1.7), (1.8), and (1.11).

As our discussions of aerodynamics progress, it will become clear that there are quantities of an even more fundamental nature than the aerodynamic forces and moments themselves. These are *dimensionless force and moment coefficients,* defined as follows. Let ρ_∞ and V_∞ be the density and velocity, respectively, in

the freestream, far ahead of the body. We define a dimensional quantity called the freestream *dynamic pressure* as

Dynamic pressure: $$q_\infty \equiv \tfrac{1}{2}\rho_\infty V_\infty^2$$

The dynamic pressure has the units of pressure (i.e., pounds per square foot or newtons per square meter). In addition, let S be a reference area and l be a reference length. The dimensionless force and moment coefficients are defined as follows:

Lift coefficient: $$C_L \equiv \frac{L}{q_\infty S}$$

Drag coefficient: $$C_D \equiv \frac{D}{q_\infty S}$$

Normal force coefficient: $$C_N \equiv \frac{N}{q_\infty S}$$

Axial force coefficient: $$C_A \equiv \frac{A}{q_\infty S}$$

Moment coefficient: $$C_M \equiv \frac{M}{q_\infty S l}$$

In the above coefficients, the reference area S and reference length l are chosen to pertain to the given geometric body shape; for different shapes, S and l may be different things. For example, for an airplane wing, S is the planform area, and l is the mean chord length, as illustrated in Figure 1.21*a*. However, for a sphere, S is the cross-sectional area, and l is the diameter, as shown in Figure 1.21*b*.

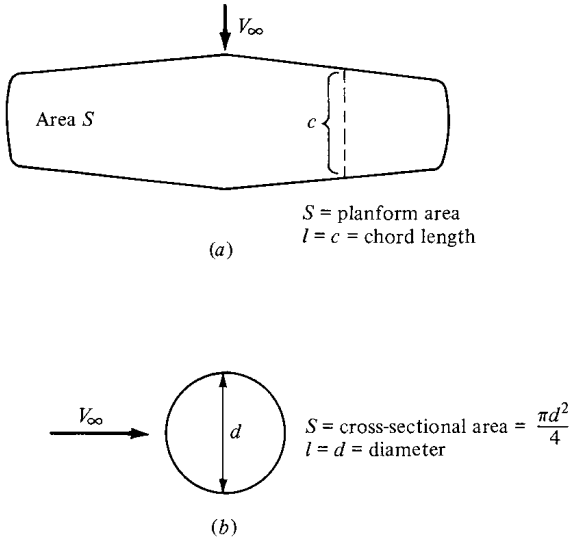

Figure 1.21 Some reference areas and lengths.

The particular choice of reference area and length is not critical; however, when using force and moment coefficient data, you must always know what reference quantities the particular data are based upon.

The symbols in capital letters listed above (i.e., C_L, C_D, C_M, and C_A) denote the force and moment coefficients for a complete three-dimensional body such as an airplane or a finite wing. In contrast, for a two-dimensional body, such as given in Figures 1.18 and 1.19, the forces and moments are per unit span. For these two-dimensional bodies, it is conventional to denote the aerodynamic coefficients by lowercase letters; for example,

$$c_l \equiv \frac{L'}{q_\infty c} \quad c_d \equiv \frac{D'}{q_\infty c} \quad c_m \equiv \frac{M'}{q_\infty c^2}$$

where the reference area $S = c(1) = c$.

Two additional dimensionless quantities of immediate use are

Pressure coefficient: $$C_p \equiv \frac{p - p_\infty}{q_\infty}$$

Skin friction coefficient: $$c_f \equiv \frac{\tau}{q_\infty}$$

where p_∞ is the freestream pressure.

The most useful forms of Equations (1.7), (1.8), and (1.11) are in terms of the dimensionless coefficients introduced above. From the geometry shown in Figure 1.22,

$$dx = ds \cos\theta \tag{1.12}$$

$$dy = -(ds \sin\theta) \tag{1.13}$$

$$S = c(1) \tag{1.14}$$

Substituting Equations (1.12) and (1.13) into Equations (1.7), (1.8), and (1.11), dividing by q_∞, and further dividing by S in the form of Equation (1.14), we

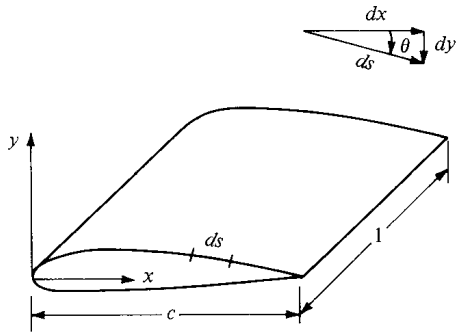

Figure 1.22 Geometrical relationship of differential lengths.

obtain the following integral forms for the force and moment coefficients:

$$c_n = \frac{1}{c}\left[\int_0^c (C_{p,l} - C_{p,u})\,dx + \int_0^c \left(c_{f,u}\frac{dy_u}{dx} + c_{f,l}\frac{dy_l}{dx}\right)dx\right] \tag{1.15}$$

$$c_a = \frac{1}{c}\left[\int_0^c \left(C_{p,u}\frac{dy_u}{dx} - C_{p,l}\frac{dy_l}{dx}\right)dx + \int_0^c (c_{f,u} + c_{f,l})\,dx\right] \tag{1.16}$$

$$\begin{aligned} c_{m_{\text{LE}}} = \frac{1}{c^2}\Bigg[&\int_0^c (C_{p,u} - C_{p,l})x\,dx - \int_0^c \left(c_{f,u}\frac{dy_u}{dx} + c_{f,l}\frac{dy_l}{dx}\right)x\,dx \\ &+ \int_0^c \left(C_{p,u}\frac{dy_u}{dx} + c_{f,u}\right)y_u\,dx + \int_0^c \left(-C_{p,l}\frac{dy_l}{dx} + c_{f,l}\right)y_l\,dx\Bigg] \end{aligned} \tag{1.17}$$

The simple algebraic steps are left as an exercise for the reader. When evaluating these integrals, keep in mind that y_u is directed above the x axis, and hence is positive, whereas y_l is directed below the x axis, and hence is negative. Also, dy/dx on both the upper and lower surfaces follow the usual rule from calculus (i.e., positive for those portions of the body with a positive slope and negative for those portions with a negative slope).

The lift and drag coefficients can be obtained from Equations (1.1) and (1.2) cast in coefficient form:

$$c_l = c_n \cos\alpha - c_a \sin\alpha \tag{1.18}$$

$$c_d = c_n \sin\alpha + c_a \cos\alpha \tag{1.19}$$

Integral forms for c_l and c_d are obtained by substituting Equations (1.15) and (1.16) into (1.18) and (1.19).

It is important to note from Equations (1.15) through (1.19) that the aerodynamic force and moment coefficients can be obtained by integrating the pressure and skin friction coefficients over the body. This is a common procedure in both theoretical and experimental aerodynamics. In addition, although our derivations have used a two-dimensional body, an analogous development can be presented for three-dimensional bodies—the geometry and equations only get more complex and involved—the principle is the same.

EXAMPLE 1.1

Consider the supersonic flow over a 5° half-angle wedge at zero angle of attack, as sketched in Figure 1.23*a*. The freestream Mach number ahead of the wedge is 2.0, and the freestream pressure and density are 1.01×10^5 N/m^2 and 1.23 kg/m^3, respectively (this corresponds to standard sea level conditions). The pressures on the upper and lower surfaces of the wedge are constant with distance s and equal to each other, namely, $p_u = p_l = 1.31 \times 10^5$ N/m^2, as shown in Figure 1.23*b*. The pressure exerted on the base of the wedge is equal to p_∞. As seen in Figure 1.23*c*, the shear stress varies over both the upper and lower surfaces as $\tau_w = 431 s^{-0.2}$. The chord length, c, of the wedge is 2 m. Calculate the drag coefficient for the wedge.

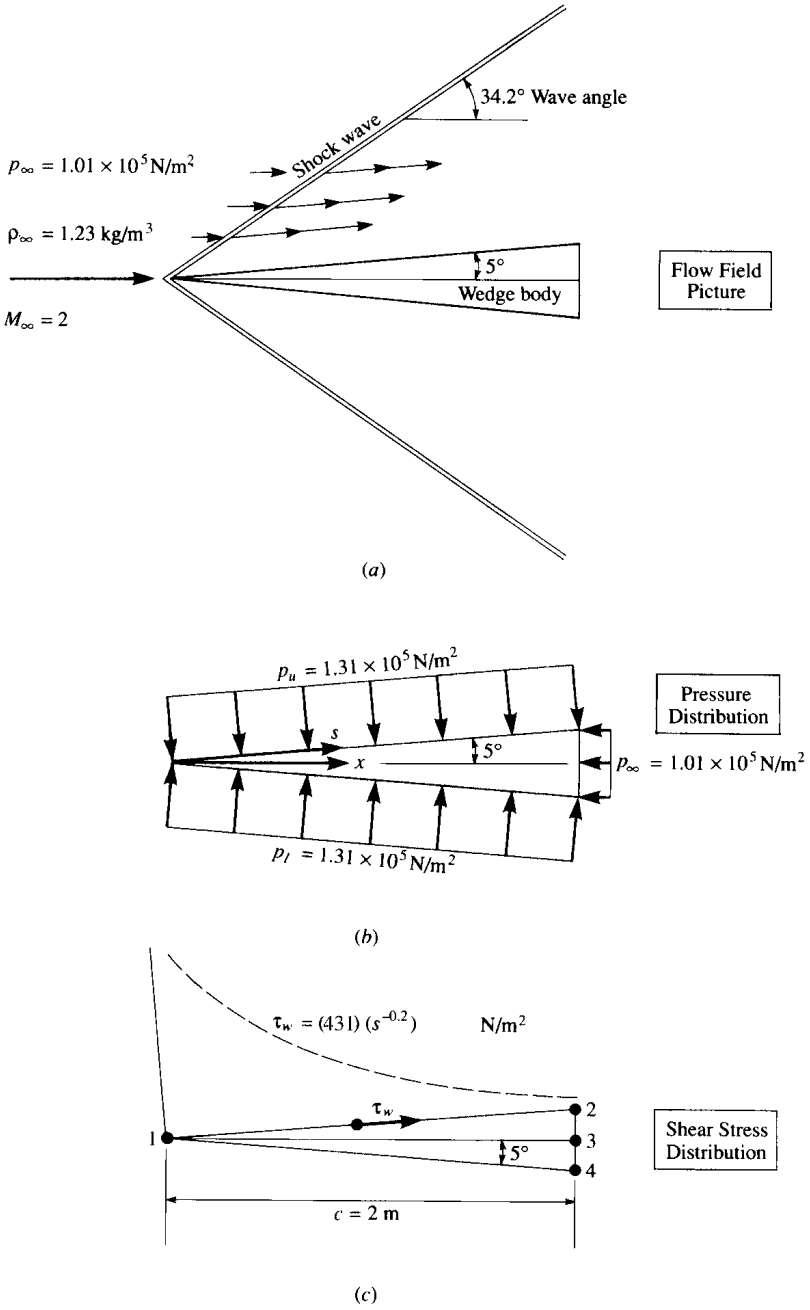

Figure 1.23 Illustration for Example 1.1.

■ Solution

We will carry out this calculation in two equivalent ways. First, we calculate the drag from Equation (1.8), and then obtain the drag coefficient. In turn, as an illustration of an alternate approach, we convert the pressure and shear stress to pressure coefficient and skin friction coefficient, and then use Equation (1.16) to obtain the drag coefficient.

Since the wedge in Figure 1.23 is at zero angle of attack, then $D' = A'$. Thus, the drag can be obtained from Equation (1.8) as

$$D' = \int_{\text{LE}}^{\text{TE}} (-p_u \sin\theta + \tau_u \cos\theta)\, ds_u + \int_{\text{LE}}^{\text{TE}} (p_l \sin\theta + \tau_l \cos\theta)\, ds_l$$

Referring to Figure 1.23*c*, recalling the sign convention for θ, and noting that integration over the upper surface goes from s_1 to s_2 on the inclined surface and from s_2 to s_3 on the base, whereas integration over the bottom surface goes from s_1 to s_4 on the inclined surface and from s_4 to s_3 on the base, we find that the above integrals become

$$\begin{aligned}
\int_{\text{LE}}^{\text{TE}} -p_u \sin\theta\, ds_u &= \int_{s_1}^{s_2} -(1.31 \times 10^5) \sin(-5^\circ)\, ds_u \\
&\quad + \int_{s_2}^{s_3} -(1.01 \times 10^5) \sin 90^\circ\, ds_u \\
&= 1.142 \times 10^4 (s_2 - s_1) - 1.01 \times 10^5 (s_3 - s_2) \\
&= 1.142 \times 10^4 \left(\frac{c}{\cos 5^\circ}\right) - 1.01 \times 10^5 (c)(\tan 5^\circ) \\
&= 1.142 \times 10^4 (2.008) - 1.01 \times 10^5 (0.175) = 5260 \text{ N}
\end{aligned}$$

$$\begin{aligned}
\int_{\text{LE}}^{\text{TE}} p_l \sin\theta\, ds_l &= \int_{s_1}^{s_4} (1.31 \times 10^5) \sin(5^\circ)\, ds_l + \int_{s_4}^{s_3} (1.01 \times 10^5) \sin(-90^\circ)\, ds_l \\
&= 1.142 \times 10^4 (s_4 - s_1) + 1.01 \times 10^5 (-1)(s_3 - s_4) \\
&= 1.142 \times 10^4 \left(\frac{c}{\cos 5^\circ}\right) - 1.01 \times 10^5 (c)(\tan 5^\circ) \\
&= 2.293 \times 10^4 - 1.767 \times 10^4 = 5260 \text{ N}
\end{aligned}$$

Note that the integrals of the pressure over the top and bottom surfaces, respectively, yield the same contribution to the drag—a result to be expected from the symmetry of the configuration in Figure 1.23:

$$\begin{aligned}
\int_{\text{LE}}^{\text{TE}} \tau_u \cos\theta\, ds_u &= \int_{s_1}^{s_2} 431 s^{-0.2} \cos(-5^\circ)\, ds_u \\
&= 429 \left(\frac{s_2^{0.8} - s_1^{0.8}}{0.8}\right) \\
&= 429 \left(\frac{c}{\cos 5^\circ}\right)^{0.8} \frac{1}{0.8} = 936.5 \text{ N}
\end{aligned}$$

$$\int_{\text{LE}}^{\text{TE}} \tau_l \cos\theta \, ds_l = \int_{s_1}^{s_4} 431 s^{-0.2} \cos(-5^\circ) \, ds_l$$
$$= 429 \left(\frac{s_4^{0.8} - s_1^{0.8}}{0.8} \right)$$
$$= 429 \left(\frac{c}{\cos 5^\circ} \right)^{0.8} \frac{1}{0.8} = 936.5 \text{ N}$$

Again, it is no surprise that the shear stresses acting over the upper and lower surfaces, respectively, give equal contributions to the drag; this is to be expected due to the symmetry of the wedge shown in Figure 1.23. Adding the pressure integrals, and then adding the shear stress integrals, we have for total drag

$$D' = \underbrace{1.052 \times 10^4}_{\substack{\text{pressure} \\ \text{drag}}} + \underbrace{0.1873 \times 10^4}_{\substack{\text{skin friction} \\ \text{drag}}} = \boxed{1.24 \times 10^4 \text{ N}}$$

Note that, for this rather slender body, but at a supersonic speed, most of the drag is pressure drag. Referring to Figure 1.23*a*, we see that this is due to the presence of an oblique shock wave from the nose of the body, which acts to create pressure drag (sometimes called *wave drag*). In this example, only 15 percent of the drag is skin friction drag; the other 85 percent is the pressure drag (wave drag). This is typical of the drag of slender supersonic bodies. In contrast, as we will see later, the drag of a slender body at subsonic speed, where there is no shock wave, is mainly skin friction drag.

The drag coefficient is obtained as follows. The velocity of the freestream is twice the sonic speed, which is given by

$$a_\infty = \sqrt{\gamma R T_\infty} = \sqrt{(1.4)(287)(288)} = 340.2 \text{ m/s}$$

(See Chapter 8 for a derivation of this expression for the speed of sound.) Note that, in the above, the standard sea level temperature of 288 K is used. Hence, $V_\infty = 2(340.2) = 680.4$ m/s. Thus,

$$q_\infty = \tfrac{1}{2} \rho_\infty V_\infty^2 = (0.5)(1.23)(680.4)^2 = 2.847 \times 10^5 \text{ N/m}^2$$

Also,
$$S = c(1) = 2.0 \text{ m}^2$$

Hence,
$$c_d = \frac{D'}{q_\infty S} = \frac{1.24 \times 10^4}{(2.847 \times 10^5)(2)} = \boxed{0.022}$$

An alternate solution to this problem is to use Equation (1.16), integrating the pressure coefficients and skin friction coefficients to obtain directly the drag coefficient. We proceed as follows:

$$C_{p,u} = \frac{p_u - p_\infty}{q_\infty} = \frac{1.31 \times 10^5 - 1.01 \times 10^5}{2.847 \times 10^5} = 0.1054$$

On the lower surface, we have the same value for C_p, that is,

$$C_{p,l} = C_{p,u} = 0.1054$$

Also,

$$c_{f,u} = \frac{\tau_w}{q_\infty} = \frac{431 s^{-0.2}}{q_\infty} = \frac{431}{2.847 \times 10^5} \left(\frac{x}{\cos 5^\circ} \right)^{-0.2} = 1.513 \times 10^{-3} x^{-0.2}$$

On the lower surface, we have the same value for c_f, that is,

$$c_{f,l} = 1.513 \times 10^{-3} x^{-0.2}$$

Also,

$$\frac{dy_u}{dx} = \tan 5^\circ = 0.0875$$

and

$$\frac{dy_l}{dx} = -\tan 5^\circ = -0.0875$$

Inserting the above information into Equation (1.16), we have

$$c_d = c_a = \frac{1}{c} \int_0^c \left(C_{p,u} \frac{dy_u}{dx} - C_{p,l} \frac{dy_l}{dx} \right) dx + \frac{1}{c} \int_0^c (c_{f,u} + c_{f,l})\, dx$$

$$= \frac{1}{2} \int_0^2 [(0.1054)(0.0875) - (0.1054)(-0.0875)]\, dx$$

$$+ \frac{1}{2} \int_0^2 2(1.513 \times 10^{-3}) x^{-0.2}\, dx$$

$$= 0.009223x \Big|_0^2 + 0.00189x^{0.8} \Big|_0^2$$

$$= 0.01854 + 0.00329 = \boxed{0.022}$$

This is the same result as obtained earlier.

EXAMPLE 1.2

Consider a cone at zero angle of attack in a hypersonic flow. (Hypersonic flow is very high-speed flow, generally defined as any flow above a Mach number of 5; hypersonic flow is further defined in Section 1.10.) The half-angle of the cone is θ_c, as shown in Figure 1.24. An approximate expression for the pressure coefficient on the surface of a hypersonic body is given by the newtonian sine-squared law (to be derived in Chapter 14):

$$C_p = 2 \sin^2 \theta_c$$

Note that C_p, hence, p, is constant along the inclined surface of the cone. Along the base of the body, we assume that $p = p_\infty$. Neglecting the effect of friction, obtain an expression for the drag coefficient of the cone, where C_D is based on the area of the base S_b.

■ Solution

We cannot use Equations (1.15) to (1.17) here. These equations are expressed for a two-dimensional body, such as the airfoil shown in Figure 1.22, whereas the cone in Figure 1.24 is a shape in three-dimensional space. Hence, we must treat this three-dimensional body as follows. From Figure 1.24, the drag force on the shaded strip of surface area is

$$(p \sin \theta_c)(2\pi r) \frac{dr}{\sin \theta_c} = 2\pi r p\, dr$$

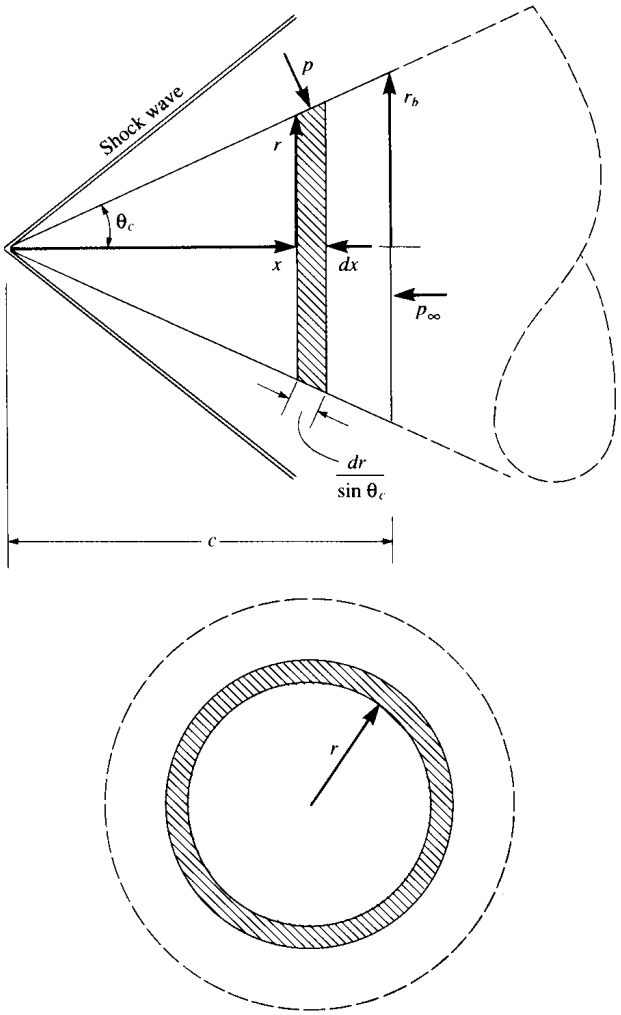

Figure 1.24 Illustration for Example 1.2.

The total drag due to the pressure acting over the total surface area of the cone is

$$D = \int_0^{r_b} 2\pi r p \, dr - \int_0^{r_b} r 2\pi p_\infty \, dr$$

The first integral is the horizontal force on the inclined surface of the cone, and the second integral is the force on the base of the cone. Combining the integrals, we have

$$D = \int_0^{r_b} 2\pi r (p - p_\infty) \, dr = \pi (p - p_\infty) r_b^2$$

Referenced to the base area, πr_b^2, the drag coefficient is

$$C_D = \frac{D}{q_\infty \pi r_b^2} = \frac{\pi r_b^2 (p - p_\infty)}{\pi r_b^2 q_\infty} = C_p$$

(*Note:* The drag coefficient for a cone is equal to its surface pressure coefficient.) Hence, using the newtonian sine-squared law, we obtain

$$\boxed{C_D = 2\sin^2\theta_c}$$

1.6 CENTER OF PRESSURE

From Equations (1.7) and (1.8), we see that the normal and axial forces on the body are due to the *distributed* loads imposed by the pressure and shear stress distributions. Moreover, these distributed loads generate a moment about the leading edge, as given by Equation (1.11). *Question:* If the aerodynamic force on a body is specified in terms of a resultant single force R, or its components such as N and A, *where* on the body should this resultant be placed? The answer is that the resultant force should be located on the body such that it produces the same effect as the distributed loads. For example, the distributed load on a two-dimensional body such as an airfoil produces a moment about the leading edge given by Equation (1.11); therefore, N' and A' must be placed on the airfoil at such a location to generate the same moment about the leading edge. If A' is placed on the chord line as shown in Figure 1.25, then N' must be located a distance x_{cp} downstream of the leading edge such that

$$M'_{LE} = -(x_{cp})N'$$

$$\boxed{x_{cp} = -\frac{M'_{LE}}{N'}} \tag{1.20}$$

In Figure 1.25, the direction of the curled arrow illustrating M'_{LE} is drawn in the positive (pitch-up) sense. (From Section 1.5, recall the standard convention that aerodynamic moments are positive if they tend to increase the angle of attack.) Examining Figure 1.25, we see that a positive N' creates a negative (pitch-down) moment about the leading edge. This is consistent with the negative sign in Equation (1.20). Therefore, in Figure 1.25, the actual moment about the leading edge is negative, and hence is in a direction opposite to the curled arrow shown.

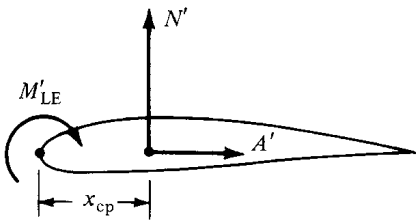

Figure 1.25 Center of pressure for an airfoil.

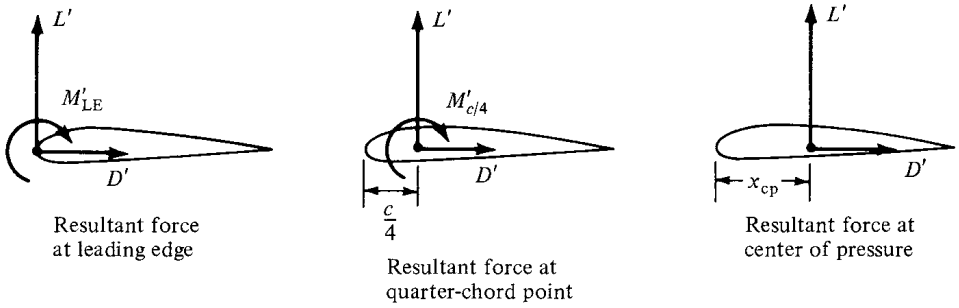

Figure 1.26 Equivalent ways of specifying the force-and-moment system on an airfoil.

In Figure 1.25 and Equation (1.20), x_{cp} is defined as the *center of pressure*. It is the location where the resultant of a distributed load effectively acts on the body. If moments were taken about the center of pressure, the integrated effect of the distributed loads would be zero. Hence, an alternate definition of the center of pressure is that point on the body about which the aerodynamic moment is zero.

In cases where the angle of attack of the body is small, $\sin\alpha \approx 0$ and $\cos\alpha \approx 1$; hence, from Equation (1.1), $L' \approx N'$. Thus, Equation (1.20) becomes

$$x_{cp} \approx -\frac{M'_{LE}}{L'} \tag{1.21}$$

Examine Equations (1.20) and (1.21). As N' and L' decrease, x_{cp} increases. As the forces approach zero, the center of pressure moves to infinity. For this reason, the center of pressure is not always a convenient concept in aerodynamics. However, this is no problem. To define the force-and-moment system due to a distributed load on a body, the resultant force can be placed at *any* point on the body, as long as the value of the moment about that point is also given. For example, Figure 1.26 illustrates three equivalent ways of specifying the force-and-moment system on an airfoil. In the left figure, the resultant is placed at the leading edge, with a finite value of M'_{LE}. In the middle figure, the resultant is placed at the quarter-chord point, with a finite value of $M'_{c/4}$. In the right figure, the resultant is placed at the center of pressure, with a zero moment about that point. By inspection of Figure 1.26, the quantitative relation between these cases is

$$M'_{LE} = -\frac{c}{4}L' + M'_{c/4} = -x_{cp}L' \tag{1.22}$$

EXAMPLE 1.3

In low-speed, incompressible flow, the following experimental data are obtained for an NACA 4412 airfoil section at an angle of attack of 4°: $c_l = 0.85$ and $c_{m,c/4} = -0.09$. Calculate the location of the center of pressure.

■ Solution

From Equation (1.22),

$$x_{cp} = \frac{c}{4} - \frac{M'_{c/4}}{L'}$$

$$\frac{x_{cp}}{c} = \frac{1}{4} - \frac{(M_{c/4}/q_\infty c^2)}{(L'/q_\infty c)} = \frac{1}{4} - \frac{c_{m,c/4}}{c_l}$$

$$= \frac{1}{4} - \frac{(-0.09)}{0.85} = \boxed{0.356}$$

(*Note:* In Chapter 4, we will learn that, for a thin, symmetrical airfoil, the center of pressure is at the quarter-chord location. However, for the NACA 4412 airfoil, which is not symmetric, the center-of-pressure location is behind the quarter-chord point.)

EXAMPLE 1.4

Consider the DC-3 shown in Fig. 1.1. Just outboard of the engine nacelle, the airfoil chord length is 15.4 ft. At cruising velocity (188 mi/h) at sea level, the moments per unit span at this airfoil location are $M'_{c/4} = -1071$ ft lb/ft and $M'_{LE} = -3213.9$ ft lb/ft. Calculate the lift per unit span and the location of the center of pressure on the airfoil.

■ Solution

From Eq. (1.22)

$$\frac{c}{4}L' = M'_{c/4} - M'_{LE} = -1071 - (-3213.9) = 2142.9$$

At this airfoil location on the wing, $\frac{c}{4} = \frac{15.4}{4} = 3.85$ ft.

Thus,

$$L' = \frac{2142.9}{3.85} = \boxed{556.6 \text{ lb/ft}}$$

Returning to Eq. (1.22)

$$-x_{cp}L' = M'_{LE}$$

$$-x_{cp} = -\frac{M'_{LE}}{L'} = -\frac{(-3213.9)}{556.6} = \boxed{5.774 \text{ ft}}$$

Note: In this section, we have shown that the force and moment system acting on an airfoil is uniquely specified by giving the lift acting at any point on the airfoil and the moment about that point. Analogously, this example proves that the force and moment system is also uniquely specified by giving the moments acting about any two points on the airfoil.

1.7 DIMENSIONAL ANALYSIS: THE BUCKINGHAM PI THEOREM

The aerodynamic forces and moments on a body, and the corresponding force and moment coefficients, have been defined and discussed in Section 1.5. *Question:*

What physical quantities determine the variation of these forces and moments? The answer can be found from the powerful method of *dimensional analysis,* which is introduced in this section.[3]

Consider a body of given shape at a given angle of attack (e.g., the airfoil sketched in Figure 1.17). The resultant aerodynamic force is R. On a physical, intuitive basis, we expect R to depend on:

1. Freestream velocity V_∞.
2. Freestream density ρ_∞.
3. Viscosity of the fluid. We have seen that shear stress τ contributes to the aerodynamic forces and moments, and that τ is proportional to the velocity gradients in the flow. For example, if the velocity gradient is given by $\partial u/\partial y$, then $\tau = \mu \partial u/\partial y$. The constant of proportionality is the viscosity coefficient μ. Hence, let us represent the influence of viscosity on aerodynamic forces and moments by the freestream viscosity coefficient μ_∞.
4. The size of the body, represented by some chosen reference length. In Figure 1.17, the convenient reference length is the chord length c.
5. The compressibility of the fluid. The technical definition of compressibility is given in Chapter 7. For our present purposes, let us just say that compressibility is related to the *variation* of density throughout the flow field, and certainly the aerodynamic forces and moments should be sensitive to any such variation. In turn, compressibility is related to the speed of sound a in the fluid, as shown in Chapter 8.[4] Therefore, let us represent the influence of compressibility on aerodynamic forces and moments by the freestream speed of sound, a_∞.

In light of the above, and without any a priori knowledge about the variation of R, we can use common sense to write

$$R = f(\rho_\infty, V_\infty, c, \mu_\infty, a_\infty) \tag{1.23}$$

Equation (1.23) is a general functional relation, and as such is not very practical for the direct calculation of R. In principle, we could mount the given body in a wind tunnel, incline it at the given angle of attack, and then systematically measure the variation of R due to variations of ρ_∞, V_∞, c, μ_∞, and a_∞, taken one at a time. By cross-plotting the vast bulk of data thus obtained, we might be able to extract a precise functional relation for Equation (1.23). However, it would be hard work, and it would certainly be costly in terms of a huge amount of required wind-tunnel time. Fortunately, we can simplify the problem and considerably reduce our time and effort by first employing the method of dimensional analysis. This method will

[3] For a more elementary treatment of dimensional analysis, see Chapter 5 of Reference 2.

[4] Common experience tells us that sound waves propagate through air at some finite velocity, much slower than the speed of light; you see a flash of lightning in the distance, and hear the thunder moments later. The speed of sound is an important physical quantity in aerodynamics and is discussed in detail in Section 8.3.

define a set of dimensionless parameters that governs the aerodynamic forces and moments; this set will considerably reduce the number of independent variables as presently occurs in Equation (1.23).

Dimensional analysis is based on the obvious fact that in an equation dealing with the real physical world, each term must have the same dimensions. For example, if

$$\psi + \eta + \zeta = \phi$$

is a physical relation, then ψ, η, ζ, and ϕ must have the same dimensions. Otherwise we would be adding apples and oranges. The above equation can be made dimensionless by dividing by any one of the terms, say, ϕ:

$$\frac{\psi}{\phi} + \frac{\eta}{\phi} + \frac{\zeta}{\phi} = 1$$

These ideas are formally embodied in the Buckingham pi theorem, stated below without derivation. (See Reference 3, pages 21–28, for such a derivation.)

Buckingham pi Theorem

Let K equal the number of fundamental dimensions required to describe the physical variables. (In mechanics, all physical variables can be expressed in terms of the dimensions of *mass, length,* and *time;* hence, $K = 3$.) Let $P_1, P_2, \ldots, P_N$ represent N physical variables in the physical relation

$$f_1(P_1, P_2, \ldots, P_N) = 0 \tag{1.24}$$

Then, the physical relation Equation (1.24) may be reexpressed as a relation of $(N - K)$ dimensionless products (called Π products),

$$f_2(\Pi_1, \Pi_2, \ldots, \Pi_{N-K}) = 0 \tag{1.25}$$

where each Π product is a dimensionless product of a set of K physical variables plus one other physical variable. Let $P_1, P_2, \ldots, P_K$ be the selected set of K physical variables. Then

$$\begin{aligned} \Pi_1 &= f_3(P_1, P_2, \ldots, P_K, P_{K+1}) \\ \Pi_2 &= f_4(P_1, P_2, \ldots, P_K, P_{K+2}) \\ &\cdots\cdots\cdots\cdots\cdots\cdots\cdots \\ \Pi_{N-K} &= f_5(P_1, P_2, \ldots, P_K, P_N) \end{aligned} \tag{1.26}$$

The choice of the repeating variables, $P_1, P_2, \ldots, P_K$ should be such that they include *all* the K dimensions used in the problem. Also, the dependent variable [such as R in Equation (1.23)] should appear in only one of the Π products.

Returning to our consideration of the aerodynamic force on a given body at a given angle of attack, Equation (1.23) can be written in the form of Equation (1.24):

$$g(R, \rho_\infty, V_\infty, c, \mu_\infty, a_\infty) = 0 \tag{1.27}$$

Following the Buckingham pi theorem, the fundamental dimensions are

$$\begin{aligned} m &= \text{dimensions of mass} \\ l &= \text{dimension of length} \\ t &= \text{dimension of time} \end{aligned}$$

Hence, $K = 3$. The physical variables and their dimensions are

$$\begin{aligned} [R] &= mlt^{-2} \\ [\rho_\infty] &= ml^{-3} \\ [V_\infty] &= lt^{-1} \\ [c] &= l \\ [\mu_\infty] &= ml^{-1}t^{-1} \\ [a_\infty] &= lt^{-1} \end{aligned}$$

Hence, $N = 6$. In the above, the dimensions of the force R are obtained from Newton's second law, force = mass $\times$ acceleration; hence, $[R] = mlt^{-2}$. The dimensions of μ_∞ are obtained from its definition [e.g., $\mu = \tau/(\partial u/\partial y)$], and from Newton's second law. (Show for yourself that $[\mu_\infty] = ml^{-1}t^{-1}$.) Choose ρ_∞, V_∞, and c as the arbitrarily selected sets of K physical variables. Then Equation (1.27) can be reexpressed in terms of $N - K = 6 - 3 = 3$ dimensionless Π products in the form of Equation (1.25):

$$f_2(\Pi_1, \Pi_2, \Pi_3) = 0 \tag{1.28}$$

From Equation (1.26), these Π products are

$$\Pi_1 = f_3(\rho_\infty, V_\infty, c, R) \tag{1.29a}$$

$$\Pi_2 = f_4(\rho_\infty, V_\infty, c, \mu_\infty) \tag{1.29b}$$

$$\Pi_3 = f_5(\rho_\infty, V_\infty, c, a_\infty) \tag{1.29c}$$

For the time being, concentrate on Π_1, from Equation (1.29a). Assume that

$$\Pi_1 = \rho_\infty^d V_\infty^b c^e R \tag{1.30}$$

where d, b, and e are exponents to be found. In dimensional terms, Equation (1.30) is

$$[\Pi_1] = (ml^{-3})^d (lt^{-1})^b (l)^e (mlt^{-2}) \tag{1.31}$$

Because Π_1 is dimensionless, the right side of Equation (1.31) must also be dimensionless. This means that the exponents of m must add to zero, and similarly

for the exponents of l and t. Hence,

For m: $d + 1 = 0$

For l: $-3d + b + e + 1 = 0$

For t: $-b - 2 = 0$

Solving the above equations, we find that $d = -1$, $b = -2$, and $e = -2$. Substituting these values into Equation (1.30), we have

$$\Pi_1 = R\rho_\infty^{-1} V_\infty^{-2} c^{-2} \tag{1.32}$$

$$= \frac{R}{\rho_\infty V_\infty^2 c^2}$$

The quantity $R/\rho_\infty V_\infty^2 c^2$ is a dimensionless parameter in which c^2 has the dimensions of an area. We can replace c^2 with any reference area we wish (such as the planform area of a wing S), and Π_1 will still be dimensionless. Moreover, we can multiply Π_1 by a pure number, and it will still be dimensionless. Thus, from Equation (1.32), Π_1 can be redefined as

$$\Pi_1 = \frac{R}{\frac{1}{2}\rho_\infty V_\infty^2 S} = \frac{R}{q_\infty S} \tag{1.33}$$

Hence, Π_1 is a force coefficient C_R, as defined in Section 1.5. In Equation (1.33), S is a reference area germane to the given body shape.

The remaining Π products can be found as follows. From Equation (1.29*b*), assume

$$\Pi_2 = \rho_\infty V_\infty^h c^i \mu_\infty^j \tag{1.34}$$

Paralleling the above analysis, we obtain

$$[\Pi_2] = (ml^{-3})(lt^{-1})^h (l)^i (ml^{-1}t^{-1})^j$$

Hence,

For m: $1 + j = 0$

For l: $-3 + h + i - j = 0$

For t: $-h - j = 0$

Thus, $j = -1$, $h = 1$, and $i = 1$. Substitution into Equation (1.34) gives

$$\Pi_2 = \frac{\rho_\infty V_\infty c}{\mu_\infty} \tag{1.35}$$

The dimensionless combination in Equation (1.35) is defined as the freestream *Reynolds number* $\mathrm{Re} = \rho_\infty V_\infty c/\mu_\infty$. The Reynolds number is physically a measure of the ratio of inertia forces to viscous forces in a flow and is one of the most powerful parameters in fluid dynamics. Its importance is emphasized in Chapters 15 to 20.

Returning to Equation (1.29*c*), assume

$$\Pi_3 = V_\infty \rho_\infty^k c^r a_\infty^s \tag{1.36}$$
$$[\Pi_3] = (lt^{-1})(ml^{-3})^k (l)^r (lt^{-1})^s$$

For m: $k = 0$

For l: $1 - 3k + r + s = 0$

For t: $-1 - s = 0$

Hence, $k = 0$, $s = -1$, and $r = 0$. Substituting Equation (1.36), we have

$$\Pi_e = \frac{V_\infty}{a_\infty} \tag{1.37}$$

The dimensionless combination in Equation (1.37) is defined as the freestream *Mach number* $M = V_\infty / a_\infty$. The Mach number is the ratio of the flow velocity to the speed of sound; it is a powerful parameter in the study of gas dynamics. Its importance is emphasized in subsequent chapters.

The results of our dimensional analysis may be organized as follows. Inserting Equations (1.33), (1.35), and (1.37) into (1.28), we have

$$f_2\left(\frac{R}{\frac{1}{2}\rho_\infty V_\infty^2 S}, \frac{\rho_\infty V_\infty c}{\mu_\infty}, \frac{V_\infty}{a_\infty}\right) = 0$$

or $$f_2(C_R, \text{Re}, M_\infty) = 0$$

or $$\boxed{C_R = f_6(\text{Re}, M_\infty)} \tag{1.38}$$

This is an important result! Compare Equations (1.23) and (1.38). In Equation (1.23), R is expressed as a general function of five independent variables. However, our dimensional analysis has shown that:

1. R can be expressed in terms of a dimensionless force coefficient, $C_R = R/\frac{1}{2}\rho_\infty V_\infty^2 S$.
2. C_R is a function of only Re and M_∞, from Equation (1.38).

Therefore, by using the Buckingham pi theorem, we have reduced the number of independent variables from five in Equation (1.23) to two in Equation (1.38). Now, if we wish to run a series of wind-tunnel tests for a given body at a given angle of attack, we need only to vary the Reynolds and Mach numbers in order to obtain data for the direct formulation of R through Equation (1.38). With a small amount of analysis, we have saved a huge amount of effort and wind-tunnel time. More importantly, we have defined two dimensionless parameters, Re and M_∞, which govern the flow. They are called *similarity parameters,* for reasons to be discussed in the following section. Other similarity parameters are introduced as our aerodynamic discussions progress.

Since the lift and drag are components of the resultant force, corollaries to Equation (1.38) are

$$C_L = f_7(\text{Re}, M_\infty) \tag{1.39}$$

$$C_D = f_8(\text{Re}, M_\infty) \tag{1.40}$$

Moreover, a relation similar to Equation (1.23) holds for the aerodynamic moments, and dimensional analysis yields

$$C_M = f_9(\text{Re}, M_\infty) \tag{1.41}$$

Keep in mind that the above analysis was for a given body shape at a given angle of attack α. If α is allowed to vary, then C_L, C_D, and C_M will in general depend on the value of α. Hence, Equations (1.39) to (1.41) can be generalized to

$$\boxed{C_L = f_{10}(\text{Re}, M_\infty, \alpha)} \tag{1.42}$$

$$\boxed{C_D = f_{11}(\text{Re}, M_\infty, \alpha)} \tag{1.43}$$

$$\boxed{C_M = f_{12}(\text{Re}, M_\infty, \alpha)} \tag{1.44}$$

Equations (1.42) to (1.44) assume a given body shape. Much of theoretical and experimental aerodynamics is focused on obtaining explicit expressions for Equations (1.42) to (1.44) for specific body shapes. This is one of the practical applications of aerodynamics mentioned in Section 1.2, and it is one of the major thrusts of this book.

For mechanical problems that also involve thermodynamics and heat transfer, the temperature, specific heat, and thermal conductivity of the fluid, as well as the temperature of the body surface (wall temperature), must be added to the list of physical variables, and the unit of temperature (say, kelvin or degree Rankine) must be added to the list of fundamental dimensions. For such cases, dimensional analysis yields additional dimensionless products such as heat transfer coefficients, and additional similarity parameters such as the ratio of specific heat at constant pressure to that at constant volume c_p/c_v, the ratio of wall temperature to freestream temperature T_w/T_∞, and the Prandtl number $\text{Pr} = \mu_\infty c_p/k_\infty$, where k_∞ is the thermal conductivity of the freestream.[5] Thermodynamics is essential to the study of compressible flow (Chapters 7 to 14), and heat transfer is part of the study of viscous flow (Chapters 15 to 20). Hence, these additional similarity parameters will be emphasized when they appear logically in our subsequent discussions. For the time being, however, the Mach and Reynolds numbers will suffice as the dominant similarity parameters for our present considerations.

[5] The *specific heat* of a fluid is defined as the amount of heat added to a system, δq, per unit increase in temperature; $c_v = \delta q/dT$ if δq is added at constant volume, and similarly, for c_p if δq is added at constant pressure. Specific heats are discussed in detail in Section 7.2. The thermal conductivity relates heat flux to temperature gradients in the fluid. For example, if $\dot{q}_x$ is the heat transferred in the x direction per second per unit area and dT/dx is the temperature gradient in the x direction, then thermal conductivity k is defined by $\dot{q}_x = -k(dT/dx)$. Thermal conductivity is discussed in detail in Section 15.3.

1.8 FLOW SIMILARITY

Consider two different flow fields over two different bodies. By definition, different flows are *dynamically similar* if:

1. The streamline patterns are geometrically similar.
2. The distributions of V/V_∞, p/p_∞, T/T_∞, etc., throughout the flow field are the same when plotted against common nondimensional coordinates.
3. The force coefficients are the same.

Actually, item 3 is a consequence of item 2; if the nondimensional pressure and shear stress distributions over different bodies are the same, then the nondimensional force coefficients will be the same.

The definition of dynamic similarity was given above. *Question:* What are the *criteria* to ensure that two flows are dynamically similar? The answer comes from the results of the dimensional analysis in Section 1.7. Two flows will be dynamically similar if:

1. The bodies and any other solid boundaries are geometrically similar for both flows.
2. The similarity parameters are the same for both flows.

So far, we have emphasized two parameters, Re and M_∞. For many aerodynamic applications, these are by far the dominant similarity parameters. Therefore, in a limited sense, but applicable to many problems, we can say that flows over geometrically similar bodies at the same Mach and Reynolds numbers are dynamically similar, and hence the lift, drag, and moment coefficients will be identical for the bodies. This is a key point in the validity of wind-tunnel testing. If a scale model of a flight vehicle is tested in a wind tunnel, the measured lift, drag, and moment coefficients will be the same as for free flight as long as the Mach and Reynolds numbers of the wind-tunnel test-section flow are the same as for the free-flight case. As we will see in subsequent chapters, this statement is not quite precise because there are other similarity parameters that influence the flow. In addition, differences in freestream turbulence between the wind tunnel and free flight can have an important effect on C_D and the maximum value of C_L. However, direct simulation of the free-flight Re and M_∞ is the primary goal of many wind-tunnel tests.

EXAMPLE 1.5

Consider the flow over two circular cylinders, one having four times the diameter of the other, as shown in Figure 1.27. The flow over the smaller cylinder has a freestream density, velocity and temperature given by ρ_1, V_1, and T_1, respectively. The flow over the larger cylinder has a freestream density, velocity, and temperature given by ρ_2, V_2, and T_2, respectively, where $\rho_2 = \rho_1/4$, $V_2 = 2V_1$, and $T_2 = 4T_1$. Assume that both μ and a are proportional to $T^{1/2}$. Show that the two flows are dynamically similar.

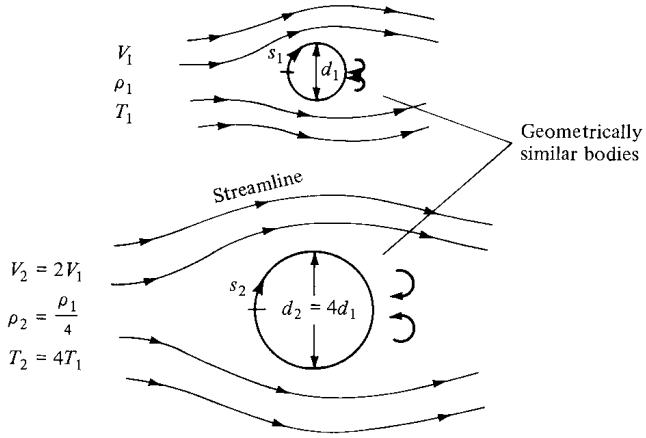

Figure 1.27 Example of dynamic flow similarity. Note that as part of the definition of dynamic similarity, the streamlines (lines along which the flow velocity is tangent at each point) are geometrically similar between the two flows.

■ Solution

Since $\mu \propto \sqrt{T}$ and $a \propto \sqrt{T}$, then

$$\frac{\mu_2}{\mu_1} = \sqrt{\frac{T_2}{T_1}} = \sqrt{\frac{4T_1}{T_1}} = 2$$

and

$$\frac{a_2}{a_1} = \sqrt{\frac{T_2}{T_1}} = 2$$

By definition,

$$M_1 = \frac{V_1}{a_1}$$

and

$$M_2 = \frac{V_2}{a_2} = \frac{2V_1}{2a_1} = \frac{V_1}{a_1} = M_1$$

Hence, the Mach numbers are the same. Basing the Reynolds number on the diameter d of the cylinder, we have by definition,

$$\text{Re}_1 = \frac{\rho_1 V_1 d_1}{\mu_1}$$

and

$$\text{Re}_2 = \frac{\rho_2 V_2 d_2}{\mu_2} = \frac{(\rho_1/4)(2V_1)(4d_1)}{2\mu_1} = \frac{\rho_1 V_1 d_1}{\mu_1} = \text{Re}_1$$

Hence, the Reynolds numbers are the same. Since the two bodies are geometrically similar and M_∞ and Re are the same, we have satisfied all the criteria; the two flows are dynamically similar. In turn, as a consequence of being similar flows, we know from the definition that:

1. The streamline patterns around the two cylinders are geometrically similar.
2. The nondimensional pressure, temperature, density, velocity, etc., distributions are the same around two cylinders. This is shown schematically in Figure 1.28, where

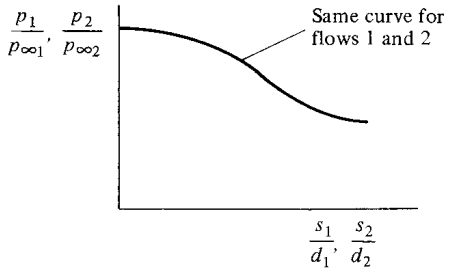

Figure 1.28 One aspect of the definition of dynamically similar flows. The nondimensional flow variable distributions are the same.

the nondimensional pressure distribution p/p_∞ is shown as a function of the nondimensional surface distance s/d. It is the same curve for both bodies.

3. The drag coefficients for the two bodies are the same. Here, $C_D = D/q_\infty S$, where $S = \pi d^2/4$. As a result of the flow similarity, $C_{D1} = C_{D2}$. (*Note:* Examining Figure 1.27, we see that the lift on the cylinders is zero because the flow is symmetrical about the horizontal axis through the center of the cylinder. The pressure distribution over the top is the same as over the bottom, and they cancel each other in the vertical direction. Therefore, drag is the only aerodynamic force on the body.)

EXAMPLE 1.6

Consider a Boeing 747 airliner cruising at a velocity of 550 mi/h at a standard altitude of 38,000 ft, where the freestream pressure and temperature are 432.6 lb/ft^2 and 390°R, respectively. A one-fiftieth scale model of the 747 is tested in a wind tunnel where the temperature is 430°R. Calculate the required velocity and pressure of the test airstream in the wind tunnel such that the lift and drag coefficients measured for the wind-tunnel model are the same as for free flight. Assume that both μ and a are proportional to $T^{1/2}$.

■ Solution

Let subscripts 1 and 2 denote the free-flight and wind-tunnel conditions, respectively. For $C_{L,1} = C_{L,2}$ and $C_{D,1} = C_{D,2}$, the wind-tunnel flow must be dynamically similar to free flight. For this to hold, $M_1 = M_2$ and $\text{Re}_1 = \text{Re}_2$:

$$M_1 = \frac{V_1}{a_1} \propto \frac{V_1}{\sqrt{T_1}}$$

and

$$M_2 = \frac{V_2}{a_2} \propto \frac{V_2}{\sqrt{T_2}}$$

Hence,
$$\frac{V_2}{\sqrt{T_2}} = \frac{V_1}{\sqrt{T_1}}$$

or
$$V_2 = V_1\sqrt{\frac{T_2}{T_1}} = 550\sqrt{\frac{430}{390}} = \boxed{577.5 \text{ mi/h}}$$

$$\text{Re}_1 = \frac{\rho_1 V_1 c_1}{\mu_1} \propto \frac{\rho_1 V_1 c_1}{\sqrt{T_1}}$$

and
$$\text{Re}_2 = \frac{\rho_2 V_2 c_2}{\mu_2} \propto \frac{\rho_2 V_2 c_2}{\sqrt{T_2}}$$

Hence,
$$\frac{\rho_1 V_1 c_1}{\sqrt{T_1}} = \frac{\rho_2 V_2 c_2}{\sqrt{T_2}}$$

or
$$\frac{\rho_2}{\rho_1} = \left(\frac{V_1}{V_2}\right)\left(\frac{c_1}{c_2}\right)\sqrt{\frac{T_2}{T_1}}$$

However, since $M_1 = M_2$, then

$$\frac{V_1}{V_2} = \sqrt{\frac{T_1}{T_2}}$$

Thus,
$$\frac{\rho_2}{\rho_1} = \frac{c_1}{c_2} = 50$$

The equation of state for a perfect gas is $p = \rho RT$, where R is the specific gas constant. Thus

$$\frac{p_2}{p_1} = \frac{\rho_2}{\rho_1}\frac{T_2}{T_1} = (50)\left(\frac{430}{390}\right) = 55.1$$

Hence,
$$p_2 = 55.1 p_1 = (55.1)(432.6) = \boxed{23{,}836 \text{ lb/ft}^2}$$

Since 1 atm = 2116 lb/ft^2, then $p_2 = 23{,}836/2116 = \boxed{11.26 \text{ atm}}$.

In Example 1.6, the wind-tunnel test stream must be pressurized far above atmospheric pressure in order to simulate the proper free-flight Reynolds number. However, most standard subsonic wind tunnels are not pressurized as such, because of the large extra financial cost involved. This illustrates a common difficulty in wind-tunnel testing, namely, the difficulty of simulating both Mach number and Reynolds number simultaneously in the same tunnel. It is interesting to note that the NACA (National Advisory Committee for Aeronautics, the predecessor of NASA) in 1922 began operating a pressurized wind tunnel at the NACA Langley Memorial Laboratory in Hampton, Virginia. This was a subsonic wind tunnel contained entirely inside a large tank pressurized to as high as 20 atm. Called the variable density tunnel (VDT), this facility was used in the 1920s and 1930s to provide essential data on the NACA family of airfoil sections at the high

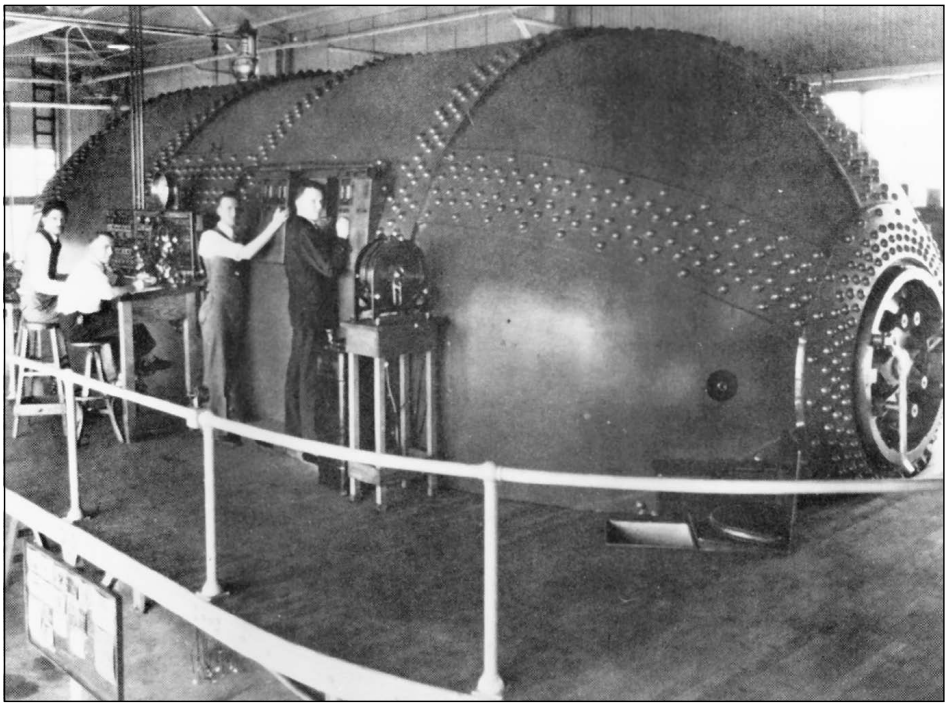

Figure 1.29 The NACA variable density tunnel (VDT). Authorized in March of 1921, the VDT was operational in October 1922 at the NACA Langley Memorial Laboratory at Hampton, Virginia. It is essentially a large, subsonic wind tunnel entirely contained within an 85-ton pressure shell, capable of 20 atm. This tunnel was instrumental in the development of the various families of NACA airfoil shapes in the 1920s and 1930s. In the early 1940s, it was decommissioned as a wind tunnel and used as a high-pressure air storage tank. In 1983, due to its age and outdated riveted construction, its use was discontinued altogether. Today, the VDT remains at the NASA Langley Research Center; it has been officially designated as a National Historic Landmark. *(Courtesy of NASA.)*

Reynolds numbers associated with free flight. A photograph of the NACA variable density tunnel is shown in Figure 1.29; notice the heavy pressurized shell in which the wind tunnel is enclosed. A cross section of the VDT inside the pressure cell is shown in Figure 1.30. These figures demonstrate the extreme measures sometimes taken in order to simulate simultaneously the free-flight values of the important similarity parameters in a wind tunnel. Today, for the most part, we do not attempt to simulate all the parameters simultaneously; rather, Mach number simulation is achieved in one wind tunnel, and Reynolds number simulation in another tunnel. The results from both tunnels are then analyzed and correlated to obtain reasonable values for C_L and C_D appropriate for free flight. In any event, this example serves to illustrate the difficulty of full free-flight simulation in a given wind tunnel and underscores the importance given to dynamically similar flows in experimental aerodynamics.

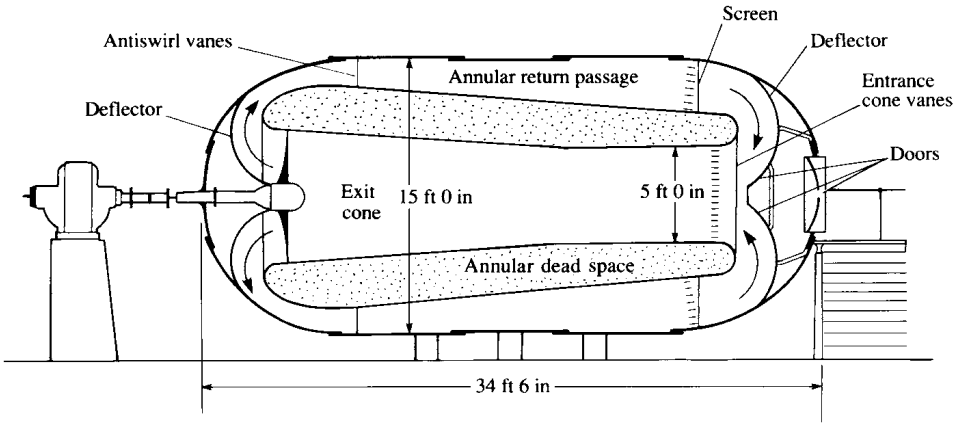

Figure 1.30 Schematic of the variable density tunnel. *(From Baals, D. D. and Carliss, W. R.,* Wind Tunnels of NASA, *NASA SP-440, 1981.)*

DESIGN BOX

Lift and drag coefficients play a strong role in the preliminary design and performance analysis of airplanes. The purpose of this design box is to enforce the importance of C_L and C_D in aeronautical engineering; they are much more than just the conveniently defined terms discussed so far—they are fundamental quantities, which make the difference between intelligent engineering and simply groping in the dark.

Consider an airplane in steady, level (horizontal) flight, as illustrated in Figure 1.31. For this case, the weight W acts vertically downward. The lift L acts vertically upward, perpendicular to the relative wind V_∞ (by definition). In order to sustain the airplane in level flight,

$$L = W$$

The thrust T from the propulsive mechanism and the drag D are both parallel to V_∞. For steady (unaccelerated) flight,

$$T = D$$

Note that for most conventional flight situations, the magnitude of L and W is much larger than the magnitude of T and D, as indicated by the sketch in Figure 1.31. Typically, for conventional cruising flight, $L/D \approx 15$ to 20.

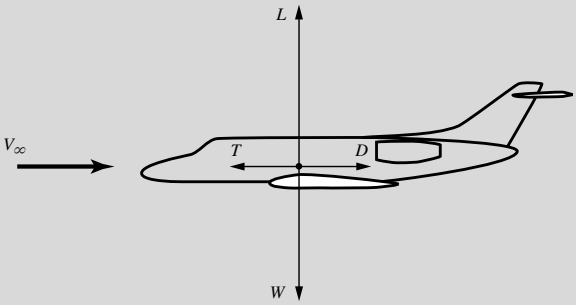

Figure 1.31 The four forces acting on an airplane in flight.

For an airplane of *given shape,* such as that sketched in Figure 1.31, at given Mach and Reynolds number, C_L and C_D are simply functions of the angle of attack, α of the airplane. This is the message conveyed by Equations (1.42) and (1.43). It is a simple and basic message—part of the beauty of nature—that the actual values of C_L and C_D for a given body shape just depend on the orientation of the body in the flow (i.e., angle of attack). Generic variations for C_L and C_D versus α are sketched in Figure 1.32. Note that C_L increases linearly with α until an angle of

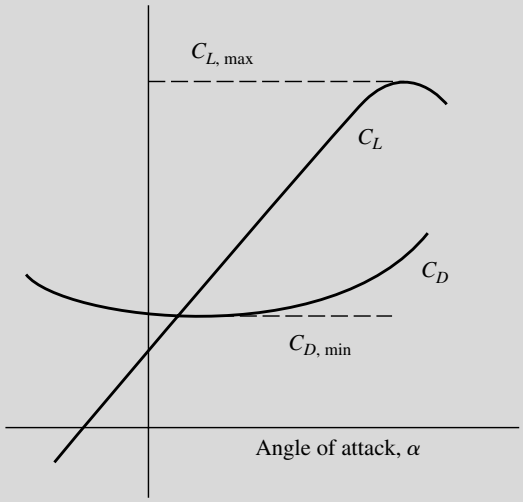

Figure 1.32 Schematic of lift and drag coefficients versus angle of attack; illustration of maximum lift coefficient and minimum drag coefficient.

attack is reached when the wing stalls, the lift coefficient reaches a peak value, and then drops off as α is further increased. The maximum value of the lift coefficient is denoted by $C_{L,\max}$, as noted in Figure 1.32.

The lowest possible velocity at which the airplane can maintain steady, level flight is the stalling velocity, V_{stall}; it is dictated by the value of $C_{L,\max}$, as follows.[6] From the definition of lift coefficient given in Section 1.5, applied for the case of level flight where $L = W$, we have

$$C_L = \frac{L}{q_\infty S} = \frac{W}{q_\infty S} = \frac{2W}{\rho_\infty V_\infty^2 S} \tag{1.45}$$

Solving Equation (1.45) for V_∞,

$$V_\infty = \sqrt{\frac{2W}{\rho_\infty S C_L}} \tag{1.46}$$

For a given airplane flying at a given altitude, W, ρ, and S are fixed values; hence from Equation (1.46) each value of velocity corresponds to a specific value of C_L. In particular, V_∞ will be the smallest when C_L is a maximum. Hence, the stalling velocity for a given airplane is determined by $C_{L,\max}$ from Equation (1.46)

$$V_{\text{stall}} = \sqrt{\frac{2W}{\rho_\infty S C_{L,\max}}} \tag{1.47}$$

For a given airplane, without the aid of any artificial devices, $C_{L,\max}$ is determined purely by nature, through the physical laws for the aerodynamic flowfield over the airplane. However, the airplane designer has some devices available that artificially increase $C_{L,\max}$ beyond that for the basic airplane shape. These mechanical devices are called *high-lift devices;* examples are flaps, slats, and slots on the wing which, when deployed by the pilot, serve to increase $C_{L,\max}$, and hence decrease the stalling speed. High-lift devices are usually deployed for landing and take-off; they are discussed in more detail in Section 4.12.

On the other extreme of flight velocity, the maximum velocity for a given airplane with a given maximum thrust from the engine is determined by the value of minimum drag coefficient, $C_{D,\min}$, where $C_{D,\min}$ is marked in Figure 1.32. From the definition of drag coefficient in Section 1.5, applied for the case of steady, level flight where $T = D$, we have

$$C_D = \frac{D}{q_\infty S} = \frac{T}{q_\infty S} = \frac{2T}{\rho_\infty V_\infty^2 S} \tag{1.48}$$

Solving Equation (1.48) for V_∞,

$$V_\infty = \sqrt{\frac{2T}{\rho_\infty S C_D}} \tag{1.49}$$

For a given airplane flying at maximum thrust $T_{\max}$ and a given altitude, from Equation (1.49) the maximum value of V_∞ corresponds to flight at $C_{D,\min}$

$$V_{\max} = \sqrt{\frac{2T_{\max}}{\rho_\infty S C_{D,\min}}} \tag{1.50}$$

From the above discussion, it is clear that the aerodynamic *coefficients* are important engineering

[6] The lowest velocity may instead be dictated by the power required to maintain level flight exceeding the power available from the powerplant. This occurs on the "back side of the power curve." The velocity at which this occurs is usually less than the stalling velocity, so is of academic interest only. See Anderson, *Aircraft Performance and Design,* McGraw-Hill, 1999, for more details.

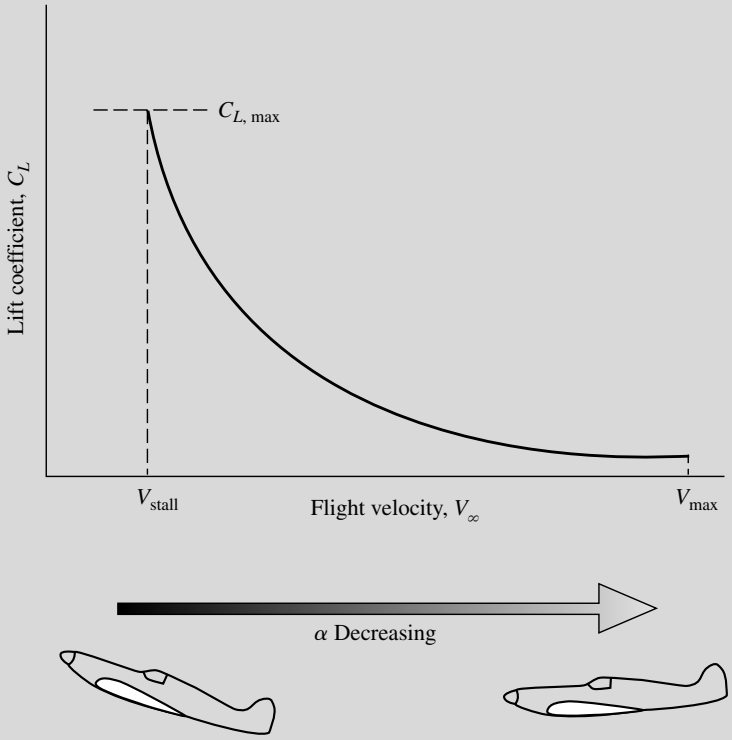

Figure 1.33 Schematic of the variation of lift coefficient with flight velocity for level flight.

quantities that dictate the performance and design of airplanes. For example, stalling velocity is determined in part by $C_{L,\max}$, and maximum velocity is determined in part by $C_{D,\min}$.

Broadening our discussion to the whole range of flight velocity for a given airplane, note from Equation (1.45) that each value of V_∞ corresponds to a specific value of C_L. Therefore, over the whole range of flight velocity from V_{stall} to $V_{\max}$, the airplane lift coefficient varies as shown generically in Figure 1.33. The values of C_L given by the curve in Figure 1.33 are *what are needed* to maintain level flight over the whole range of velocity at a given altitude. The airplane designer must design the airplane to *achieve* these values of C_L for an airplane of given weight and wing area. Note that the required values of C_L decrease as V_∞ increases. Examining the lift coefficient variation with angle of attack shown in Figure 1.33, note that as the airplane flies faster, the angle of attack must be smaller, as also shown in Figure 1.33. Hence, at high speeds, airplanes are at low α, and at low speeds, airplanes are at high α; the specific angle of attack which the airplane must have at a specific V_∞ is dictated by the specific value of C_L required at that velocity.

Obtaining raw lift on a body is relatively easy—even a barn door creates lift at angle of attack. The name of the game is to obtain the necessary lift with as *low* a drag as possible. That is, the values of C_L required over the entire flight range for an airplane, as represented by Figure 1.33, can sometimes be obtained even for the least effective lifting shape—just make the angle of attack high enough. But C_D also varies with V_∞, as governed by Equation (1.48); the generic variation of C_D with V_∞ is sketched in Figure 1.34. A poor aerodynamic shape, even though it generates the necessary values of C_L shown in Figure 1.33, will have inordinately high values of C_D (i.e., the C_D curve in Figure 1.34 will ride high on the

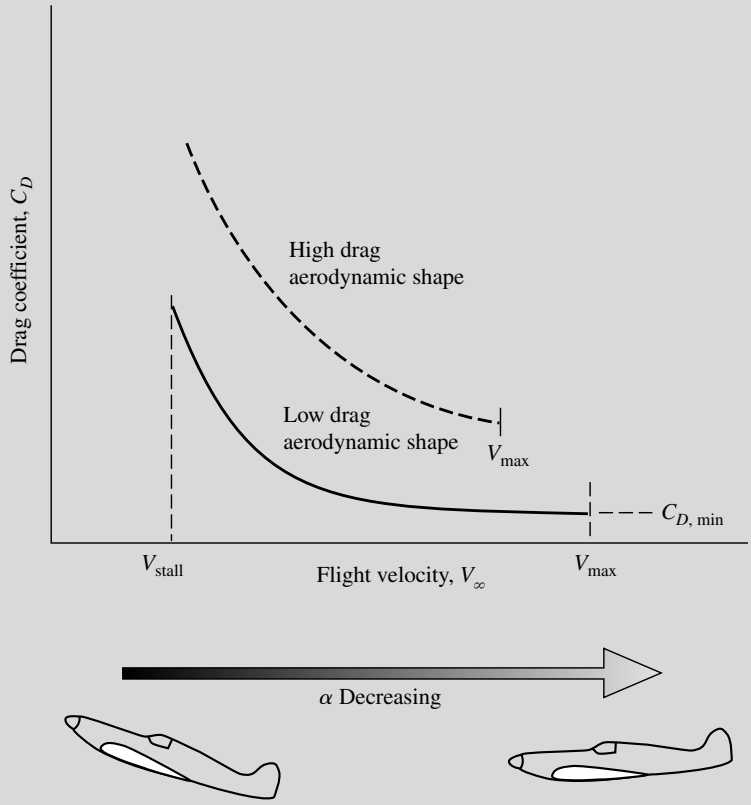

Figure 1.34 Schematic of the variation of drag coefficient with flight velocity for level flight. Comparison between high and low drag aerodynamic bodies, with the consequent effect on maximum velocity.

graph), as denoted by the dashed curve in Figure 1.34. An aerodynamically efficient shape, however, will produce the requisite values of C_L prescribed by Figure 1.33 with much lower drag, as denoted by the solid curve in Figure 1.34. An undesirable by-product of the high-drag shape is a lower value of the maximum velocity for the same maximum thrust, as also indicated in Figure 1.34.

Finally, we emphasize that a true measure of the aerodynamic efficiency of a body shape is its *lift-to-drag ratio,* given by

$$\frac{L}{D} = \frac{q_\infty S C_L}{q_\infty S C_D} = \frac{C_L}{C_D} \tag{1.51}$$

Since the value of C_L necessary for flight at a given velocity and altitude is determined by the airplane's weight and wing area (actually, by the *ratio* of W/S, called the *wing loading*) through the relationship given by Equation (1.45), the value of L/D at this velocity is controlled by C_D, the denominator in Equation (1.51). At any given velocity, we want L/D to be as high as possible; the higher is L/D, the more aerodynamically efficient is the body. For a given airplane at a given altitude, the variation of L/D as a function of velocity is sketched generically in Figure 1.35. Note that, as V_∞ increases from a low value, L/D first increases, reaches a maximum at some intermediate velocity, and then decreases. Note that, as V_∞ increases, the angle of attack of the airplane decreases, as explained earlier. From a strictly aerodynamic consideration, L/D for a given body shape depends on angle of attack. This can be seen from Figure 1.32,

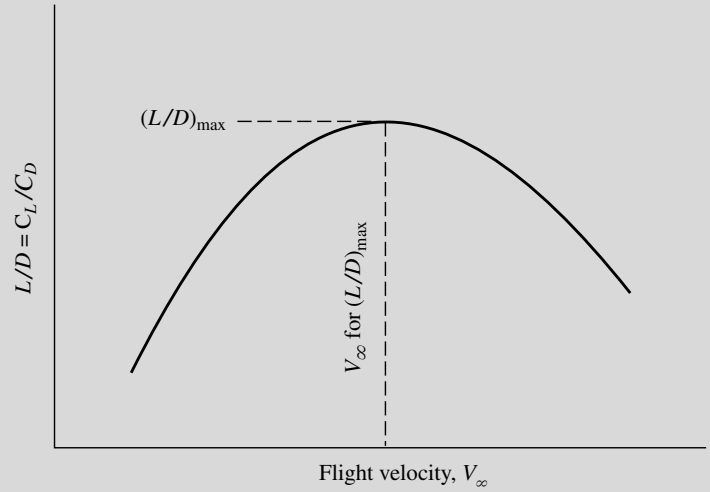

Figure 1.35 Schematic of the variation of lift-to-drag ratio with flight velocity for level flight.

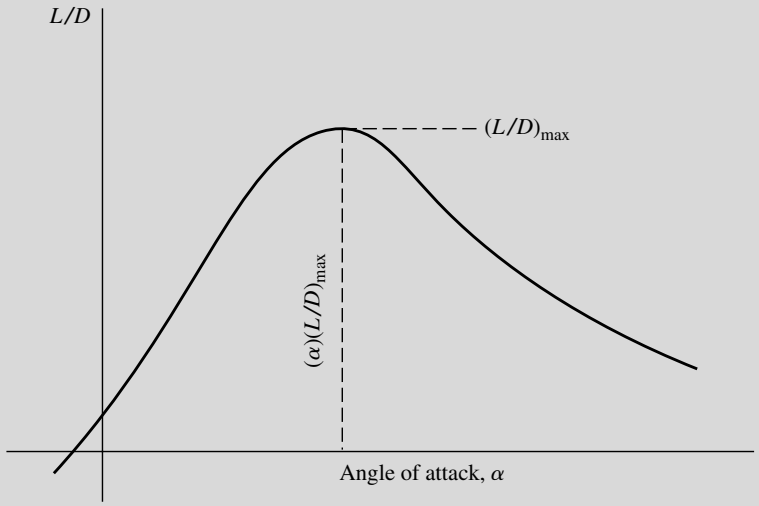

Figure 1.36 Schematic of the variation of lift-to-drag ratio with angle of attack.

where C_L and C_D are given as a function of α. If these two curves are ratioed, the result is L/D as a function of angle of attack, as sketched generically in Figure 1.36. The relationship of Figure 1.35 to Figure 1.36 is that, when the airplane is flying at the velocity that corresponds to $(L/D)_{max}$ as shown in Figure 1.35, it *is* at the angle of attack for $(L/D)_{max}$ as shown in Figure 1.36.

In summary, the purpose of this design box is to emphasize the important role played by the aerodynamic *coefficients* in the performance analysis and design of airplanes. In this discussion, what has

been important is not the lift and drag per se, but rather C_L and C_D. These coefficients are a wonderful intellectual construct that helps us to better understand the aerodynamic characteristics of a body, and to make reasoned, intelligent calculations. Hence they are more than just conveniently defined quantities as might first appear when introduced in Section 1.5.

For more insight to the engineering value of these coefficients, see Anderson, *Aircraft Performance and Design,* McGraw-Hill, 1999, and Anderson, *Introduction to Flight,* 6th edition, McGraw-Hill, 2008. Also, homework problem 1.15 at the end of this chapter gives you the opportunity to construct specific curves for C_L, C_D, and L/D versus velocity for an actual airplane so that you can obtain a feel for some real numbers that have been only generically indicated in the figures here. (In our present discussion, the use of generic figures has been intentional for pedagogic reasons.) Finally, an historical note on the origins of the use of aerodynamic coefficients is given in Section 1.14.

EXAMPLE 1.7

Consider an executive jet transport patterned after the Cessna 560 Citation V shown in three-view in Figure 1.37. The airplane is cruising at a velocity of 492 mph at an altitude of 33,000 ft, where the ambient air density is 7.9656×10^{-4} slug/ft^3. The weight and wing planform areas of the airplane are 15,000 lb and 342.6 ft^2, respectively. The drag coefficient at cruise is 0.015. Calculate the lift coefficient and the lift-to-drag ratio at cruise.

■ Solution

The units of miles per hour for velocity are not consistent units. In the English engineering system of units, feet per second are consistent units for velocity (see Section 2.4 of Reference 2). To convert between mph and ft/s, it is useful to remember that 88 ft/s = 60 mph.

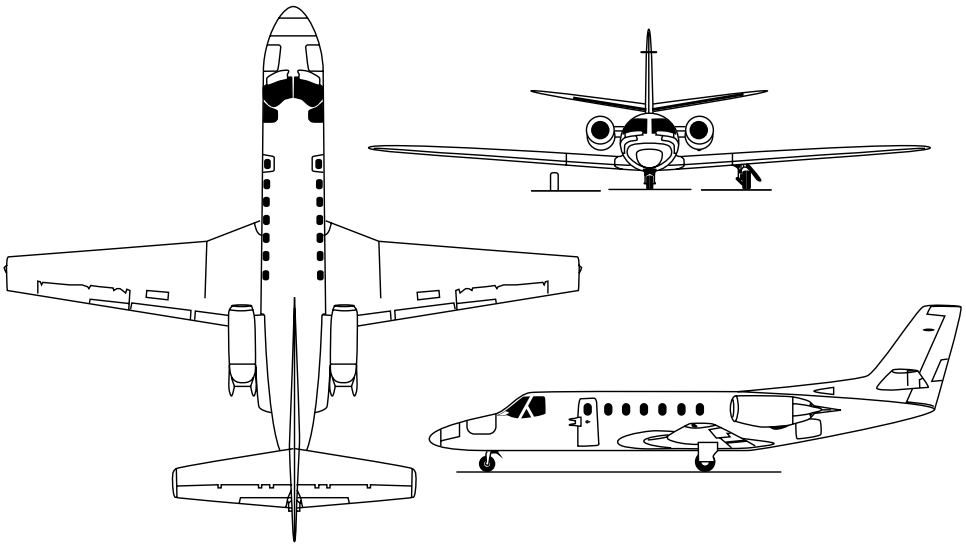

Figure 1.37 Cessna 560 Citation V.

For the present example,

$$V_\infty = 492\left(\tfrac{88}{60}\right) = 721.6 \text{ ft/s}$$

From Equation (1.45),

$$C_L = \frac{2W}{\rho_\infty V_\infty^2 S} = \frac{2(15{,}000)}{(7.9659 \times 10^{-4})(721.6)^2(342.6)} = \boxed{0.21}$$

From Equation (1.51),

$$\frac{L}{D} = \frac{C_L}{C_D} = \frac{0.21}{0.015} = \boxed{14}$$

Remarks: For a conventional airplane such as shown in Figure 1.37, almost all the lift at cruising conditions is produced by the wing; the lift of the fuselage and tail are very small by comparison. Hence, the wing can be viewed as an aerodynamic "lever." In this example, the lift-to-drag ratio is 14, which means that for the expenditure of one pound of thrust to overcome one pound of drag, the wing is lifting 14 pounds of weight—quite a nice leverage.

EXAMPLE 1.8

The same airplane as described in Example 1.7 has a stalling speed at sea level of 100 mph at the maximum take-off weight of 15,900 lb. The ambient air density at standard sea level is 0.002377 slug/ft^3. Calculate the value of the maximum lift coefficient for the airplane.

■ Solution

Once again we have to use consistent units, so

$$V_{\text{stall}} = 100\tfrac{88}{60} = 146.7 \text{ ft/s}$$

Solving Equation (1.47) for $C_{L,\max}$, we have

$$C_{L,\max} = \frac{2W}{\rho_\infty V_{\text{stall}}^2 S} = \frac{2(15{,}900)}{(0.002377)(146.7)^2(342.6)} = \boxed{1.81}$$

1.9 FLUID STATICS: BUOYANCY FORCE

In aerodynamics, we are concerned about fluids in motion, and the resulting forces and moments on bodies due to such motion. However, in this section, we consider the special case of *no* fluid motion (i.e., *fluid statics*). A body immersed in a fluid will still experience a force even if there is no relative motion between the body and the fluid. Let us see why.

To begin, we must first consider the force on an element of fluid itself. Consider a stagnant fluid above the xz plane, as shown in Figure 1.38. The vertical direction is given by y. Consider an infinitesimally small fluid element with sides of length dx, dy, and dz. There are two types of forces acting on this fluid element: pressure forces from the surrounding fluid exerted on the surface of the

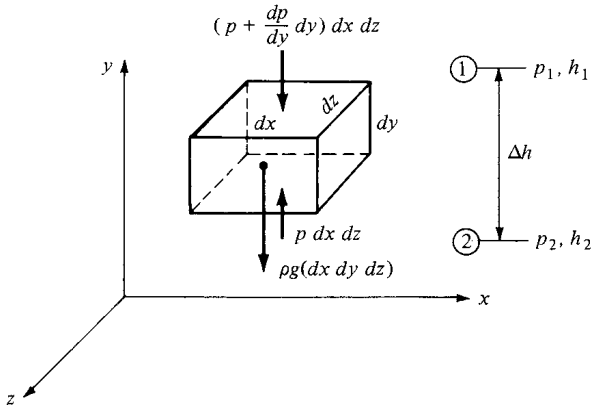

Figure 1.38 Forces on a fluid element in a stagnant fluid.

element, and the gravity force due to the weight of the fluid inside the element. Consider forces in the y direction. The pressure on the bottom surface of the element is p, and hence the force on the bottom face is $p(dx\,dz)$ in the upward direction, as shown in Figure 1.38. The pressure on the top surface of the element will be slightly different from the pressure on the bottom because the top surface is at a different location in the fluid. Let dp/dy denote the rate of change of p with respect to y. Then the pressure exerted on the top surface will be $p + (dp/dy)\,dy$, and the pressure force on the top of the element will be $[p + (dp/dy)\,dy](dx\,dz)$ in the downward direction, as shown in Figure 1.38. Hence, letting upward force be positive, we have

$$\text{Net pressure force} = p(dx\,dz) - \left(p + \frac{dp}{dy}dy\right)(dx\,dz)$$

$$= -\frac{dp}{dy}(dx\,dy\,dz)$$

Let ρ be the mean density of the fluid element. The total mass of the element is $\rho(dx\,dy\,dz)$. Therefore,

$$\text{Gravity force} = -\rho(dx\,dy\,dz)g$$

where g is the acceleration of gravity. Since the fluid element is stationary (in equilibrium), the sum of the forces exerted on it must be zero:

$$-\frac{dp}{dy}(dx\,dy\,dz) - g\rho(dx\,dy\,dz) = 0$$

or

$$\boxed{dp = -g\rho\,dy} \tag{1.52}$$

Equation (1.52) is called the *Hydrostatic equation;* it is a differential equation which relates the change in pressure dp in a fluid with a change in vertical height dy.

The net force on the element acts only in the vertical direction. The pressure forces on the front and back faces are equal and opposite and hence cancel; the same is true for the left and right faces. Also, the pressure forces shown in Figure 1.38 act at the center of the top and bottom faces, and the center of gravity is at the center of the elemental volume (assuming the fluid is homogeneous); hence, the forces in Figure 1.38 are colinear, and as a result, there is no moment on the element.

Equation (1.52) governs the variation of atmospheric properties as a function of altitude in the air above us. It is also used to estimate the properties of other planetary atmospheres such as for Venus, Mars, and Jupiter. The use of Equation (1.52) in the analysis and calculation of the "standard atmosphere" is given in detail in Reference 2; hence the details will not be repeated here. Appendices D and E, however, contain a tabulation of the properties of the 1959 ARDC model atmosphere for earth as compiled by the U.S. Air Force. These standard atmosphere tables are included in this book for use in solving certain worked examples and some end-of-chapter homework problems. Moreover, Example 1.10 at the end of this section illustrates how the Hydrostatic equation is used to obtain some of the entries in Appendices D and E.

Let the fluid be a liquid, for which we can assume ρ is constant. Consider points 1 and 2 separated by the vertical distance Δh as sketched on the right side of Figure 1.38. The pressure and y locations at these points are p_1, h_1, and p_2, h_2, respectively. Integrating Equation (1.52) between points 1 and 2, we have

$$\int_{p_1}^{p_2} dp = -\rho g \int_{h_1}^{h_2} dy$$

or

$$p_2 - p_1 = -\rho g(h_2 - h_1) = \rho g\, \Delta h \tag{1.53}$$

where $\Delta h = h_1 - h_2$. Equation (1.53) can be more conveniently expressed as

$$p_2 + \rho g h_2 = p_1 + \rho g h_1$$

or

$$\boxed{p + \rho g h = \text{constant}} \tag{1.54}$$

Note that in Equations (1.53) and (1.54), increasing values of h are in the positive (upward) y direction.

A simple application of Equation (1.54) is the calculation of the pressure distribution on the walls of a container holding a liquid, and open to the atmosphere at the top. This is illustrated in Figure 1.39, where the top of the liquid is at a height h_1. The atmospheric pressure p_a is impressed on the top of the liquid; hence, the pressure at h_1 is simply p_a. Applying Equation (1.54) between the top (where $h = h_1$) and an arbitrary height h, we have

$$p + \rho g h = p_1 + \rho g h_1 = p_a + \rho g h_1$$

or

$$p = p_a + \rho g(h_1 - h) \tag{1.55}$$

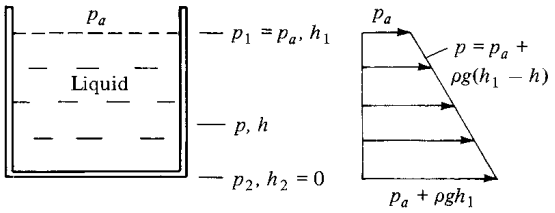

Figure 1.39 Hydrostatic pressure distribution on the walls of a container.

Equation (1.55) gives the pressure distribution on the vertical sidewall of the container as a function of h. Note that the pressure is a *linear* function of h as sketched on the right of Figure 1.39, and that p increases with depth below the surface.

Another simple and very common application of Equation (1.54) is the liquid-filled U-tube manometer used for measuring pressure differences, as sketched in Figure 1.40. The manometer is usually made from hollow glass tubing bent in the shape of the letter U. Imagine that we have an aerodynamic body immersed in an airflow (such as in a wind tunnel), and we wish to use a manometer to measure the surface pressure at point b on the body. A small pressure orifice (hole) at point b is connected to one side of the manometer via a long (usually flexible) pressure tube. The other side of the manometer is open to the atmosphere, where the pressure p_a is a known value. The U tube is partially filled with a liquid of known density ρ. The tops of the liquid on the left and right sides of the U tube are at points 1 and 2, with heights h_1 and h_2, respectively. The body surface pressure p_b is transmitted through the pressure tube and impressed on the top of the liquid at point 1. The atmospheric pressure p_a is impressed on the top of the liquid at point 2. Because in general $p_b \neq p_a$, the tops of the liquid will be at different heights; (i.e., the two sides of the manometer will show a displacement $\Delta h = h_1 - h_2$ of the fluid). We wish to obtain the value of the surface pressure

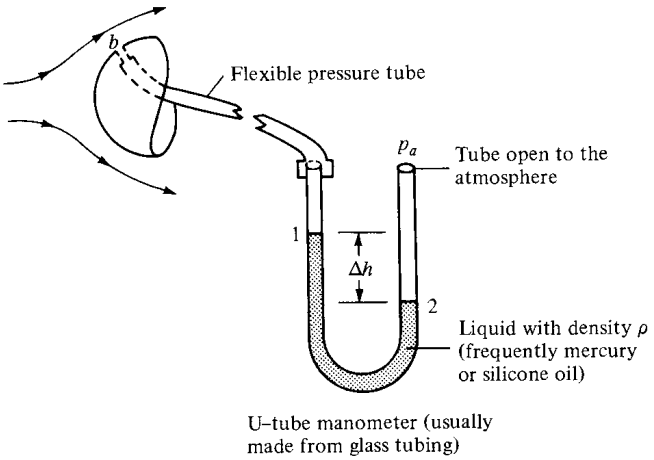

Figure 1.40 The use of a U-tube manometer.

at point b on the body by reading the value of Δh from the manometer. From Equation (1.54) applied between points 1 and 2,

$$p_b + \rho g h_1 = p_a + \rho g h_2$$

or

$$p_b = p_a - \rho g(h_1 - h_2)$$

or

$$p_b = p_a - \rho g\, \Delta h \tag{1.56}$$

In Equation (1.56), p_a, ρ, and g are known, and Δh is read from the U tube, thus allowing p_b to be measured.

At the beginning of this section, we stated that a solid body immersed in a fluid will experience a force even if there is no relative motion between the body and the fluid. We are now in a position to derive an expression for this force, henceforth called the *buoyancy force*. We will consider a body immersed in either a stagnant gas or liquid, hence ρ can be a variable. For simplicity, consider a rectangular body of unit width, length l, and height $(h_1 - h_2)$, as shown in Figure 1.41. Examining Figure 1.41, we see that the vertical force F on the body due to the pressure distribution over the surface is

$$F = (p_2 - p_1)l(1) \tag{1.57}$$

There is no horizontal force because the pressure distributions over the vertical faces of the rectangular body lead to equal and opposite forces which cancel each other. In Equation (1.57), an expression for $p_2 - p_1$ can be obtained by integrating the hydrostatic equation, Equation (1.52), between the top and bottom faces:

$$p_2 - p_1 = \int_{p_1}^{p_2} dp = -\int_{h_1}^{h_2} \rho g\, dy = \int_{h_2}^{h_1} \rho g\, dy$$

Substituting this result into Equation (1.57), we obtain for the buoyancy force

$$F = l(1) \int_{h_2}^{h_1} \rho g\, dy \tag{1.58}$$

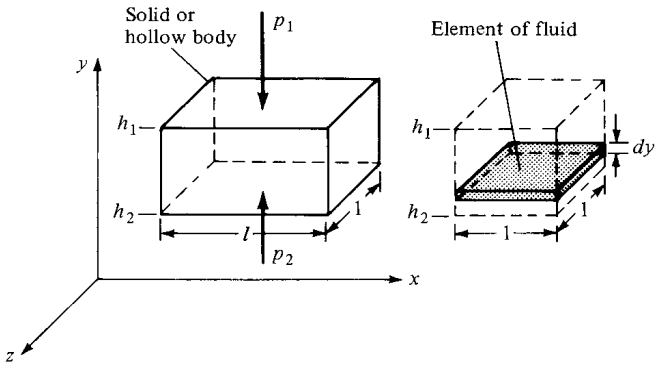

Figure 1.41 Source of the buoyancy force on a body immersed in a fluid.

Consider the physical meaning of the integral in Equation (1.58). The weight of a small element of fluid of height dy and width and length of unity as shown at the right of Figure 1.41 is $\rho g\, dy$ (1)(1). In turn, the weight of a column of fluid with a base of unit area and a height $(h_1 - h_2)$ is

$$\int_{h_2}^{h_1} \rho g\, dy$$

which is precisely the integral in Equation (1.58). Moreover, if we place l of these fluid columns side by side, we would have a volume of fluid equal to the volume of the body on the left of Figure 1.41, and the *weight* of this total volume of *fluid* would be

$$l \int_{h_2}^{h_1} \rho g\, dy$$

which is precisely the right-hand side of Equation (1.58). Therefore, Equation (1.58) states in words that

Buoyancy force on body	=	weight of fluid displaced by body

We have just proved the well-known *Archimedes principle,* first advanced by the Greek scientist, Archimedes of Syracuse (287–212 B.C.). Although we have used a rectangular body to simplify our derivation, the Archimedes principle holds for bodies of any general shape. (See Problem 1.14 at the end of this chapter.) Also, note from our derivation that the Archimedes principle holds for both gases and liquids and does not require that the density be constant.

The density of liquids is usually several orders of magnitude larger than the density of gases (e.g., for water $\rho = 10^3$ kg/m^3, whereas for air $\rho = 1.23$ kg/m^3). Therefore, a given body will experience a buoyancy force a thousand times greater in water than in air. Obviously, for naval vehicles buoyancy force is all important, whereas for airplanes it is negligible. On the other hand, lighter-than-air vehicles, such as blimps and hot-air balloons, rely on buoyancy force for sustenation; they obtain sufficient buoyancy force simply by displacing huge volumes of air. For most problems in aerodynamics, however, buoyancy force is so small that it can be readily neglected.

EXAMPLE 1.9

A hot-air balloon with an inflated diameter of 30 ft is carrying a weight of 800 lb, which includes the weight of the hot air inside the balloon. Calculate (a) its upward acceleration at sea level the instant the restraining ropes are released and (b) the maximum altitude it can achieve. Assume that the variation of density in the standard atmosphere is given by $\rho = 0.002377(1 - 7 \times 10^{-6}h)^{4.21}$, where h is the altitude in feet and ρ is in slug/ft^3.

■ Solution

(a) At sea level, where $h = 0$, $\rho = 0.002377$ slug/ft^3. The volume of the inflated balloon is $\frac{4}{3}\pi(15)^3 = 14{,}137$ ft^3. Hence,

$$\text{Buoyancy force} = \text{weight of displaced air}$$

$$= g\rho\mathcal{V}$$

where g is the acceleration of gravity and $\mathcal{V}$ is the volume.

$$\text{Buoyancy force} \equiv B = (32.2)(0.002377)(14{,}137) = 1082 \text{ lb}$$

The net upward force at sea level is $F = B - W$, where W is the weight. From Newton's second law,

$$F = B - W = ma$$

where m is the mass, $m = \frac{800}{32.2} = 24.8$ slug. Hence,

$$a = \frac{B - W}{m} = \frac{1082 - 800}{24.8} = \boxed{11.4 \text{ ft/s}^2}$$

(b) The maximum altitude occurs when $B = W = 800$ lb. Since $B = g\rho\mathcal{V}$, and assuming the balloon volume does not change,

$$\rho = \frac{B}{g\mathcal{V}} = \frac{800}{(32.2)(14{,}137)} = 0.00176 \text{ slug/ft}^3$$

From the given variation of ρ with altitude, h,

$$\rho = 0.002377(1 - 7 \times 10^{-6}h)^{4.21} = 0.00176$$

Solving for h, we obtain

$$h = \frac{1}{7 \times 10^{-6}}\left[1 - \left(\frac{0.00176}{0.002377}\right)^{1/4.21}\right] = \boxed{9842 \text{ ft}}$$

EXAMPLE 1.10

The purpose of this example is to show how the standard altitude tables in Appendices D and E are constructed with the use of the Hydrostatic equation. A complete discussion on the construction and use of the standard altitude tables is given in Chapter 3 of Ref. 2.

From sea level to an altitude of 11 km, the standard altitude is based on a linear variation of temperature with altitude, h, where T decreases at a rate of -6.5 K per kilometer (the lapse rate). At sea level, the standard pressure, density, and temperature are 1.01325×10^5 N/m^2, 1.2250 kg/m^3, and 288.16 K, respectively. Calculate the pressure, density, and temperature at a standard altitude of 5 km.

■ Solution

Repeating Eq. (1.52),

$$dp = -g\rho\, dy = -g\rho\, dh$$

The equation of state for a perfect gas is given in Chapter 7 as Eq. (7.1),

$$p = \rho RT$$

where R is the specific gas constant. Dividing Eq. (1.52) by (7.1), we have

$$\frac{dp}{p} = -\frac{g}{R}\frac{dh}{T} \tag{E1.1}$$

Denoting the lapse rate by a, we have by definition

$$a \equiv \frac{dT}{dh}$$

or

$$dh = \frac{dT}{a} \tag{E1.2}$$

Substituting (E1.2) into (E1.1), we obtain

$$\frac{dp}{p} = -\frac{g}{aR}\frac{dT}{T} \tag{E1.3}$$

Integrate Eq. (E1.3) from sea level where the standard values of pressure and temperature are denoted by p_s and T_s, respectively, and a given altitude h where the values of pressure and temperature are p and T, respectively.

$$\int_{p_s}^{p} \frac{dp}{p} = -\int_{T_s}^{T} \frac{g}{aR}\frac{dT}{T}$$

or

$$ln\,\frac{P}{p_s} = -\int_{T_s}^{T} \frac{g}{aR}\frac{dT}{T} \tag{E1.4}$$

In Eq. (E1.4), a and R are constants, but the acceleration of gravity, g, varies with altitude. The integral in Eq. (E1.4) is simplified by assuming that g is constant with altitude, equal to its value at sea level, g_s. With this assumption, Eq. (E1.4) becomes

$$ln\,\frac{P}{p_s} = -\frac{g_s}{aR}\,ln\,\frac{T}{T_s}$$

or

$$\frac{p}{p_s} = \left(\frac{T}{T_s}\right)^{-g_s/aR} \tag{E1.5}$$

Note: Here we must make a distinction between the geometric altitude, h_G, which is the actual "tape measure" altitude above sea level, and the geopotential altitude, h, which is a slightly fictitious altitude consistent with the assumption of a constant value of g. That is, when we write the Hydrostatic equation as

$$dp = -g\rho\, dh_G$$

we are treating g as a variable with altitude and hence the altitude is the actual geometric altitude, h_G. On the other hand, when we assume that g is constant, say equal to its value

at sea level, g_s, the Hydrostatic equation is

$$p = -g_s \rho \, dh \tag{E1.6}$$

where h is denoted as the geopotential altitude, consistent with the assumption of constant g. For reasonable altitudes associated with conventional atmospheric flight, the difference between h_G and h is very small. Observe from Appendix D that altitude is listed under two columns, the first being the geometric altitude, h_G, and the second being the geopotential altitude, h. For the current example we are calculating the properties at an altitude of 5 km. This is the real "tape measure" altitude, h_G. The corresponding value of geopotential altitude, h, is 4.996 km, only a 0.08 percent difference. The calculation of h for a given h_G is derived in Reference 2; it is not important to our discussions here. What is important, however, is that when we use Eq. (E1.5), or any other such equation assuming a constant value of g, we must use the geopotential altitude. For the calculations in this example, where we are calculating properties at a geometric altitude of 5 km, we must use the value of the geopotential altitude, 4.996 km, in the equations.

Eq. (E1.5) explicitly gives the variation of pressure with temperature, and implicitly the variation with altitude because temperature is a known function of altitude via the given lapse rate $a = dT/dh = -6.5 \; K/km$. Specifically, because T varies linearly with altitude for the altitude region under consideration here, we have

$$T - T_s = ah \tag{E1.7}$$

In Eq. (E1.7), h is the geopotential altitude. The given value of $a = -6.5$ K/km $= -0.0065$/m is based on the change in geopotential altitude. Thus, from Eq. (E1.7), we have at the specified geometric altitude of 5 km,

$$T - 288.16 = -(0.0065)(4996) = -32.474$$

$$T = 288.16 - 32.474 = \boxed{255.69 \text{ K}}$$

Note that this value of T is precisely the value entered in Appendix D for a geometric altitude of 5000 m.

In Eq. (E1.5), for air, $R = 287$ J/kg K.
Thus, the exponent is

$$\frac{-g_s}{aR} = -\frac{(9.80)}{(-0.0065)(287)} = 5.25328$$

and

$$\frac{p}{p_s} = \left(\frac{T}{T_s}\right)^{-g_s/aR} = \left(\frac{255.69}{288.16}\right)^{5.25328} = 0.53364$$

$$p = 0.53364 p_s = 0.53364(1.01325 \times 10^5)$$

$$p = \boxed{5.407 \times 10^4 \text{ N/m}^2}$$

This value of pressure agrees within 0.04 percent with the value entered in Appendix D. The very slight difference is due to the value of $R = 287$ J/(kg)(K) used here, which

depends on the molecular weight of air, which in turn varies slightly from one source to another.

Finally, the density can be obtained from the equation of state

$$\rho = \frac{p}{RT} = \frac{5.407 \times 10^4}{(287)(255.69)} = \boxed{0.7368 \text{ kg/m}^3}$$

which agrees within 0.05 percent with the value entered in Appendix D.

EXAMPLE 1.11

Consider a U-tube mercury manometer oriented vertically. One end is completely sealed with a total vacuum above the column of mercury. The other end is open to the atmosphere where the atmospheric pressure is that for standard sea level. What is the displacement height of the mercury in centimeters, and in which end is the mercury column the highest? The density of mercury is 1.36×10^4 kg/m^3.

■ Solution

Examining Fig. 1.40, consider the sealed end with the total vacuum to be on the left, where $p_b = 0$, and the height of the mercury column is h_1. This is balanced by the right column of mercury with height h_2 plus the atmospheric pressure p_a exerted on the top of the column. Clearly, when these two columns of mercury are balanced, the left column must be higher to account for the finite pressure being exerted at the top of the right column, i.e., $h_1 > h_2$. From Eq. (1.56), we have

$$p_b = p_a - \rho g \, \Delta h$$

where

$$\Delta h = h_1 - h_2$$

Thus,

$$\Delta h = \frac{p_a}{\rho g}$$

From Appendix D, at sea level $p_a = 1.013 \times 10^5$ N/m^2. Hence,

$$\Delta h = \frac{p_a}{\rho g} = \frac{1.013 \times 10^5}{\left(1.36 \times 10^4\right)(9.8)} = 0.76 \text{ m} = \boxed{76 \text{ cm}}$$

Note: Since 2.54 cm = 1 inch, then $\Delta h = 76/2.54 = 29.92$ in. The above calculation explains why, on a day when the atmospheric pressure happens to be that for standard sea level, the meteorologist on television will usually say that the pressure is now "76 cm, or 760 mm, or 29.92 in." You rarely hear the pressure quoted in terms of "pounds per square foot", or "pounds per square inch," and hardly ever in "newtons per square meter."

1.10 TYPES OF FLOW

An understanding of aerodynamics, like that of any other physical science, is obtained through a "building-block" approach—we dissect the discipline, form the parts into nice polished blocks of knowledge, and then later attempt to reassemble the blocks to form an understanding of the whole. An example of this process is the way that different types of aerodynamic flows are categorized and visualized. Although nature has no trouble setting up the most detailed and complex flow with a whole spectrum of interacting physical phenomena, we must attempt to understand such flows by modeling them with less detail, and neglecting some of the (hopefully) less significant phenomena. As a result, a study of aerodynamics has evolved into a study of numerous and distinct types of flow. The purpose of this section is to itemize and contrast these types of flow, and to briefly describe their most important physical phenomena.

1.10.1 Continuum Versus Free Molecule Flow

Consider the flow over a body, say, for example, a circular cylinder of diameter d. Also, consider the fluid to consist of individual molecules, which are moving about in random motion. The mean distance that a molecule travels between collisions with neighboring molecules is defined as the *mean-free path* λ. If λ is orders of magnitude smaller than the scale of the body measured by d, then the flow appears to the body as a continuous substance. The molecules impact the body surface so frequently that the body cannot distinguish the individual molecular collisions, and the surface feels the fluid as a continuous medium. Such flow is called *continuum flow*. The other extreme is where λ is on the same order as the body scale; here the gas molecules are spaced so far apart (relative to d) that collisions with the body surface occur only infrequently, and the body surface can feel distinctly each molecular impact. Such flow is called *free molecular flow*. For manned flight, vehicles such as the space shuttle encounter free molecular flow at the extreme outer edge of the atmosphere, where the air density is so low that λ becomes on the order of the shuttle size. There are intermediate cases, where flows can exhibit some characteristics of both continuum and free molecule flows; such flows are generally labeled "low-density flows" in contrast to continuum flow. By far, the vast majority of practical aerodynamic applications involve continuum flows. Low-density and free molecule flows are just a small part of the total spectrum of aerodynamics. Therefore, in this book we will always deal with continuum flow; that is, we will always treat the fluid as a continuous medium.

1.10.2 Inviscid Versus Viscous Flow

A major facet of a gas or liquid is the ability of the molecules to move rather freely, as explained in Section 1.2. When the molecules move, even in a very random fashion, they obviously transport their mass, momentum, and energy from one location to another in the fluid. This transport on a molecular scale gives rise to the phenomena of mass diffusion, viscosity (friction), and thermal conduction.

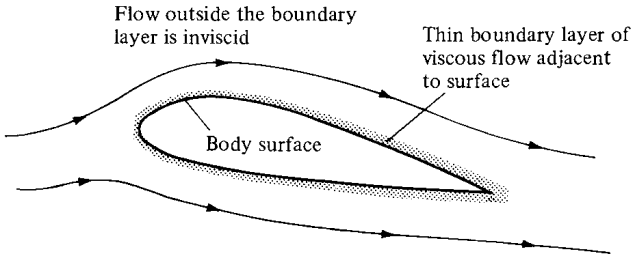

Figure 1.42 The division of a flow into two regions: (1) the thin viscous boundary layer adjacent to the body surface and (2) the inviscid flow outside the boundary layer.

Such "transport phenomena" will be discussed in detail in Chapter 15. For our purposes here, we need only to recognize that all real flows exhibit the effects of these transport phenomena; such flows are called *viscous flows*. In contrast, a flow that is assumed to involve no friction, thermal conduction, or diffusion is called an *inviscid flow*. Inviscid flows do not truly exist in nature; however, there are many practical aerodynamic flows (more than you would think) where the influence of transport phenomena is small, and we can *model* the flow as being inviscid. For this reason, more than 70 percent of this book (Chapters 3 to 14) deals primarily with inviscid flows.

Theoretically, inviscid flow is approached in the limit as the Reynolds number goes to infinity (to be proved in Chapter 15). However, for practical problems, many flows with high but finite Re can be assumed to be inviscid. For such flows, the influence of friction, thermal conduction, and diffusion is limited to a very thin region adjacent to the body surface called the boundary layer, and the remainder of the flow outside this thin region is essentially inviscid. This division of the flow into two regions is illustrated in Figure 1.42. Hence, most of the material discussed in Chapters 3 to 14 applies to the flow outside the boundary layer. For flows over slender bodies, such as the airfoil sketched in Figure 1.42, inviscid theory adequately predicts the pressure distribution and lift on the body and gives a valid representation of the streamlines and flow field away from the body. However, because friction (shear stress) is a major source of aerodynamic drag, inviscid theories by themselves cannot adequately predict total drag.

In contrast, there are some flows that are dominated by viscous effects. For example, if the airfoil in Figure 1.42 is inclined to a high incidence angle to the flow (high angle of attack), then the boundary layer will tend to separate from the top surface, and a large wake is formed downstream. The separated flow is sketched at the top of Figure 1.43; it is characteristic of the flow field over a "stalled" airfoil. Separated flow also dominates the aerodynamics of blunt bodies, such as the cylinder at the bottom of Figure 1.43. Here, the flow expands around the front face of the cylinder, but separates from the surface on the rear face, forming a rather fat wake downstream. The types of flow illustrated in Figure 1.43 are dominated by viscous effects; no inviscid theory can independently predict the

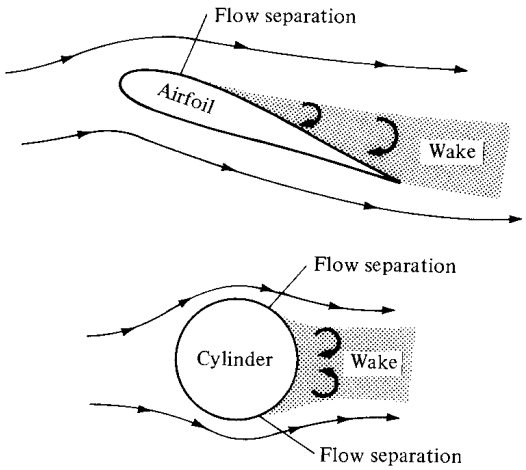

Figure 1.43 Examples of viscous-dominated flow.

aerodynamics of such flows. They require the inclusion of viscous effects, to be presented in Part 4.

1.10.3 Incompressible Versus Compressible Flows

A flow in which the density ρ is constant is called *incompressible*. In contrast, a flow where the density is variable is called *compressible*. A more precise definition of compressibility will be given in Chapter 7. For our purposes here, we will simply note that all flows, to a greater or lesser extent, are compressible; truly incompressible flow, where the density is precisely constant, does not occur in nature. However, analogous to our discussion of inviscid flow, there are a number of aerodynamic problems that can be modeled as being incompressible without any detrimental loss of accuracy. For example, the flow of homogeneous liquids is treated as incompressible, and hence most problems involving hydrodynamics assume $\rho =$ constant. Also, the flow of gases at a low Mach number is essentially incompressible; for $M < 0.3$, it is always safe to assume $\rho =$ constant. (We will prove this in Chapter 8.) This was the flight regime of all airplanes from the Wright brothers' first flight in 1903 to just prior to World War II. It is still the flight regime of most small, general aviation aircraft of today. Hence, there exists a large bulk of aerodynamic experimental and theoretical data for incompressible flows. Such flows are the subject of Chapters 3 to 6. On the other hand, high-speed flow (near Mach 1 and above) must be treated as compressible; for such flows ρ can vary over wide latitudes. Compressible flow is the subject of Chapters 7 to 14.

1.10.4 Mach Number Regimes

Of all the ways of subdividing and describing different aerodynamic flows, the distinction based on the Mach number is probably the most prevalent. If M is the

local Mach number at an arbitrary point in a flow field, then by definition the flow is locally:

Subsonic if $M < 1$
Sonic if $M = 1$
Supersonic if $M > 1$

Looking at the whole field simultaneously, four different speed regimes can be identified using Mach number as the criterion:

1. *Subsonic flow* ($M < 1$ everywhere). A flow field is defined as *subsonic* if the Mach number is less than 1 at every point. Subsonic flows are characterized by smooth streamlines (no discontinuity in slope), as sketched in Figure 1.44*a*. Moreover, since the flow velocity is everywhere less than the speed of sound, disturbances in the flow (say, the sudden deflection of the trailing edge of the airfoil in Figure 1.44*a*) propagate both upstream and downstream, and are felt throughout the entire flow field. Note that a freestream Mach number M_∞ less than 1 does not guarantee a totally subsonic flow over the body. In expanding over an aerodynamic shape, the flow velocity increases above the freestream value, and if M_∞ is close enough to 1, the local Mach number may become supersonic in certain regions of the flow. This gives rise to a rule of thumb that $M_\infty < 0.8$ for subsonic flow over slender bodies. For blunt bodies, M_∞ must be even lower to ensure totally subsonic flow. (Again, emphasis is made that the above is just a loose rule of thumb and should not be taken as a precise quantitative definition.) Also, we will show later that incompressible flow is a special limiting case of subsonic flow where $M \to 0$.
2. *Transonic flow* (mixed regions where $M < 1$ and $M > 1$). As stated above, if M_∞ is subsonic but is near unity, the flow can become locally supersonic ($M > 1$). This is sketched in Figure 1.44*b*, which shows pockets of supersonic flow over both the top and bottom surfaces of the airfoil, terminated by weak shock waves behind which the flow becomes subsonic again. Moreover, if M_∞ is increased slightly above unity, a bow shock wave is formed in front of the body; behind this shock wave the flow is locally subsonic, as shown in Figure 1.44*c*. This subsonic flow subsequently expands to a low supersonic value over the airfoil. Weak shock waves are usually generated at the trailing edge, sometimes in a "fishtail" pattern as shown in Figure 1.44*c*. The flow fields shown in Figure 1.44*b* and *c* are characterized by mixed subsonic-supersonic flows and are dominated by the physics of both types of flow. Hence, such flow fields are called *transonic flows*. Again, as a rule of thumb for slender bodies, transonic flows occur for freestream Mach numbers in the range $0.8 < M_\infty < 1.2$.
3. *Supersonic flow* ($M > 1$ everywhere). A flow field is defined as *supersonic* if the Mach number is greater than 1 at every point. Supersonic flows are frequently characterized by the presence of shock waves across which the flow properties and streamlines change discontinuously (in contrast to the

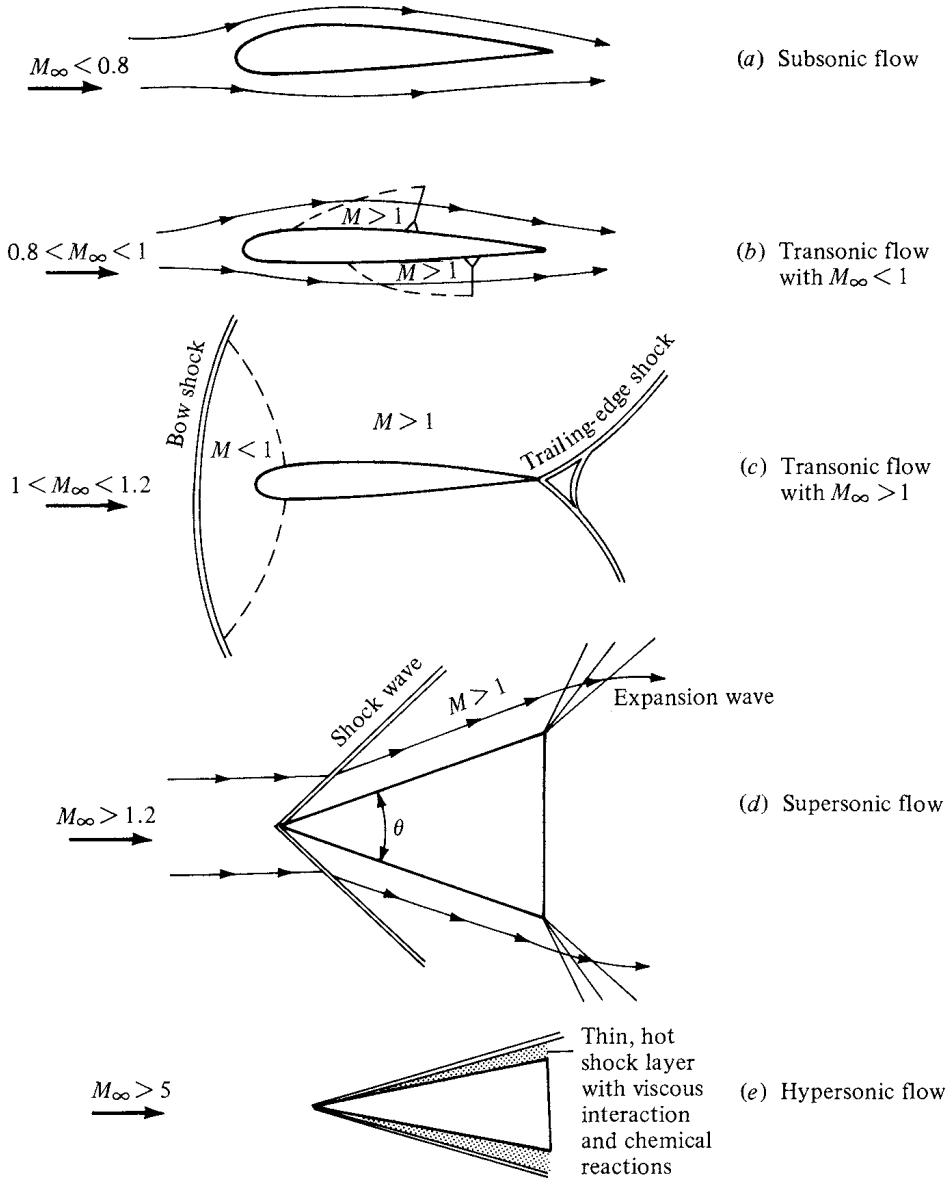

Figure 1.44 Different regimes of flow.

smooth, continuous variations in subsonic flows). This is illustrated in Figure 1.44*d* for supersonic flow over a sharp-nosed wedge; the flow remains supersonic behind the oblique shock wave from the tip. Also shown are distinct expansion waves, which are common in supersonic flow. (Again, the listing of $M_\infty > 1.2$ is strictly a rule of thumb. For example, in Figure 1.44*d*, if θ is made large enough, the oblique shock wave will detach from the tip of the wedge and will form a strong, curved bow shock ahead of the wedge with a substantial region of subsonic flow behind the wave. Hence, the totally supersonic flow sketched in

Figure 1.44*d* is destroyed if θ is too large for a given M_∞. This shock detachment phenomenon can occur at any value of $M_\infty > 1$, but the value of θ at which it occurs increases as M_∞ increases. In turn, if θ is made infinitesimally small, the flow field in Figure 1.44*d* holds for $M_\infty \geq 1.0$. These matters will be considered in detail in Chapter 9. However, the above discussion clearly shows that the listing of $M_\infty > 1.2$ in Figure 1.44*d* is a very tenuous rule of thumb and should not be taken literally.) In a supersonic flow, because the local flow velocity is greater than the speed of sound, disturbances created at some point in the flow *cannot* work their way upstream (in contrast to subsonic flow). This property is one of the most significant physical differences between subsonic and supersonic flows. It is the basic reason why shock waves occur in supersonic flows, but do not occur in steady subsonic flow. We will come to appreciate this difference more fully in Chapters 7 to 14.

4. *Hypersonic flow* (very high supersonic speeds). Refer again to the wedge in Figure 1.44*d*. Assume θ is a given, fixed value. As M_∞ increases above 1, the shock wave moves closer to the body surface. Also, the strength of the shock wave increases, leading to higher temperatures in the region between the shock and the body (the shock layer). If M_∞ is sufficiently large, the shock layer becomes very thin, and interactions between the shock wave and the viscous boundary layer on the surface occur. Also, the shock layer temperature becomes high enough that chemical reactions occur in the air. The O_2 and N_2 molecules are torn apart; that is, the gas molecules dissociate. When M_∞ becomes large enough such that viscous interaction and/or chemically reacting effects begin to dominate the flow (Figure 1.44*e*), the flow field is called *hypersonic*. (Again, a somewhat arbitrary but frequently used rule of thumb for hypersonic flow is $M_\infty > 5$.) Hypersonic aerodynamics received a great deal of attention during the period 1955–1970 because atmospheric entry vehicles encounter the atmosphere at Mach numbers between 25 (ICBMs) and 36 (the Apollo lunar return vehicle). Again during the period 1985–1995, hypersonic flight received a great deal of attention with the concept of air-breathing supersonic-combustion ramjet-powered transatmospheric vehicles to provide single-stage-to-orbit capability. Today, hypersonic aerodynamics is just part of the whole spectrum of realistic flight speeds. Some basic elements of hypersonic flow are treated in Chapter 14.

In summary, we attempt to organize our study of aerodynamic flows according to one or more of the various categories discussed in this section. The block diagram in Figure 1.45 is presented to help emphasize these categories and to show how they are related. Indeed, Figure 1.45 serves as a road map for this entire book. All the material to be covered in subsequent chapters fits into these blocks, which are lettered for easy reference. For example, Chapter 2 contains discussions of some fundamental aerodynamic principles and equations which fit into both blocks C and D. Chapters 3 to 6 fit into blocks D and E, Chapter 7 fits into blocks D and F, etc. As we proceed with our development of aerodynamics, we

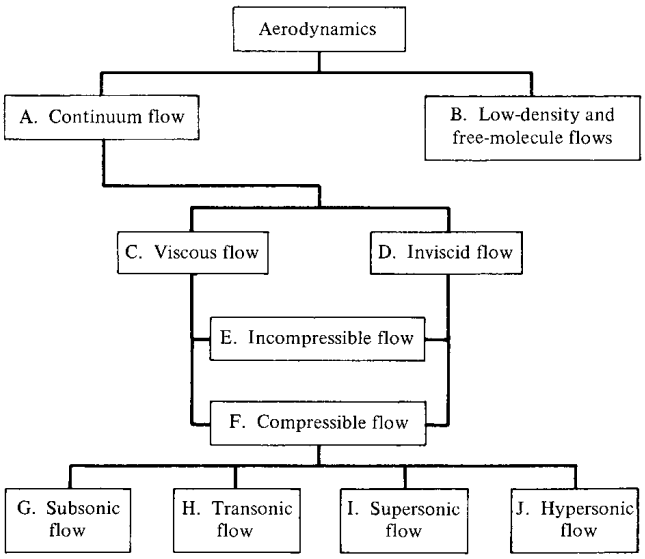

Figure 1.45 Block diagram categorizing the types of aerodynamic flows.

will frequently refer to Figure 1.45 in order to help put specific, detailed material in proper perspective relative to the whole of aerodynamics.

1.11 VISCOUS FLOW: INTRODUCTION TO BOUNDARY LAYERS

Section 1.10.2 speaks to the problem of friction in an aerodynamic flow. Frictional shear stress is defined in Section 1.4; shear stress, τ, exists at any point in a flow where there is a velocity gradient across streamlines. For most problems in aerodynamics, the local shear stress has a meaningful effect on the flow only where the velocity gradients are substantial. Consider, for example, the flow over the body shown in Figure 1.42. For the vast region of the flow field away from the body, the velocity gradients are relatively small, and friction plays virtually no role. For the thin region of the flow adjacent to the surface, however, the velocity gradients are large, and friction plays a defining role. This natural division of the flow into two regions, one where friction is much more important than the other, was recognized by the famous German fluid dynamicist Ludwig Prandtl in 1904. Prandtl's concept of the boundary layer created a breakthrough in aerodynamic analysis. Since that time theoretical analyses of most aerodynamic flows have treated the region away from the body as an *inviscid flow* (i.e., no dissipative effects due to friction, thermal conduction, or mass diffusion), and the thin region immediately adjacent to the body surface as a *viscous flow* where these dissipative effects are included. The thin viscous region adjacent to the body is called the *boundary layer;* for most aerodynamic problems of interest, the boundary layer is very thin compared to the extent of the rest of the flow. But what an effect this thin boundary layer has! It is the source of the friction drag on an aerodynamic

body. The friction drag on an Airbus 380 jumbo jet, for example, is generated by the boundary layer that wets the entire surface of the airplane in flight. The phenomena of flow separation, as sketched in Figure 1.43, is associated with the presence of the boundary layer; when the flow separates from the surface, it dramatically changes the pressure distribution over the surface resulting in a large increase in drag called *pressure drag*. So this thin viscous boundary layer adjacent to the body surface, although small in extent compared to the rest of the flow, is extremely important in aerodynamics.

Parts II and III of this book deal primarily with inviscid flows; viscous flow is the subject of Part IV. However, at the end of some of the chapters in Parts II and III, you will find a "viscous flow section" (such as the present section) for the benefit of those readers who are interested in examining the practical impact of boundary layers on the inviscid flows studied in the given chapters. These viscous flow sections are stand-alone sections and do not break the continuity of the inviscid flow discussion in Parts II and III; they simply complement those discussions.

Why are the velocity gradients inside the boundary layer so large? To help answer this question, first consider the purely inviscid flow over the airfoil shape in Figure 1.46. By definition there is no friction effect, so the streamline that is right on the surface of the body *slips* over the surface; for example, the flow velocity at point b on the surface is a finite value, unhindered by the effect of friction. In actuality, due to friction the infinitesimally thin layer of air molecules immediately adjacent to the body surface sticks to the surface, thus it has *zero* velocity relative to the surface. This is the *no-slip* condition, and it is the cause of the large velocity gradients within the boundary layer. To see why, consider the flow illustrated in Figure 1.47; here the boundary layer is shown greatly magnified

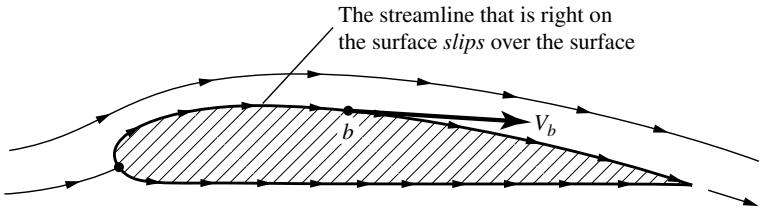

Figure 1.46 Inviscid (frictionless) flow.

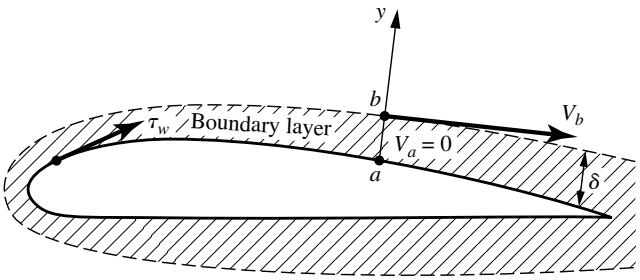

Figure 1.47 Flow in real life, with friction. The thickness of the boundary layer is greatly overemphasized for clarity.

in thickness for clarity. The flow velocity at point a on the body surface is zero due to the no-slip condition. Above point a, the velocity increases until it reaches the value of V_b at point b at the outer edge of the boundary layer. Because the boundary layer is so thin, V_b at point b in Figure 1.47 is assumed to be the same as V_b at point b on the body in the inviscid flow shown in Figure 1.46. Conventional boundary layer analysis assumes that the flow conditions at the outer edge of the boundary layer are the same as the surface flow conditions from an inviscid flow analysis. Examining Figure 1.47, because the flow velocity inside the boundary layer increases from zero at point a to a significant finite velocity at point b, and this increase takes place over a very short distance because the boundary layer is so thin, then the velocity gradients, the local values of dV/dy, are large. Hence the boundary layer is a region of the flow where frictional effects are dominant.

Also identified in Figure 1.47 is the shear stress at the wall, τ_w, and the boundary layer thickness, δ. Both τ_w and δ are important quantities, and a large part of boundary layer theory is devoted to their calculation.

It can be shown experimentally and theoretically that the pressure through the boundary layer in a direction perpendicular to the surface is constant. That is, letting p_a and p_b be the pressures at point a and b, respectively, in Figure 1.47, where the y-axis is perpendicular to the body at point a, then $p_a = p_b$. This is an important phenomenon. This is why the surface pressure distribution calculated for an inviscid flow (Figure 1.46) gives accurate results for the real-life surface pressures; it is because the inviscid calculations give the correct pressure at the outer edge of the thin boundary layer (point b in Figure 1.47), and these pressures are impressed without change through the boundary layer right down to the surface (point a). The preceding statements are reasonable for thin boundary layers that remain attached to the body surface; they do not hold for regions of separated flow such as those sketched in Figure 1.43. Such separated flows are discussed in Sections 4.12 and 4.13.

Looking more closely at the boundary layer, Figure 1.48 illustrates the *velocity profile* through the boundary layer. The velocity starts out at zero at the surface and increases continuously to its value of V_b at the outer edge. Let us set up coordinate axes x and y such that x is parallel to the surface and y is normal to the surface, as shown in Figure 1.48. By definition, a *velocity profile* gives the variation of velocity in the boundary layer as a function of y. In general, the velocity profiles at different x stations are different. Similarly, the *temperature profile* through the boundary layer is shown in Figure 1.49. The gas

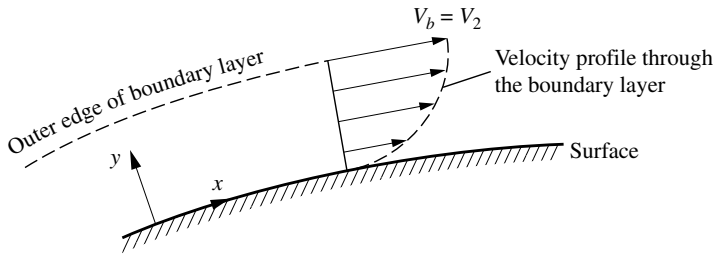

Figure 1.48 Velocity profile through a boundary layer.

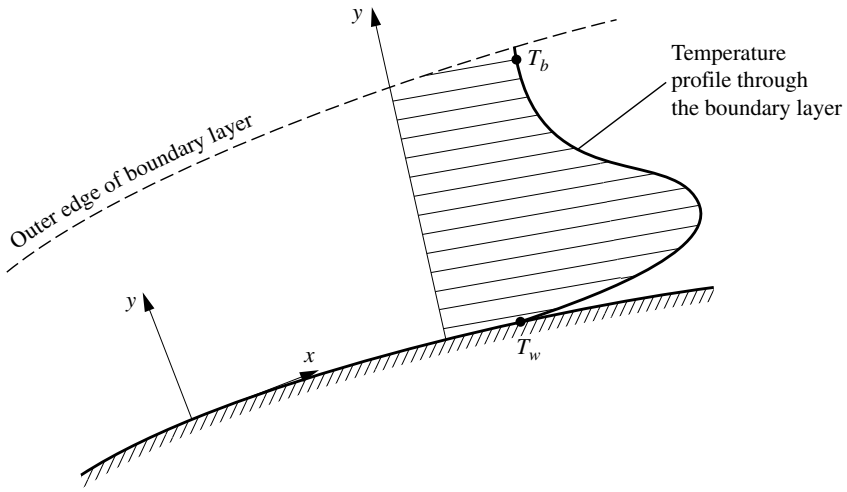

Figure 1.49 Temperature profile through a boundary layer.

temperature at the wall (which is the same as the surface temperature of the wall itself—a kind of "no slip" condition on temperature) is T_w, and the temperature at the outer edge of the boundary layer is T_b. As before, the value of T_b is the same as the gas temperature at the surface calculated from an inviscid flow analysis. By definition, a *temperature profile* gives the variation of temperature in the boundary layer as a function of y. In general, the temperature profiles at different x stations are different. The temperature inside the boundary layer is governed by the combined mechanisms of thermal conduction and frictional dissipation. Thermal conduction is the transfer of heat from a hotter region to a colder region by random molecular motion. Frictional dissipation, in a very simplistic sense, is the local heating of the gas due to one streamline rubbing over another, somewhat analogous to warming your hands by vigorously rubbing them together. A better explanation of frictional dissipation is that, as a fluid element moves along a streamline inside the boundary layer, it slows down due to frictional shear stress acting on it, and some of the original kinetic energy it had before it entered the boundary layer is converted to internal energy inside the boundary layer, hence increasing the gas temperature inside the boundary layer.

The slope of the velocity profile at the wall is of particular importance because it governs the wall shear stress. Let $(dV/dy)_{y=0}$ be defined as the velocity gradient at the wall. Then the shear stress at the wall is given by

$$\tau_w = \mu \left(\frac{dV}{dy} \right)_{y=0} \tag{1.59}$$

where μ is the *absolute viscosity coefficient* (or simply the *viscosity*) of the gas. The viscosity coefficient has dimensions of mass/(length)(time), as can be verified from Equation (1.59) combined with Newton's second law. It is a physical property of the fluid; μ is different for different gases and liquids. Also, μ varies with T. For liquids, μ decreases as T increases (we all know that oil gets "thinner" when the temperature is increased). But for gases, μ increases as T increases (air

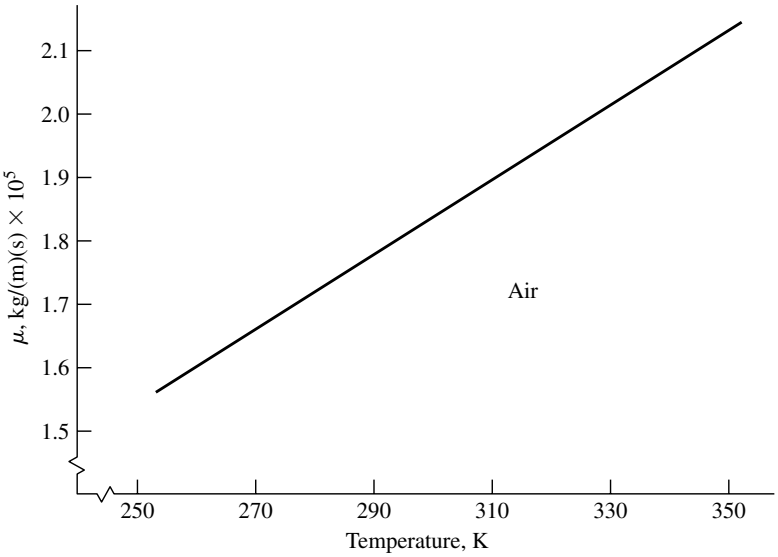

Figure 1.50 Variation of viscosity coefficient with temperature.

gets "thicker" when the temperature is increased). For air at standard sea-level temperature,

$$\mu = 1.7894 \times 10^{-5}\text{kg/(m)(s)} = 3.7373 \times 10^{-7}\text{slug/(ft)(s)}$$

The temperature variation of μ for air over a small range of interest is given in Figure 1.50.

Similarly, the slope of the temperature profile at the wall is very important; it dictates the aerodynamic heating to or from the wall. Let $(dT/dy)_{y=0}$ be defined as the temperature gradient at the wall. Then the aerodynamic heating rate (energy per second per unit area) at the wall is given by

$$\dot{q}_w = -k\left(\frac{dT}{dy}\right)_{y=0} \tag{1.60}$$

where k is the *thermal conductivity* of the gas, and the minus sign connotes that heat is conducted from a warm region to a cooler region, in the opposite direction as the temperature gradient. That is, if the temperature gradient in Equation (1.60) is positive (temperature increases in the direction above the wall), the heat transfer is from the gas *into* the wall, opposite to the direction of increasing temperature. If the temperature gradient is negative (temperature decreases in the direction above the wall), the heat transfer is *away* from the wall into the gas, again opposite to the direction of increasing temperature. Frequently, the heating or cooling of a wall by a flow over the wall is called "convective heat transfer," although from Equation (1.60) the actual mechanism by which heat is transferred between the gas and the wall is thermal *conduction*. In this book, we will label the heat transfer taking place between the boundary layer and the wall as *aerodynamic heating*. Aerodynamic heating is important in high-speed flows, particularly supersonic

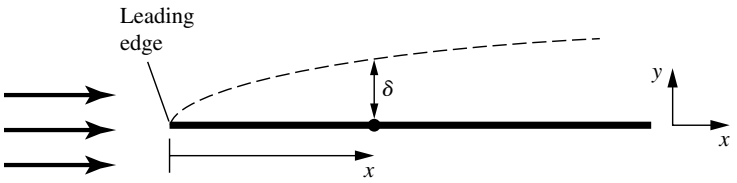

Figure 1.51 Growth of the boundary layer thickness.

flows, and it becomes absolutely dominant in hypersonic flows. Finally, we note that k in Equation (1.60), like μ in Equation (1.59), is a physical property of the fluid, and is a function of temperature. For air at standard sea-level temperature,

$$k = 2.53 \times 10^{-2} \text{J/(m)(s)(K)} = 3.16 \times 10^{-3} \text{lb/(s)(°R)}$$

Thermal conductivity is essentially proportional to the viscosity coefficient (i.e, k = (constant) $\times$ μ), so the temperature variation of k is proportional to that shown in Figure 1.49 for μ.

Sections 1.7 and 1.8 introduced the Reynolds number as an important similarity parameter. Consider the development of a boundary layer on a surface, such as the flat plate sketched in Figure 1.51. Let x be measured from the leading edge, that is, from the tip of the plate. Let V_∞ be the flow velocity far upstream of the plate. The *local* Reynolds number at a local distance x from the leading edge is defined as

$$\text{Re}_x = \frac{\rho_\infty V_\infty x}{\mu_\infty} \tag{1.61}$$

where the subscript ∞ is used to denote conditions in the freestream ahead of the plate. The local values of τ_w and δ are functions of Re_x; this is shown in Chapter 4, and in more detail in Part IV of this book. The Reynolds number has a powerful influence over the properties of a boundary layer, and it governs the nature of viscous flows in general. We will encounter the Reynolds number frequently in this book.

Up to this point in our discussion, we have considered flow streamlines to be smooth and regular curves in space. However, in a viscous flow, and particularly in boundary layers, life is not quite so simple. There are two basic types of viscous flow:

1. *Laminar flow,* in which the streamlines are smooth and regular and a fluid element moves smoothly along a streamline.
2. *Turbulent flow,* in which the streamlines break up and a fluid element moves in a random, irregular, and tortuous fashion.

If you observe smoke rising from a lit cigarette, as sketched in Figure 1.52, you see first a region of smooth flow—laminar flow—and then a transition to irregular, mixed-up flow—turbulent flow. The differences between laminar and turbulent flow are dramatic, and they have a major impact on aerodynamics. For example, consider the velocity profiles through a boundary layer, as sketched in Figure 1.53. The profiles are different, depending on whether the flow is laminar

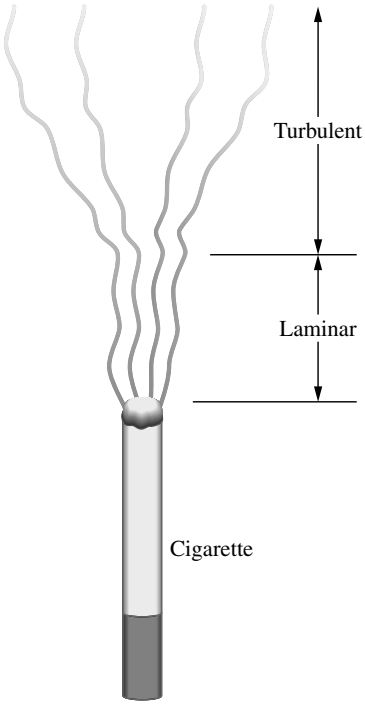

Figure 1.52 Smoke pattern illustrating transition from laminar to turbulent flow.

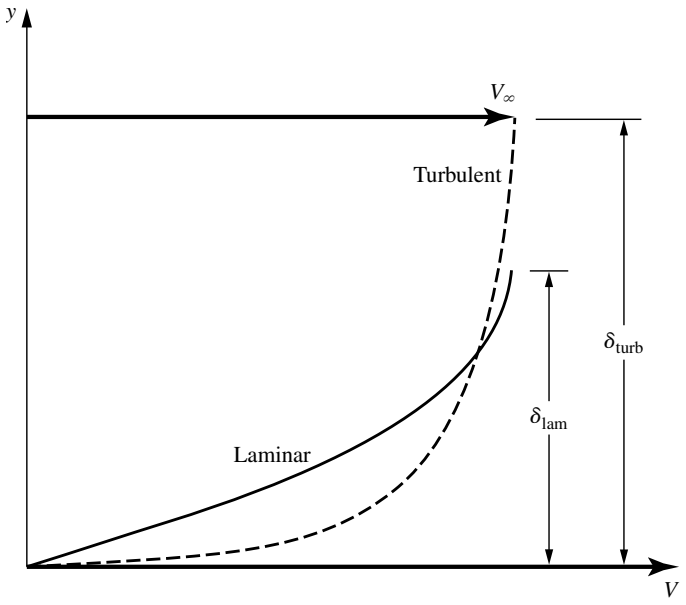

Figure 1.53 Velocity profiles for laminar and turbulent boundary layers. Note that the turbulent boundary layer thickness is larger than the laminar boundary layer thickness.

or turbulent. The turbulent profile is "fatter," or fuller, than the laminar profile. For the turbulent profile, from the outer edge to a point near the surface, the velocity remains reasonably close to the free-stream velocity; it then rapidly decreases to zero at the surface. In contrast, the laminar velocity profile gradually decreases to zero from the outer edge to the surface. Now consider the velocity gradient at the wall, $(dV/dy)_{y=0}$, which is the reciprocal of the slope of the curves shown in Figure 1.52 evaluated at $y = 0$. From Figure 1.53, it is clear that

$$\left(\frac{dV}{dy}\right)_{y=0} \text{for laminar flow} < \left(\frac{dV}{dy}\right)_{y=0} \text{for turbulent flow}$$

Recalling Equation (1.59) for τ_w leads us to the fundamental and highly important fact that *laminar shear stress is less than turbulent shear stress:*

$$(\tau_w)_{\text{laminar}} < (\tau_w)_{\text{turbulent}}$$

This obviously implies that the skin friction exerted on an airplane wing or body will depend on whether the boundary layer on the surface is laminar or turbulent, with laminar flow yielding the smaller skin friction drag.

The same trends hold for aerodynamic heating. We have for the temperature gradients at the wall:

$$\left(\frac{dT}{dy}\right)_{y=0} \text{for laminar flow} < \left(\frac{dT}{dy}\right)_{y=0} \text{for turbulent flow}$$

Recalling Equation (1.60) for q_w, we see that turbulent aerodynamic heating is larger than laminar aerodynamic heating, sometimes *considerably* larger. At hypersonic speeds, turbulent heat transfer rates can be almost a factor of 10 larger than laminar heat transfer rates—a showstopper in some hypersonic vehicle designs. We will have a lot to say about the effects of turbulent versus laminar flows in subsequent sections of this book.

In summary, in this section we have presented some introductory thoughts about friction, viscous flows, and boundary layers, in keeping with the introductory nature of this chapter. In subsequent chapters we will expand on these thoughts, including discussions on how to calculate some of the important practical quantities such as τ_w, q_w, and δ.

1.12 APPLIED AERODYNAMICS: THE AERODYNAMIC COEFFICIENTS—THEIR MAGNITUDES AND VARIATIONS

With the present section, we begin a series of special sections in this book under the general heading of "applied aerodynamics." The main thrust of this book is to present the *fundamentals* of aerodynamics, as is reflected in the book's title. However, *applications* of these fundamentals are liberally sprinkled throughout the book, in the text material, in the worked examples, and in the homework problems. The term *applied aerodynamics* normally implies the application of

aerodynamics to the practical evaluation of the aerodynamic characteristics of real configurations such as airplanes, missiles, and space vehicles moving through an atmosphere (the earth's, or that of another planet). Therefore, to enhance the reader's appreciation of such applications, sections on applied aerodynamics will appear near the end of many of the chapters. To be specific, in this section, we address the matter of the aerodynamic coefficients defined in Section 1.5; in particular, we focus on lift, drag, and moment coefficients. These nondimensional coefficients are the primary language of applications in external aerodynamics (the distinction between external and internal aerodynamics was made in Section 1.2). It is important for you to obtain a feeling for typical values of the aerodynamic coefficients. (For example, do you expect a drag coefficient to be as low as 10^{-5}, or maybe as high as 1000—does this make sense?) The purpose of this section is to begin to provide you with such a feeling, at least for some common aerodynamic body shapes. As you progress through the remainder of this book, make every effort to note the typical magnitudes of the aerodynamic coefficients that are discussed in various sections. Having a realistic feel for these magnitudes is part of your technical maturity.

Question: What are some typical drag coefficients for various aerodynamic configurations? Some basic values are shown in Figure 1.54. The dimensional analysis described in Section 1.7 proved that $C_D = f(M, \text{Re})$. In Figure 1.54, the drag-coefficient values are for low speeds, essentially incompressible flow; therefore, the Mach number does not come into the picture. (For all practical purposes, for an incompressible flow, the Mach number is theoretically zero, not because the velocity goes to zero, but rather because the speed of sound is infinitely large. This will be made clear in Section 8.3.) Thus, for a low-speed flow, the aerodynamic coefficients for a fixed shape at a fixed orientation to the flow are functions of just the Reynolds number. In Figure 1.54, the Reynolds numbers are listed at the left and the drag-coefficient values at the right. In Figure 1.54*a*, a flat plate is oriented perpendicular to the flow; this configuration produces the largest possible drag coefficient of any conventional configuration, namely, $C_D = D'/q_\infty S = 2.0$, where S is the frontal area per unit span, i.e., $S = (d)(1)$, where d is the height of the plate. The Reynolds number is based on the height d; that is, $\text{Re} = \rho_\infty V_\infty d/\mu_\infty = 10^5$. Figure 1.54*b* illustrates flow over a circular cylinder of diameter d; here, $C_D = 1.2$, considerably smaller than the vertical plate value in Figure 1.54*a*. The drag coefficient can be reduced dramatically by streamlining the body, as shown in Figure 1.54*c*. Here, $C_D = 0.12$; this is an order of magnitude smaller than the circular cylinder in Figure 1.54*b*. The Reynolds numbers for Figure 1.54*a*, *b*, and *c* are all the same value, based on d (diameter). The drag coefficients are all defined the same, based on a reference area per unit span of $(d)(1)$. Note that the flow fields over the configurations in Figure 1.54*a*, *b*, and *c* show a wake downstream of the body; the wake is caused by the flow separating from the body surface, with a low-energy, recirculating flow inside the wake. The phenomenon of flow separation will be discussed in detail in Part 4 of this book, dealing with viscous flows. However, it is clear that the wakes diminish in size as we progressively go from Figure 1.54*a*, *b*, and *c*. The fact that C_D also diminishes progressively from Figure 1.54*a*, *b*, and *c* is no accident—it

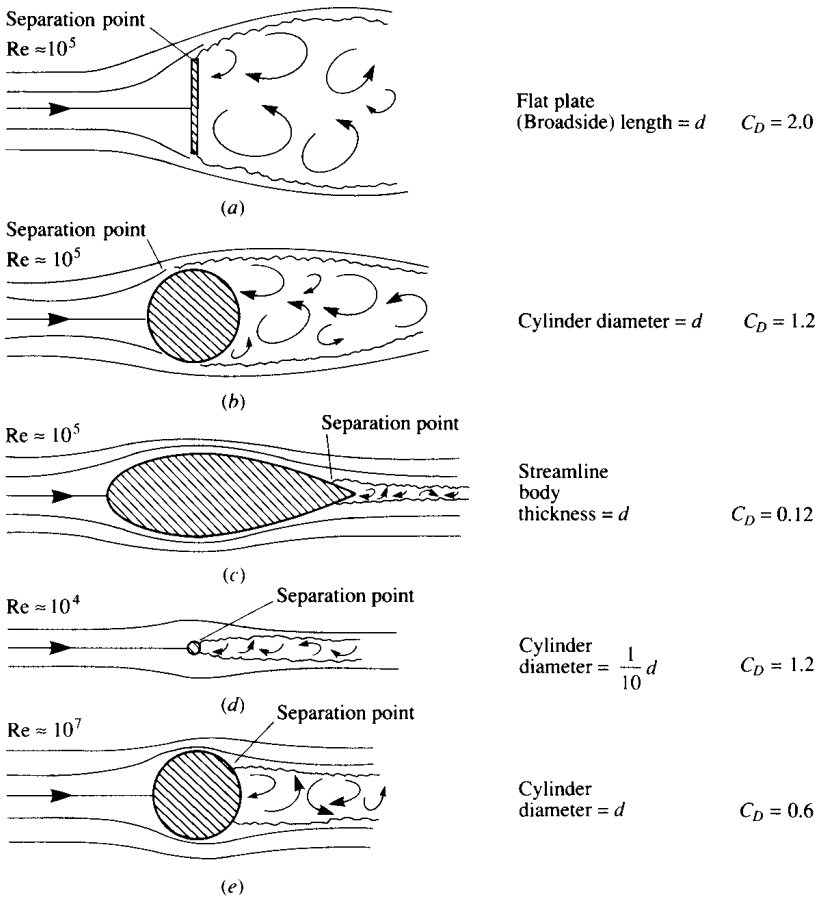

Figure 1.54 Drag coefficients for various aerodynamic shapes. (*Source:* Talay, T. A., *Introduction to the Aerodynamics of Flight,* NASA SP-367, 1975.)

is a direct result of the regions of separated flow becoming progressively smaller. Why is this so? Simply consider this as one of the many interesting questions in aerodynamics—a question that will be answered in due time in this book. Note, in particular that the physical effect of the streamlining in Figure 1.54*c* results in a very small wake, hence a small value for the drag coefficient.

Consider Figure 1.54*d*, where once again a circular cylinder is shown, but of much smaller diameter. Since the diameter here is $0.1d$, the Reynolds number is now 10^4 (based on the same freestream V_∞, ρ_∞, and μ_∞ as Figure 1.54*a*, *b*, and *c*). It will be shown in Chapter 3 that C_D for a circular cylinder is relatively independent of Re between $\text{Re} = 10^4$ and 10^5. Since the body *shape* is the same between Figure 1.54*d* and *b*, namely, a circular cylinder, then C_D is the same value of 1.2 as shown in the figure. However, since the drag is given by $D' = q_\infty S C_D$, and S is one-tenth smaller in Figure 1.54*d*, then the *drag force* on the small cylinder in Figure 1.54*d* is one-tenth smaller than that in Figure 1.54*b*.

Another comparison is illustrated in Figure 1.54*c* and *d*. Here we are comparing a large streamlined body of thickness d with a small circular cylinder of

diameter $0.1d$. For the large streamlined body in Figure 1.54*c*,

$$D' = q_\infty S C_D = 0.12 q_\infty d$$

For the small circular cylinder in Figure 1.54*d*,

$$D' = q_\infty S C_D = q_\infty (0.1d)(1.2) = 0.12 q_\infty d$$

The drag values are the same! Thus, Figure 1.54*c* and *d* illustrate that the drag on a circular cylinder is the same as that on the streamlined body which is 10 times thicker—another way of stating the aerodynamic value of streamlining.

As a final note in regard to Figure 1.54, the flow over a circular cylinder is again shown in Figure 1.54*e*. However, now the Reynolds number has been increased to 10^7, and the cylinder drag coefficient has decreased to 0.6—a dramatic factor of two less than in Figure 1.54*b* and *d*. Why has C_D decreased so precipitously at the higher Reynolds number? The answer must somehow be connected with the smaller wake behind the cylinder in Figure 1.54*e* compared to Figure 1.54*b*. What is going on here? This is one of the fascinating questions we will answer as we progress through our discussions of aerodynamics in this book—an answer that will begin with Section 3.18 and culminate in Part 4 dealing with viscous flow.

At this stage, pause for a moment and note the *values* of C_D for the aerodynamic shapes in Figure 1.54. With C_D based on the *frontal projected area* ($S = d(1)$ per unit span), the values of C_D range from a maximum of 2 to numbers as low as 0.12. These are typical values of C_D for aerodynamic bodies.

Also, note the values of Reynolds number given in Figure 1.54. Consider a circular cylinder of diameter 1 m in a flow at standard sea level conditions ($\rho_\infty = 1.23$ kg/m^3 and $\mu_\infty = 1.789 \times 10^{-5}$ kg/m $\cdot$ s) with a velocity of 45 m/s (close to 100 mi/h). For this case,

$$\text{Re} = \frac{\rho_\infty V_\infty d}{\mu_\infty} = \frac{(1.23)(45)(1)}{1.789 \times 10^{-5}} = 3.09 \times 10^6$$

Note that the Reynolds number is over 3 million; values of Re in the millions are typical of practical applications in aerodynamics. Therefore, the large numbers given for Re in Figure 1.54 are appropriate.

Let us examine more closely the nature of the drag exerted on the various bodies in Figure 1.54. Since these bodies are at zero angle of attack, the drag is equal to the axial force. Hence, from Equation (1.8) the drag per unit span can be written as

$$\begin{aligned} D' = & \underbrace{\int_{\text{LE}}^{\text{TE}} -p_u \sin\theta \, ds_u + \int_{\text{LE}}^{\text{TE}} p_l \sin\theta \, ds_l}_{\text{pressure drag}} \\ & + \underbrace{\int_{\text{LE}}^{\text{TE}} \tau_u \cos\theta \, ds_u + \int_{\text{LE}}^{\text{TE}} \tau_l \cos\theta \, ds_l}_{\text{skin friction drag}} \end{aligned} \tag{1.62}$$

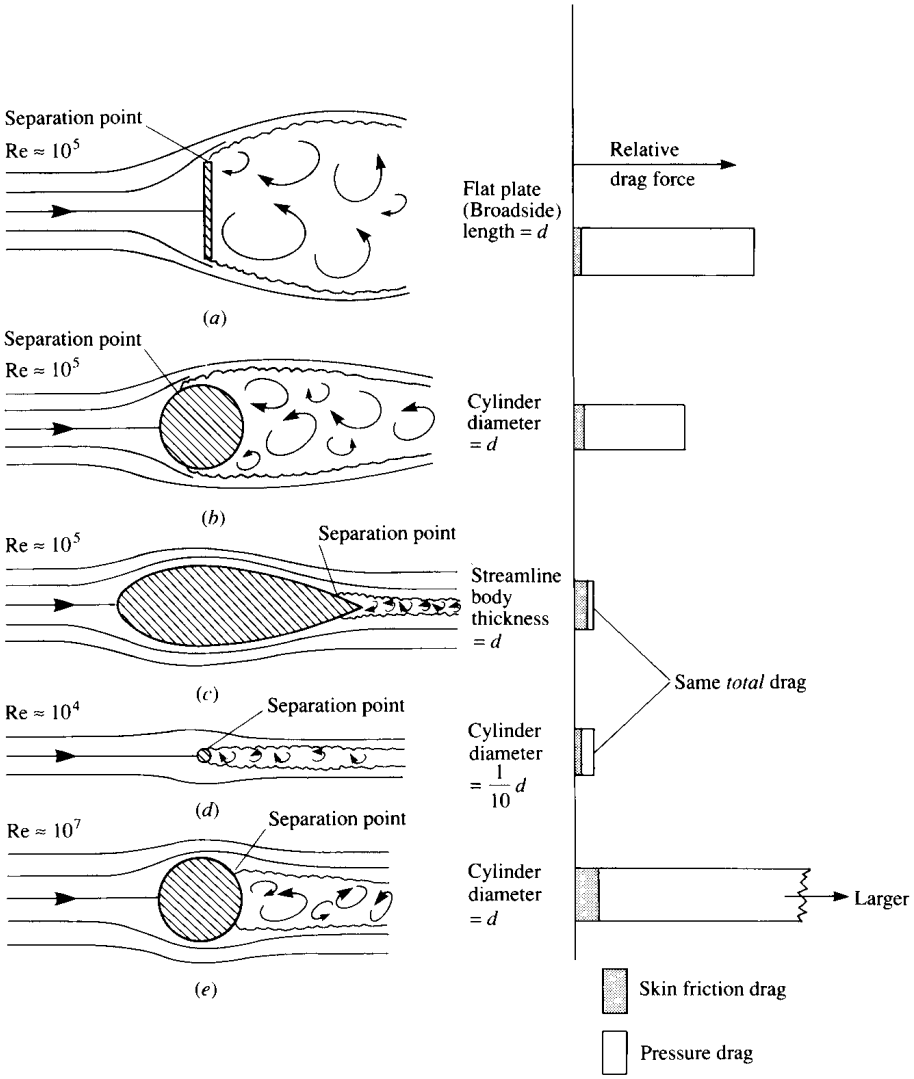

Figure 1.55 The relative comparison between skin friction drag and pressure drag for various aerodynamic shapes. (*Source:* Talay, T. A., *Introduction to the Aerodynamics of Flight,* NASA SP-367, 1975.)

That is, the drag on any aerodynamic body is composed of pressure drag and skin friction drag; this is totally consistent with our discussion in Section 1.5, where it is emphasized that the only two basic sources of aerodynamic force on a body are the pressure and shear stress distributions exerted on the body surface. The division of total drag onto its components of pressure and skin friction drag is frequently useful in analyzing aerodynamic phenomena. For example, Figure 1.55 illustrates the comparison of skin friction drag and pressure drag for the cases shown in Figure 1.54. In Figure 1.55, the bar charts at the right of the figure give the relative drag force on each body; the cross-hatched region denotes the amount

of skin friction drag, and the blank region is the amount of pressure drag. The freestream density and viscosity are the same for Figure 1.55*a* to *e*; however, the freestream velocity V_∞ is varied by the necessary amount to achieve the Reynolds numbers shown. That is, comparing Figure 1.55*b* and *e*, the value of V_∞ is much larger for Figure 1.55*e*. Since the drag force is given by

$$D' = \tfrac{1}{2}\rho_\infty V_\infty^2 S C_D$$

then the drag for Figure 1.55*e* is much larger than for Figure 1.55*b*. Also shown in the bar chart is the equal drag between the streamlined body of thickness d and the circular cylinder of diameter $0.1d$—a comparison discussed earlier in conjunction with Figure 1.54. Of most importance in Figure 1.55, however, is the relative amounts of skin friction and pressure drag for each body. Note that the drag of the vertical flat plate and the circular cylinders is dominated by pressure drag, whereas, in contrast, most of the drag of the streamlined body is due to skin friction. Indeed, this type of comparison leads to the definition of two generic body shapes in aerodynamics, as follows:

Blunt body = a body where most of the drag is pressure drag

Streamlined body = a body where most of the drag is skin friction drag

In Figures 1.54 and 1.55, the vertical flat plate and the circular cylinder are clearly *blunt bodies*.

The large pressure drag of blunt bodies is due to the massive regions of flow separation which can be seen in Figures 1.54 and 1.55. The reason why flow separation causes drag will become clear as we progress through our subsequent discussions. Hence, the pressure drag shown in Figure 1.55 is more precisely denoted as "pressure drag due to flow separation"; this drag is frequently called *form drag*. (For an elementary discussion of form drag and its physical nature, see Reference 2.)

Let us now examine the drag on a flat plate at zero angle of attack, as sketched in Figure 1.56. Here, the drag is completely due to shear stress; there is no pressure force in the drag direction. The skin friction drag coefficient is defined as

$$C_f = \frac{D'}{q_\infty S} = \frac{D'}{q_\infty c(1)}$$

where the reference area is the *planform* area per unit span, that is, the surface area as seen by looking down on the plate from above. C_f will be discussed further in Chapters 4 and 16. However, the purpose of Figure 1.56 is to demonstrate that:

1. C_f is a strong function of Re, where Re is based on the chord length of the plate, $\text{Re} = \rho_\infty V_\infty c/\mu_\infty$. Note that C_f decreases as Re increases.
2. The value of C_f depends on whether the flow over the plate surface is laminar or turbulent, with the turbulent C_f being higher than the laminar C_f at the same Re. What is going on here? What is laminar flow? What is turbulent flow? Why does it affect C_f? The answers to these questions will be addressed in Chapters 4, 15, 17, and 18.

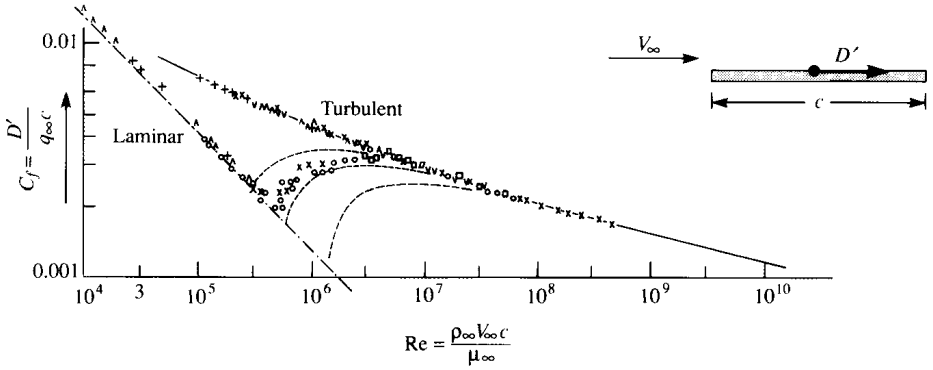

Figure 1.56 Variation of laminar and turbulent skin friction coefficient for a flat plate as a function of Reynolds number based on the chord length of the plate. The intermediate dashed curves are associated with various transition paths from laminar flow to turbulent flow.

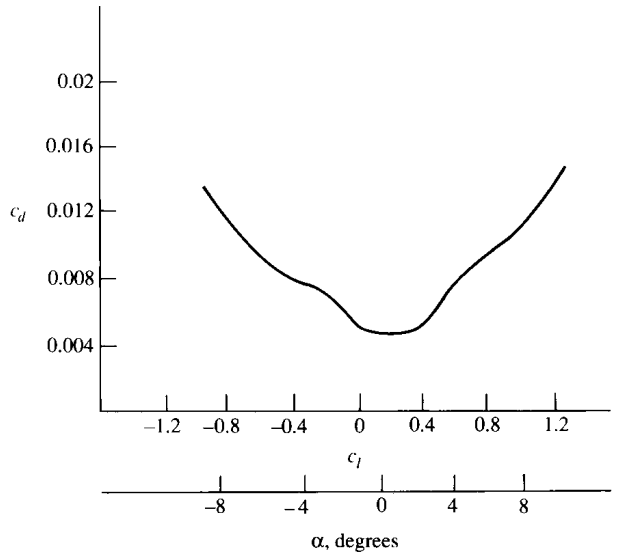

Figure 1.57 Variation of section drag coefficient for an NACA 63-210 airfoil. Re $= 3 \times 10^6$.

3. The magnitudes of C_f range typically from 0.001 to 0.01 over a large range of Re. These numbers are considerably smaller than the drag coefficients listed in Figure 1.54. This is mainly due to the different reference areas used. In Figure 1.54, the reference area is a cross-sectional area normal to the flow; in Figure 1.56, the reference area is the *planform* area.

A flat plate is not a very practical aerodynamic body—it simply has no volume. Let us now consider a body with thickness, namely, an airfoil section. An NACA 63-210 airfoil section is one such example. The variation of the drag coefficient, c_d, with angle of attack is shown in Figure 1.57. Here, as usual, c_d is

defined as

$$c_d = \frac{D'}{q_\infty c}$$

where D' is the drag per unit span. Note that the lowest value of c_d is about 0.0045. The NACA 63-210 airfoil is classified as a "laminar-flow airfoil" because it is designed to promote such a flow at small α. This is the reason for the bucketlike appearance of the c_d curve at low α; at higher α, transition to turbulent flow occurs over the airfoil surface, causing a sharp increase in c_d. Hence, the value of $c_d = 0.0045$ occurs in a laminar flow. Note that the Reynolds number is 3 million. Once again, a reminder is given that the various aspects of laminar and turbulent flows will be discussed in Part 4. The main point here is to demonstrate that typical airfoil drag-coefficient values are on the order of 0.004 to 0.006. As in the case of the streamlined body in Figures 1.54 and 1.55, most of this drag is due to skin friction. However, at higher values of α, flow separation over the top surface of the airfoil begins to appear and pressure drag due to flow separation (form drag) begins to increase. This is why c_d increases with increasing α in Figure 1.57.

Let us now consider a complete airplane. In Chapter 3, Figure 3.2 is a photograph of the Seversky P-35, a typical fighter aircraft of the late 1930s. Figure 1.58 is a detailed drag breakdown for this type of aircraft. Configuration 1 in Figure 1.58 is the stripped-down, aerodynamically cleanest version of this aircraft; its drag coefficient (measured at an angle of attack corresponding to a lift coefficient of $C_L = 0.15$) is $C_D = 0.0166$. Here, C_D is defined as

$$C_D = \frac{D}{q_\infty S}$$

where D is the airplane drag and S is the planform area of the wing. For configurations 2 through 18, various changes are progressively made in order to bring the aircraft to its conventional, operational configuration. The incremental drag increases due to each one of these additions are tabulated in Figure 1.58. Note that the drag coefficient is increased by more than 65 percent by these additions; the value of C_D for the aircraft in full operational condition is 0.0275. This is a typical airplane drag-coefficient value. The data shown in Figure 1.58 were obtained in the full-scale wind tunnel at the NACA Langley Memorial Laboratory just prior to World War II. (The full-scale wind tunnel has test-section dimensions of 30 by 60 ft, which can accommodate a whole airplane—hence the name "full-scale.")

The values of drag coefficients discussed so far in this section have applied to low-speed flows. In some cases, their variation with the Reynolds number has been illustrated. Recall from the discussion of dimensional analysis in Section 1.7 that drag coefficient also varies with the Mach number. *Question:* What is the effect of increasing the Mach number on the drag coefficient of an airplane?

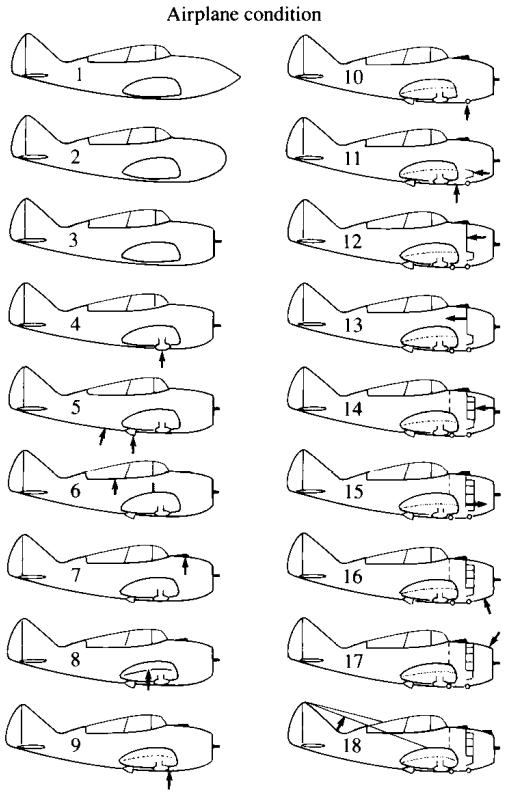

Condition number	Description	C_D ($C_L = 0.15$)	ΔC_D	ΔC_D, %[a]
1	Completely faired condition, long nose fairing	0.0166		
2	Completely faired condition, blunt nose fairing	0.0169		
3	Original cowling added, no airflow through cowling	0.0186	0.0020	12.0
4	Landing-gear seals and fairing removed	0.0188	0.0002	1.2
5	Oil cooler installed	0.0205	0.0017	10.2
6	Canopy fairing removed	0.0203	−0.0002	−1.2
7	Carburetor air scoop added	0.0209	0.0006	3.6
8	Sanded walkway added	0.0216	0.0007	4.2
9	Ejector chute added	0.0219	0.0003	1.8
10	Exhaust stacks added	0.0225	0.0006	3.6
11	Intercooler added	0.0236	0.0011	6.6
12	Cowling exit opened	0.0247	0.0011	6.6
13	Accessory exit opened	0.0252	0.0005	3.0
14	Cowling fairing and seals removed	0.0261	0.0009	5.4
15	Cockpit ventilator opened	0.0262	0.0001	0.6
16	Cowling venturi installed	0.0264	0.0002	1.2
17	Blast tubes added	0.0267	0.0003	1.8
18	Antenna installed	0.0275	0.0008	4.8
	Total		0.0109	

[a]Percentages based on completely faired condition with long nose fairing.

Figure 1.58 The breakdown of various sources of drag on a late 1930s airplane, the Seversky XP-41 (derived from the Seversky P-35 shown in Figure 3.2). [*Source:* Experimental data from Coe, Paul J., "Review of Drag Cleanup Tests in Langley Full-Scale Tunnel (From 1935 to 1945) Applicable to Current General Aviation Airplanes," NASA TN-D-8206, 1976.]

Consider the answer to this question for a Northrop T-38A jet trainer, shown in Figure 1.59. The drag coefficient for this airplane is given in Figure 1.60 as a function of the Mach number ranging from low subsonic to supersonic. The aircraft is at a small negative angle of attack such that the lift is zero, hence the C_D in Figure 1.60 is called the *zero-lift drag coefficient*. Note that the value of C_D is relatively constant from $M = 0.1$ to about 0.86. Why? At Mach numbers of about 0.86, the C_D rapidly increases. This large increase in C_D near Mach one is typical of all flight vehicles. Why? Stay tuned; the answers to these questions will become clear in Part 3 dealing with compressible flow. Also, note in Figure 1.60 that at low subsonic speeds, C_D is about 0.015. This is considerably lower than the 1930s-type airplane illustrated in Figure 1.58; of course, the T-38 is a more modern, sleek, streamlined airplane, and its drag coefficient should be smaller.

We now turn our attention to lift coefficient and examine some typical values. As a complement to the drag data shown in Figure 1.57 for an NACA 63-210

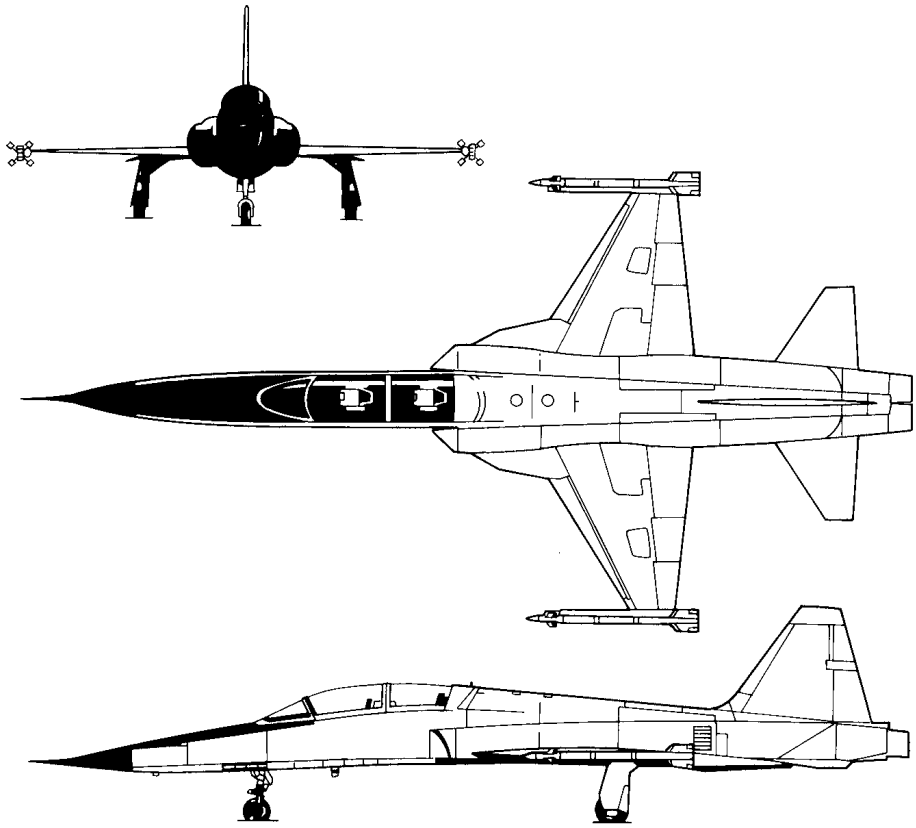

Figure 1.59 Three-view of the Northrop T-38 jet trainer. *(Courtesy of the U.S. Air Force.)*

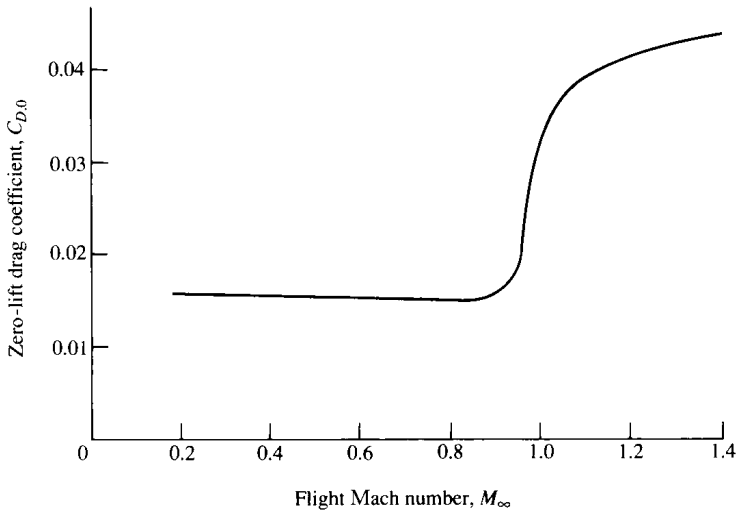

Figure 1.60 Zero-lift drag coefficient variation with Mach number for the T-38. *(Courtesy of the U.S. Air Force.)*

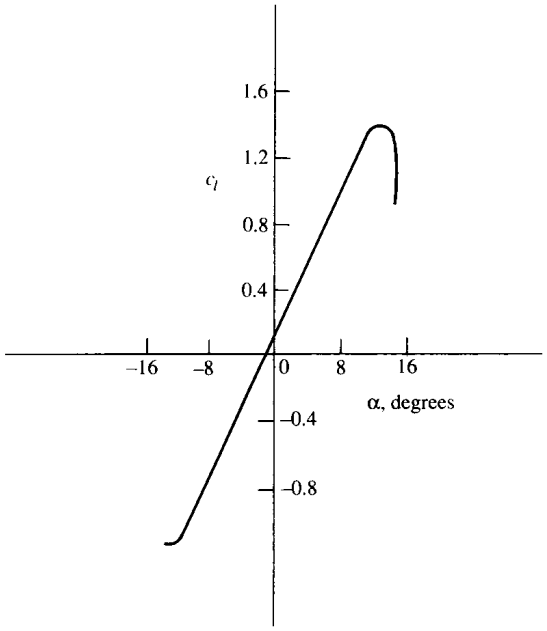

Figure 1.61 Variation of section lift coefficient for an NACA 63-210 airfoil. Re $= 3 \times 10^6$. No flap deflection.

airfoil, the variation of lift coefficient versus angle of attack for the same airfoil is shown in Figure 1.61. Here, we see c_l increasing linearly with α until a maximum value is obtained near $\alpha = 14^\circ$, beyond which there is a precipitous drop in lift. Why does c_l vary with α in such a fashion—in particular, what causes the sudden drop in c_l beyond $\alpha = 14^\circ$? An answer to this question will evolve over the ensuing chapters. For our purpose in the present section, observe the *values* of c_l; they vary from about -1.0 to a maximum of 1.5, covering a range of α from -12 to 14°. Conclusion: For an airfoil, the magnitude of c_l is about a factor of 100 larger than c_d. A particularly important figure of merit in aerodynamics is the *ratio* of lift to drag, the so-called L/D ratio; many aspects of the flight performance of a vehicle are directly related to the L/D ratio (see, e.g., Reference 2). Other things being equal, a higher L/D means better flight performance. For an airfoil—a configuration whose primary function is to produce lift with as little drag as possible—values of L/D are large. For example, from Figures 1.57 and 1.61, at $\alpha = 4^\circ$, $c_l = 0.6$ and $c_d = 0.0046$, yielding $L/D = \frac{0.6}{0.0046} = 130$. This value is much larger than those for a complete airplane, as we will soon see.

To illustrate the lift coefficient for a complete airplane, Figure 1.62 shows the variation of C_L with α for the T-38 in Figure 1.59. Three curves are shown, each for a different flap deflection angle. (Flaps are sections of the wing at the trailing edge which, when deflected downward, increase the lift of the wing. See Section 5.17 of Reference 2 for a discussion of the aerodynamic properties of flaps.) Note that at a given α, the deflection of the flaps increases C_L. The values of C_L shown

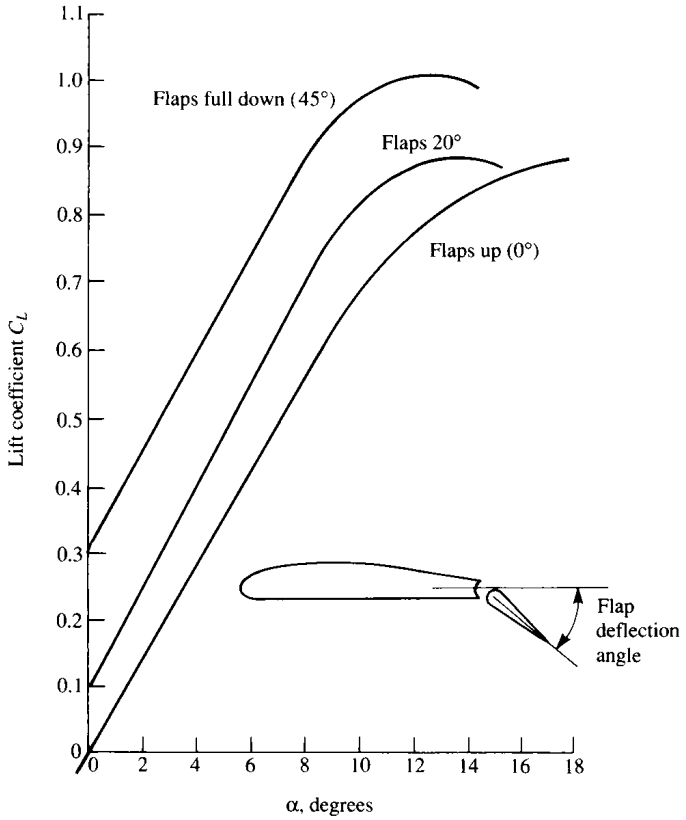

Figure 1.62 Variation of lift coefficient with angle of attack for the T-38. Three curves are shown corresponding to three different flap deflections. Freestream Mach number is 0.4. *(Courtesy of the U.S. Air Force.)*

in Figure 1.62 are about the same as that for an airfoil—on the order of 1. On the other hand, the maximum L/D ratio of the T-38 is about 10—considerably smaller than that for an airfoil alone. Of course, an airplane has a fuselage, engine nacelles, etc., which are elements with other functions than just producing lift, and indeed produce only small amounts of lift while at the same time adding a lot of drag to the vehicle. Thus, the L/D ratio for an airplane is expected to be much less than that for an airfoil alone. Moreover, the wing on an airplane experiences a much higher pressure drag than an airfoil due to the adverse aerodynamic effects of the wing tips (a topic for Chapter 5). This additional pressure drag is called induced drag, and for short, stubby wings, such as on the T-38, the induced drag can be large. (We must wait until Chapter 5 to find out about the nature of induced drag.) As a result, the L/D ratio of the T-38 is fairly small as most airplanes go. For example, the maximum L/D ratio for the Boeing B-52 strategic bomber is 21.5 (see Reference 48). However, this value is still considerably smaller than that for an airfoil alone.

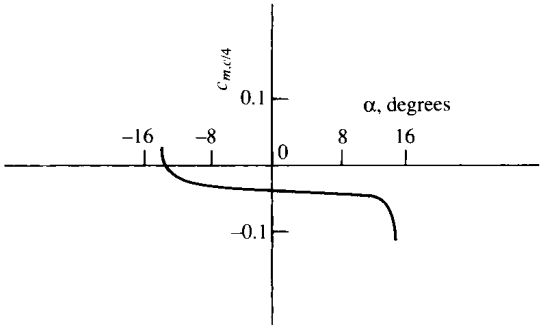

Figure 1.63 Variation of section moment coefficient about the quarter chord for an NACA 63-210 airfoil. $\text{Re} = 3 \times 10^6$.

Finally, we turn our attention to the values of moment coefficients. Figure 1.63 illustrates the variation of $c_{m,c/4}$ for the NACA 63-210 airfoil. Note that this is a *negative* quantity; all conventional airfoils produce negative, or "pitch-down," moments. (Recall the sign convention for moments given in Section 1.5.) Also, notice that its value is on the order of -0.035. This value is typical of a moment coefficient—on the order of hundredths.

With this, we end our discussion of typical values of the aerodynamic coefficients defined in Section 1.5. At this stage, you should reread this section, now from the overall perspective provided by a first reading, and make certain to fix in your mind the typical values discussed—it will provide a useful "calibration" for our subsequent discussions.

EXAMPLE 1.12

Consider the Seversky P-35 shown in Figure 3.2. Assume that the drag breakdown given in Figure 1.58 for the XP-41 applies also to the P-35. Note that the data given in Figure 1.58 apply for the specific condition where $C_L = 0.15$. The wing planform area and the gross weight of the P-35 are 220 ft^2 and 5599 lb, respectively. Calculate the horsepower required for the P-35 to fly in steady level flight with $C_L = 0.15$ at standard sea level.

■ Solution

From basic mechanics, if **F** is a force exerted on a body moving with a velocity **V**, the power generated by this system is $P = \mathbf{F} \cdot \mathbf{V}$. When **F** and **V** are in the same direction, then the dot product becomes $P = FV$ where F and V are the scalar magnitudes of force and velocity, respectively. When the airplane is in steady level flight (no acceleration) the thrust obtained from the engine exactly counteracts the drag, i.e., $T = D$. Hence the power required for the airplane to fly at a given velocity V_∞ is

$$P = TV_\infty = DV_\infty \tag{E1.12.1}$$

To obtain the power required for the P-35 to fly in steady level flight with $C_L = 0.15$, at standard sea level, we must first calculate both D and V_∞ for this flight condition.

To obtain V_∞, we note that in steady level flight the weight is exactly balanced by the aerodynamic lift; i.e.,

$$W = L \tag{E1.12.2}$$

From Section 1.5, we have

$$W = L = q_\infty S C_L = 1/2 \rho_\infty V_\infty^2 S C_L \tag{E1.12.3}$$

where S is the planform area of the wing. Solving Eq. (E1.12.3) for V_∞, we have

$$V_\infty = \sqrt{\frac{2W}{\rho_\infty S C_L}} \tag{E1.12.4}$$

At standard sea level, from Appendix E (using English engineering units, consistent with the units used in this example), $\rho_\infty = 0.002377$ slug/ft^3. Also, for the P-35 in this example, $S = 220$ ft^2, $W = 5599$ lb, and $C_L = 0.15$. Hence, from Eq. (E1.12.3), we have

$$V_\infty = \sqrt{\frac{2(5599)}{(0.002377)(220)(0.15)}} = 377.8 \text{ ft/s}$$

This is the flight velocity when the airplane is flying at standard sea level such that its lift coefficient is 0.15. We note that to fly in steady level flight at any other velocity the lift coefficient would have to be different; to fly slower C_L must be larger and to fly faster C_L must be smaller. Recall that C_L for a given airplane is a function of angle of attack, so our flight condition in this example with $C_L = 0.15$ corresponds to a specific angle of attack of the airplane.

Noting that 88 ft/s = 60 mi/h, V_∞ in miles per hour is $(377.8)\left(\frac{60}{88}\right) = 257.6$ mi/h. In the reference book *The American Fighter* by Enzo Angelucci and Peter Bowers, Orion Books, New York, 1985, the cruising speed of the Seversky P-35 is given as 260 mi/h. Thus, for all practical purposes, the value of $C_L = 0.15$ pertains to cruise velocity at sea level, and this explains why the drag data given in Figure 1.58 was given for a lift coefficient of 0.15.

To complete the calculation of power required, we need the value of D. From Figure 1.58, the drag coefficient for the airplane in full configuration is $C_D = 0.0275$. For the calculated flight velocity, the dynamic pressure is

$$q_\infty = 1/2 \rho_\infty V_\infty^2 = 1/2(0.002377)(377.8)^2 = 169.6 \text{ lb/ft}^2$$

Thus,

$$D = q_\infty S C_D = (169.6)(220)(0.0275) = 1026 \text{ lb}$$

From Eq. (E1.12.1),

$$P = D V_\infty = (1026)(377.8) = 3.876 \times 10^5 \text{ ft lb/s}$$

Note that 1 horsepower is 550 ft lb/s. Thus, in horsepower,

$$P = \frac{3.876 \times 10^5}{550} = \boxed{704 \text{ hp}}$$

The P-35 was equipped with a Pratt & Whitney R-1830-45 engine rated at 1050 hp. The power required at cruising velocity calculated here is 704 hp, consistent with this engine throttled back for efficient cruise conditions.

The purpose of this worked example is to illustrate typical values of C_L and C_D for a real airplane flying at real conditions, consistent with the subtitle of this section "Applied Aerodynamics : The Aerodynamic Coefficients—Their Magnitudes and Variations." Moreover, we have shown how these coefficients are used to calculate useful aerodynamic performance characteristics for an airplane, such as cruising velocity and power required for steady level flight. This example also underscores the importance and utility of aerodynamic *coefficients*. We made these calculations for a given airplane knowing only the values of the lift and drag *coefficients,* thus again reinforcing the importance of the dimensional analysis given in Section 1.7 and the powerful concept of flow similarity discussed in Section 1.8.

1.13 HISTORICAL NOTE: THE ILLUSIVE CENTER OF PRESSURE

The center of pressure of an airfoil was an important matter during the development of aeronautics. It was recognized in the nineteenth century that, for a heavier-than-air machine to fly at stable, equilibrium conditions (e.g., straight-and-level flight), the moment about the vehicle's center of gravity must be zero (see Chapter 7 of Reference 2). The wing lift acting at the center of pressure, which is generally a distance away from the center of gravity, contributes substantially to this moment. Hence, the understanding and prediction of the center of pressure was felt to be absolutely necessary in order to design a vehicle with proper equilibrium. On the other hand, the early experimenters had difficulty measuring the center of pressure, and much confusion reigned. Let us examine this matter further.

The first experiments to investigate the center of pressure of a lifting surface were conducted by the Englishman George Cayley (1773–1857) in 1808. Cayley was the inventor of the modern concept of the airplane, namely, a vehicle with fixed wings, a fuselage, and a tail. He was the first to separate conceptually the functions of lift and propulsion; prior to Cayley, much thought had gone into ornithopters—machines that flapped their wings for both lift and thrust. Cayley rejected this idea, and in 1799, on a silver disk now in the collection of the Science Museum in London, he inscribed a sketch of a rudimentary airplane with all the basic elements we recognize today. Cayley was an active, inventive, and long-lived man, who conducted numerous pioneering aerodynamic experiments and fervently believed that powered, heavier-than-air, manned flight was inevitable.

(See Chapter 1 of Reference 2 for an extensive discussion of Cayley's contributions to aeronautics.)

In 1808, Cayley reported on experiments of a winged model which he tested as a glider and as a kite. His comments on the center of pressure are as follows:

> By an experiment made with a large kite formed of an hexagon with wings extended from it, all so constructed as to present a hollow curve to the current, I found that when loaded nearly to 1 lb to a foot and 1/2, it required the center of gravity to be suspended so as to leave the anterior and posterior portions of the surface in the ratio of 3 to 7. But as this included the tail operating with a double leverage behind, I think such hollow surfaces relieve about an equal pressure on each part, when they are divided in the ratio of 5 to 12, 5 being the anterior portion. It is really surprising to find so great a difference, and it obliges the center of gravity of flying machines to be much forwarder of the center of bulk (the centroid) than could be supposed a priori.

Here, Cayley is saying that the center of pressure is 5 units from the leading edge and 12 units from the trailing edge (i.e., $x_{cp} = 5/17c$). Later, he states in addition: "I tried a small square sail in one plane, with the weight nearly the same, and I could not perceive that the center-of-resistance differed from the center of bulk." That is, Cayley is stating that the center of pressure in this case is $1/2c$.

There is no indication from Cayley's notes that he recognized that center of pressure moves when the lift, or angle of attack, is changed. However, there is no doubt that he was clearly concerned with the location of the center of pressure and its effect on aircraft stability.

The center of pressure on a flat surface inclined at a small angle to the flow was studied by Samuel P. Langley during the period 1887–1896. Langley was the secretary of the Smithsonian at that time, and devoted virtually all his time and much of the Smithsonian's resources to the advancement of powered flight. Langley was a highly respected physicist and astronomer, and he approached the problem of powered flight with the systematic and structured mind of a scientist. Using a whirling arm apparatus as well as scores of rubber-band powered models, he collected a large bulk of aerodynamic information with which he subsequently designed a full-scale aircraft. The efforts of Langley to build and fly a successful airplane resulted in two dismal failures in which his machine fell into the Potomac River—the last attempt being just 9 days before the Wright brothers' historic first flight on December 17, 1903. In spite of these failures, the work of Langley helped in many ways to advance powered flight. (See Chapter 1 of Reference 2 for more details.)

Langley's observations on the center of pressure for a flat surface inclined to the flow are found in the *Langley Memoir on Mechanical Flight, Part I, 1887 to 1896,* by Samuel P. Langley, and published by the Smithsonian Institution in 1911—5 years after Langley's death. In this paper, Langley states:

> The center-of-pressure in an advancing plane in soaring flight is always in advance of the center of figure, and moves forward as the angle-of-inclination of the sustaining

> surfaces diminishes, and, to a less extent, as horizontal flight increases in velocity. These facts furnish the elementary ideas necessary in discussing the problem of equilibrium, whose solution is of the most vital importance to successful flight.
>
> The solution would be comparatively simple if the position of the center-of-pressure could be accurately known beforehand, but how difficult the solution is may be realized from a consideration of one of the facts just stated, namely, that the position of the center-of-pressure in horizontal flight shifts with velocity of the flight itself.

Here, we see that Langley is fully aware that the center of pressure moves over a lifting surface, but that its location is hard to pin down. Also, he notes the correct variation for a flat plate, namely, x_{cp} moves forward as the angle of attack decreases. However, he is puzzled by the behavior of x_{cp} for a curved (cambered) airfoil. In his own words:

> Later experiments conducted under my direction indicate that upon the curved surfaces I employed, the center-of-pressure moves forward with an increase in the angle of elevation, and backward with a decrease, so that it may lie even behind the center of the surface. Since for some surfaces the center-of-pressure moves backward, and for others forward, it would seem that there might be some other surface for which it will be fixed.

Here, Langley is noting the totally opposite behavior of the travel of the center of pressure on a cambered airfoil in comparison to a flat surface, and is indicating ever so slightly some of his frustration in not being able to explain his results in a rational scientific way.

Three-hundred-fifty miles to the west of Langley, in Dayton, Ohio, Orville and Wilbur Wright were also experimenting with airfoils. As described in Section 1.1, the Wrights had constructed a small wind tunnel in their bicycle shop with which they conducted aerodynamic tests on hundreds of different airfoil and wing shapes during the fall, winter, and spring of 1901–1902. Clearly, the Wrights had an appreciation of the center of pressure, and their successful airfoil design used on the 1903 Wright Flyer is a testimonial to their mastery of the problem. Interestingly enough, in the written correspondence of the Wright brothers, only one set of results for the center of pressure can be found. This appears in Wilbur's notebook, dated July 25, 1905, in the form of a table and a graph. The graph is shown in Figure 1.64—the original form as plotted by Wilbur. Here, the center of pressure, given in terms of the percentage of distance from the leading edge, is plotted versus angle of attack. The data for two airfoils are given, one with large curvature (maximum height to chord ratio = 1/12) and one with more moderate curvature (maximum height to chord ratio = 1/20). These results show the now familiar travel of the center of pressure for a curved airfoil, namely, x_{cp} moves forward as the angle of attack is increased, at least for small to moderate values of α. However, the most forward excursion of x_{cp} in Figure 1.64 is 33 percent behind the leading edge—the center of pressure is always behind the quarter-chord point.

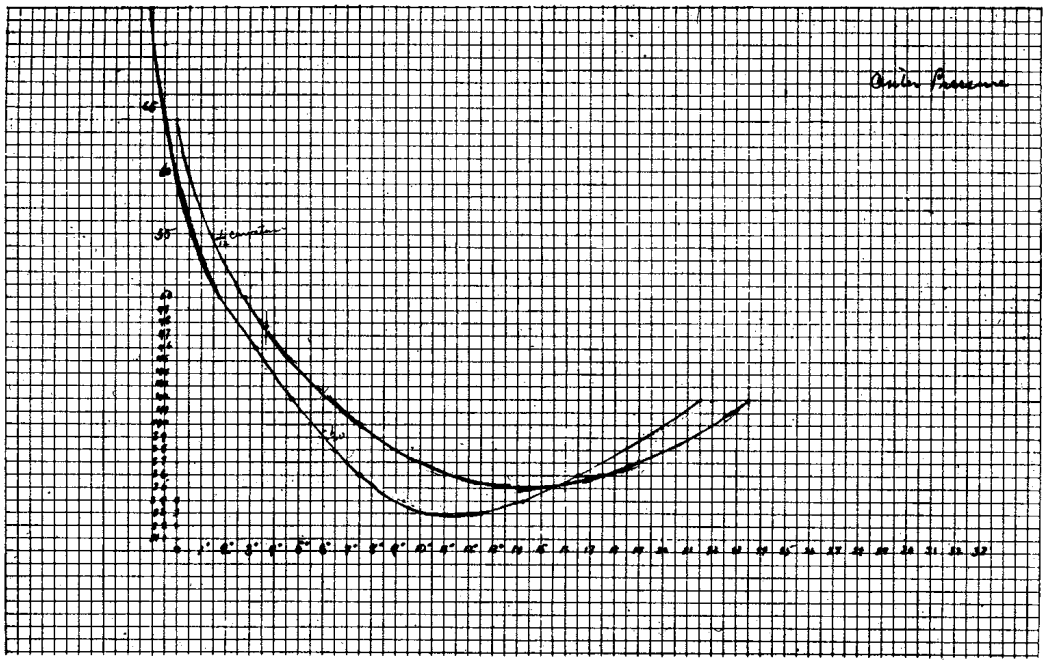

Figure 1.64 Wright brothers' measurements of the center of pressure as a function of angle of attack for a curved (cambered) airfoil. Center of pressure is plotted on the ordinate in terms of percentage distance along the chord from the leading edge. This figure shows the actual data as hand-plotted by Wilbur Wright, which appears in Wilbur's notebook dated July 25, 1905.

The first practical airfoil theory, valid for thin airfoils, was developed by Ludwig Prandtl and his colleagues at Göttingen, Germany, during the period just prior to and during World War I. This thin airfoil theory is described in detail in Chapter 4. The result for the center of pressure for a curved (cambered) airfoil is given by Equation (4.66), and shows that x_{cp} moves forward as the angle of attack (hence c_l) increases, and that it is always behind the quarter-chord point for finite, positive values of c_l. This theory, in concert with more sophisticated wind-tunnel measurements that were being made during the period 1915–1925, finally brought the understanding and prediction of the location of the center of pressure for a cambered airfoil well into focus.

Because x_{cp} makes such a large excursion over the airfoil as the angle of attack is varied, its importance as a basic and practical airfoil property has diminished. Beginning in the early 1930s, the National Advisory Committee for Aeronautics (NACA), at its Langley Memorial Aeronautical Laboratory in Virginia, measured the properties of several systematically designed families of airfoils—airfoils which became a standard in aeronautical engineering. These NACA airfoils are discussed in Sections 4.2 and 4.3. Instead of giving the airfoil data in terms of lift, drag, and center of pressure, the NACA chose the alternate systems of reporting lift, drag, and moments about either the quarter-chord point or the aerodynamic

center. These are totally appropriate alternative methods of defining the force-and-moment system on an airfoil, as discussed in Section 1.6 and illustrated in Figure 1.26. As a result, the center of pressure is rarely given as part of modern airfoil data. On the other hand, for three-dimensional bodies, such as slender projectiles and missiles, the location of the center of pressure still remains an important quantity, and modern missile data frequently include x_{cp}. Therefore, a consideration of center of pressure still retains its importance when viewed over the whole spectrum of flight vehicles.

1.14 HISTORICAL NOTE: AERODYNAMIC COEFFICIENTS

In Section 1.5, we introduced the convention of expressing aerodynamic force in terms of an aerodynamic *coefficient,* such as

$$L = \tfrac{1}{2}\rho_\infty V_\infty^2 S C_L$$

and

$$D = \tfrac{1}{2}\rho_\infty V_\infty^2 S C_D$$

where L and D are lift and drag, respectively, and C_L and C_D are the lift coefficient and drag coefficient, respectively. This convention, expressed in the form shown above, dates from about 1920. But the use of some type of aerodynamic coefficients goes back much further. In this section, let us briefly trace the genealogy of aerodynamic coefficients. For more details, see the author's recent book, *A History of Aerodynamics and Its Impact on Flying Machines* (Reference 62).

The first person to define and use aerodynamic force coefficients was Otto Lilienthal, the famous German aviation pioneer at the end of the nineteenth century. Interested in heavier-than-flight from his childhood, Lilienthal carried out the first definitive series of aerodynamic force measurements on cambered (curved) airfoil shapes using a whirling arm. His measurements were obtained over a period of 23 years, culminating in the publication of his book *Der Vogelflug als Grundlage der Fliegekunst (Birdflight as the Basis of Aviation*) in 1889. Many of the graphs in his book are plotted in the form that today we identify as a drag polar, that is, a plot of drag coefficient versus lift coefficient, with the different data points being measured at angles of attack ranging from below zero to 90°. Lilienthal had a degree in Mechanical Engineering, and his work reflected a technical professionalism greater than most at that time. Beginning in 1891, he put his research into practice by designing several gliders, and executing over 2000 successful glider flights before his untimely death in a crash on August 9, 1896. At the time of his death, Lilienthal was working on the design of an engine to power his machines. Had he lived, there is some conjecture that he would have beaten the Wright brothers in the race for the first heavier-than-air, piloted, powered flight.

In his book, Lilienthal introduced the following equations for the normal and axial forces, which he denoted by N and T, respectively (for normal and

"tangential")

$$N = 0.13\eta F V^2 \tag{1.63}$$

and

$$T = 0.13\theta F V^2 \tag{1.64}$$

where, in Lilienthal's notation, F was the reference planform area of the wing in m^2, V is the freestream velocity in m/s, and N and T are in units of kilogram force (the force exerted on one kilogram of mass by gravity at sea level). The number 0.13 is Smeaton's coefficient, a concept and quantity stemming from measurements made in the eighteenth century on flat plates oriented perpendicular to the flow. Smeaton's coefficient is proportional to the density of the freestream; its use is archaic, and it went out of favor at the beginning of the twentieth century. By means of Equations (1.63) and (1.64) Lilienthal introduced the "normal" and "tangential" coefficients, η and θ versus angle of attack. A copy of this table, reproduced in a paper by Octave Chanute in 1897, is shown in Figure 1.65. This became famous as the "Lilienthal Tables," and was used by the Wright brothers for the design of their early gliders. It is proven in Reference 62 that Lilienthal did not use Equations (1.63) and (1.64) explicitly to reduce his experimental data to coefficient form, but rather determined his experimental values for η and θ by dividing the experimental measurements for N and T by his measured force on the wing at 90° angle of attack. In so doing, he divided out the influence of uncertainties in Smeaton's coefficient and the velocity, the former being particularly important because the classical value of Smeaton's coefficient of 0.13 was in error by almost 40 percent. (See Reference 62 for more details.) Nevertheless, we have Otto Lilienthal to thank for the concept of aerodynamic force coefficients, a tradition that has been followed in various modified forms to the present time.

Following on the heals of Lilienthal, Samuel Langley at the Smithsonian Institution published whirling arm data for the resultant aerodynamic force R on a flat plate as a function of angle of attack, using the following equation:

$$R = kSV^2 F(\alpha) \tag{1.65}$$

where S is the planform area, k is the *more accurate* value of Smeaton's coefficient (explicitly measured by Langley on his whirling arm), and $F(\alpha)$ was the corresponding force coefficient, a function of angle of attack.

The Wright brothers preferred to deal in terms of lift and drag, and used expressions patterned after Lilienthal and Langley to define lift and drag coefficients:

$$L = kSV^2 C_L \tag{1.66}$$

$$D = kSV^2 C_D \tag{1.67}$$

The Wrights were among the last to use expressions written explicitly in terms of Smeaton's coefficient k. Gustave Eiffel in 1909 defined a "unit force coefficient" K_i as

$$R = K_i SV^2 \tag{1.68}$$

TABLE OF NORMAL AND TANGENTIAL PRESSURES

Deduced by Lilienthal from the diagrams on Plate VI., in his book "Bird-flight as the Basis of the Flying Art."

α Angle.	η Normal.	ϑ Tangential.	α Angle.	η Normal.	ϑ Tangential.
− 9°	0.000	+ 0.070	16°	0.909	− 0.075
− 8°	0.040	+ 0.067	17°	0.915	− 0.073
− 7°	0.080	+ 0.064	18°	0.919	− 0.070
− 6°	0.120	+ 0.060	19°	0.921	− 0.065
− 5°	0.160	+ 0.055	20°	0.922	− 0.059
− 4°	0.200	+ 0.049	21°	0.923	− 0.053
− 3°	0.242	+ 0.043	22°	0.924	− 0.047
− 2°	0.286	+ 0.037	23°	0.924	− 0.041
− 1°	0.332	+ 0.031	24°	0.923	− 0.036
0°	0.381	+ 0.024	25°	0.922	− 0.031
+ 1°	0.434	+ 0.016	26°	0.920	− 0.026
+ 2°	0.489	+ 0.008	27°	0.918	− 0.021
+ 3°	0.546	0.000	28°	0.915	− 0.016
+ 4°	0.600	− 0.007	29°	0.912	− 0.012
+ 5°	0.650	− 0.014	30°	0.910	− 0.008
+ 6°	0.696	− 0.021	32°	0.906	0.000
+ 7°	0.737	− 0.028	35°	0.896	+ 0.010
+ 8°	0.771	− 0.035	40°	0.890	+ 0.016
+ 9°	0.800	− 0.042	45°	0.888	+ 0.020
10°	0.825	− 0.050	50°	0.888	+ 0.023
11°	0.846	− 0.058	55°	0.890	+ 0.026
12°	0.864	− 0.064	60°	0.900	+ 0.028
13°	0.879	− 0.070	70°	0.930	+ 0.030
14°	0.891	− 0.074	80°	0.960	+ 0.015
15°	0.901	− 0.076	90°	1.000	0.000

Figure 1.65 The Lilienthal Table of normal and axial force coefficients. This is a facsimile of the actual table that was published by Octave Chanute in an article entitled "Sailing Flight," *The Aeronautical Annual,* 1897, which was subsequently used by the Wright Brothers.

In Equation (1.68), Smeaton's coefficient is nowhere to be seen; it is buried in the direct measurement of K_i. (Eiffel, of Eiffel Tower fame, built a large wind tunnel in 1909, and for the next 14 years reigned as France's leading aerodynamicist until his death in 1923.) After Eiffel's work, Smeaton's coefficient was never used in the aerodynamic literature—it was totally passé.

Gorrell and Martin, in wind tunnel tests carried out in 1917 at MIT on various airfoil shapes, adopted Eiffel's approach, giving expressions for lift and drag:

$$L = K_y A V^2 \tag{1.69}$$

$$D = K_x A V^2 \tag{1.70}$$

where A denoted planform area and K_y and K_x were the lift and drag coefficients, respectively. For a short period, the use of K_y and K_x became popular in the United States.

However, also by 1917 the density ρ began to appear explicitly in expressions for force coefficients. In NACA Technical Report No. 20, entitled "Aerodynamic Coefficients and Transformation Tables," we find the following expression:

$$F = C\rho S V^2$$

where F is the total force acting on the body, ρ is the freestream density, and C is the force coefficient, which was described as "an abstract number, varying for a given airfoil with its angle of incidence, independent of the choice of units, provided these are consistently used for all four quantities (F, ρ, S, and V)."

Finally, by the end of World War I, Ludwig Prandtl at Gottingen University in Germany established the nomenclature that is accepted as standard today. Prandtl was already famous by 1918 for his pioneering work on airfoil and wing aerodynamics, and for his conception and development of boundary layer theory. (See Section 5.8 for a biographical description of Prandtl.) Prandtl reasoned that the dynamic pressure, $\frac{1}{2}\rho_\infty V_\infty^2$ (he called it "dynamical pressure"), was well suited to describe aerodynamic force. In his 1921 English-language review of works performed at Gottingen before and during World War I (Reference 63), he wrote for the aerodynamic force,

$$W = cFq \tag{1.71}$$

where W is the force, F is the area of the surface, q is the dynamic pressure, and c is a "pure number" (i.e., the force coefficient). It was only a short, quick step to express lift and drag as

$$L = q_\infty S C_L \tag{1.72}$$

and

$$D = q_\infty S C_D \tag{1.73}$$

where C_L and C_D are the "pure numbers" referred to by Prandtl (i.e., the lift and drag coefficients). And this is the way it has been ever since.

1.15 SUMMARY

Refer again to the road map for Chapter 1 given in Figure 1.11. Read again each block in this diagram as a reminder of the material we have covered. If you feel uncomfortable about some of the concepts, or if your memory is slightly "foggy" on certain points, go back and reread the pertinent sections until you have mastered the material.

This chapter has been primarily qualitative, emphasizing definitions and basic concepts. However, some of the more important quantitative relations are summarized below:

The normal, axial, lift, drag, and moment coefficients for an aerodynamic body can be obtained by integrating the pressure and skin friction coefficients over the body surface from the leading to the trailing edge. For a two-dimensional body,

$$c_n = \frac{1}{c}\left[\int_0^c (C_{p,l} - C_{p,u})\,dx + \int_0^c \left(c_{f,u}\frac{dy_u}{dx} + c_{f,l}\frac{dy_l}{dx}\right)dx\right] \tag{1.15}$$

$$c_a = \frac{1}{c}\left[\int_0^c \left(C_{p,u}\frac{dy_u}{dx} - C_{p,l}\frac{dy_l}{dx}\right)dx + \int_0^c (c_{f,u} + c_{f,l})\,dx\right] \tag{1.16}$$

$$c_{m_{\text{LE}}} = \frac{1}{c^2}\left[\int_0^c (C_{p,u} - C_{p,l})x\,dx - \int_0^c \left(c_{f,u}\frac{dy_u}{dx} + c_{f,l}\frac{dy_l}{dx}\right)x\,dx + \int_0^c \left(C_{p,u}\frac{dy_u}{dx} + c_{f,u}\right)y_u\,dx + \int_0^c \left(-C_{p,l}\frac{dy_l}{dx} + c_{f,l}\right)y_l\,dx\right] \tag{1.17}$$

$$c_l = c_n\cos\alpha - c_a\sin\alpha \tag{1.18}$$

$$c_d = c_n\sin\alpha + c_a\cos\alpha \tag{1.19}$$

The center of pressure is obtained from

$$x_{\text{cp}} = -\frac{M'_{\text{LE}}}{N'} \approx -\frac{M'_{\text{LE}}}{L'} \tag{1.20) and (1.21}$$

The criteria for two or more flows to be dynamically similar are:

1. The bodies and any other solid boundaries must be geometrically similar.
2. The similarity parameters must be the same. Two important similarity parameters are Mach number $M = V/a$ and Reynolds number $\text{Re} = \rho V c/\mu$.

If two or more flows are dynamically similar, then the force coefficients C_L, C_D, etc., are the same.

In fluid statics, the governing equation is the hydrostatic equation:

$$dp = -g\rho\, dy \tag{1.52}$$

For a constant density medium, this integrates to

$$p + \rho g h = \text{constant} \tag{1.54}$$

or

$$p_1 + \rho g h_1 = p_2 + \rho g h_2$$

Such equations govern, among other things, the operation of a manometer, and also lead to Archimedes' principle that the buoyancy force on a body immersed in a fluid is equal to the weight of the fluid displaced by the body.

1.16 PROBLEMS

1.1 For most gases at standard or near standard conditions, the relationship among pressure, density, and temperature is given by the perfect gas equation of state: $p = \rho RT$, where R is the specific gas constant. For air at near standard conditions, $R = 287$ J/(kg · K) in the International System of Units and $R = 1716$ ft · lb/(slug · °R) in the English Engineering System of Units. (More details on the perfect gas equation of state are given in Chapter 7.) Using the above information, consider the following two cases:

a. At a given point on the wing of a Boeing 727, the pressure and temperature of the air are 1.9×10^4N/m^2 and 203 K, respectively. Calculate the density at this point.

b. At a point in the test section of a supersonic wind tunnel, the pressure and density of the air are 1058 lb/ft^2 and 1.23×10^{-3} slug/ft^3, respectively. Calculate the temperature at this point.

1.2 Starting with Equations (1.7), (1.8), and (1.11), derive in detail Equations (1.15), (1.16), and (1.17).

1.3 Consider an infinitely thin flat plate of chord c at an angle of attack α in a supersonic flow. The pressures on the upper and lower surfaces are different but constant over each surface; that is, $p_u(s) = c_1$ and $p_l(s) = c_2$, where c_1 and c_2 are constants and $c_2 > c_1$. Ignoring the shear stress, calculate the location of the center of pressure.

1.4 Consider an infinitely thin flat plate with a 1 m chord at an angle of attack of 10° in a supersonic flow. The pressure and shear stress distributions on the upper and lower surfaces are given by $p_u = 4 \times 10^4(x-1)^2 + 5.4 \times 10^4$, $p_l = 2 \times 10^4(x-1)^2 + 1.73 \times 10^5$, $\tau_u = 288x^{-0.2}$, and $\tau_l = 731x^{-0.2}$, respectively, where x is the distance from the leading edge in meters and p and τ are in newtons per square meter. Calculate the normal and axial forces, the lift and drag, moments about the leading

edge, and moments about the quarter chord, all per unit span. Also, calculate the location of the center of pressure.

1.5 Consider an airfoil at 12° angle of attack. The normal and axial force coefficients are 1.2 and 0.03, respectively. Calculate the lift and drag coefficients.

1.6 Consider an NACA 2412 airfoil (the meaning of the number designations for standard NACA airfoil shapes is discussed in Chapter 4). The following is a tabulation of the lift, drag, and moment coefficients about the quarter chord for this airfoil, as a function of angle of attack.

α (degrees)	c_l	c_d	$c_{m,c/4}$
−2.0	0.05	0.006	−0.042
0	0.25	0.006	−0.040
2.0	0.44	0.006	−0.038
4.0	0.64	0.007	−0.036
6.0	0.85	0.0075	−0.036
8.0	1.08	0.0092	−0.036
10.0	1.26	0.0115	−0.034
12.0	1.43	0.0150	−0.030
14.0	1.56	0.0186	−0.025

From this table, plot on graph paper the variation of x_{cp}/c as a function of α.

1.7 The drag on the hull of a ship depends in part on the height of the water waves produced by the hull. The potential energy associated with these waves therefore depends on the acceleration of gravity g. Hence, we can state that the wave drag on the hull is $D = f(\rho_\infty, V_\infty, c, g)$ where c is a length scale associated with the hull, say, the maximum width of the hull. Define the drag coefficient as $C_D \equiv D/q_\infty c^2$. Also, define a similarity parameter called the *Froude number,* $\text{Fr} = V/\sqrt{gc}$. Using Buckingham's pi theorem, prove that $C_D = f(\text{Fr})$.

1.8 The shock waves on a vehicle in supersonic flight cause a component of drag called supersonic wave drag D_w. Define the wave-drag coefficient as $C_{D,w} = D_w/q_\infty S$, where S is a suitable reference area for the body. In supersonic flight, the flow is governed in part by its thermodynamic properties, given by the specific heats at constant pressure c_p and at constant volume c_v. Define the ratio $c_p/c_v \equiv \gamma$. Using Buckingham's pi theorem, show that $C_{D,w} = f(M_\infty, \gamma)$. Neglect the influence of friction.

1.9 Consider two different flows over geometrically similar airfoil shapes, one airfoil being twice the size of the other. The flow over the smaller airfoil has freestream properties given by $T_\infty = 200$ K, $\rho_\infty = 1.23$ kg/m^3, and $V_\infty = 100$ m/s. The flow over the larger airfoil is described by $T_\infty = 800$ K, $\rho_\infty = 1.739$ kg/m^3, and $V_\infty = 200$ m/s. Assume that both μ and a are proportional to $T^{1/2}$. Are the two flows dynamically similar?

1.10 Consider a Lear jet flying at a velocity of 250 m/s at an altitude of 10 km, where the density and temperature are 0.414 kg/m^3 and 223 K, respectively. Consider also a one-fifth scale model of the Lear jet being tested in a wind tunnel in the laboratory. The pressure in the test section of the wind tunnel is 1 atm $= 1.01 \times 10^5$ N/m^2. Calculate the necessary velocity, temperature, and density of the airflow in the wind-tunnel test section such that the lift and drag coefficients are the same for the wind-tunnel model and the actual airplane in flight. *Note:* The relation among pressure, density, and temperature is given by the equation of state described in Problem 1.1.

1.11 A U-tube mercury manometer is used to measure the pressure at a point on the wing of a wind-tunnel model. One side of the manometer is connected to the model, and the other side is open to the atmosphere. Atmospheric pressure and the density of liquid mercury are 1.01×10^5 N/m^2 and 1.36×10^4 kg/m^3, respectively. When the displacement of the two columns of mercury is 20 cm, with the high column on the model side, what is the pressure on the wing?

1.12 The German Zeppelins of World War I were dirigibles with the following typical characteristics: volume $= 15{,}000$ m^3 and maximum diameter $=$ 14.0 m. Consider a Zeppelin flying at a velocity of 30 m/s at a standard altitude of 1000 m (look up the corresponding density in Appendix D). The Zeppelin is at a small angle of attack such that its lift coefficient is 0.05 (based on the maximum cross-sectional area). The Zeppelin is flying in straight-and-level flight with no acceleration. Calculate the total weight of the Zeppelin.

1.13 Consider a circular cylinder in a hypersonic flow, with its axis perpendicular to the flow. Let ϕ be the angle measured between radii drawn to the leading edge (the stagnation point) and to any arbitrary point on the cylinder. The pressure coefficient distribution along the cylindrical surface is given by $C_p = 2\cos^2\phi$ for $0 \leq \phi \leq \pi/2$ and $3\pi/2 \leq \phi \leq 2\pi$ and $C_p = 0$ for $\pi/2 \leq \phi \leq 3\pi/2$. Calculate the drag coefficient for the cylinder, based on projected frontal area of the cylinder.

1.14 Derive Archimedes' principle using a body of general shape.

1.15 Consider a light, single-engine, propeller-driven airplane similar to a Cessna Skylane. The airplane weight is 2950 lb and the wing reference area is 174 ft^2. The drag coefficient of the airplane C_D is a function of the lift coefficient C_L for reasons that are given in Chapter 5; this function for the given airplane is $C_D = 0.025 + 0.054C_L^2$.

a. For steady, level flight at sea level, where the ambient atmospheric density is 0.002377 slug/ft^3, plot on a graph the variation of C_L, C_D, and the lift-to-drag ratio L/D with flight velocity ranging between 70 ft/s and 250 ft/s.

b. Make some observations about the variation of these quantities with velocity.

1.16 Consider a flat plate at zero angle of attack in a hypersonic flow at Mach 10 at standard sea level conditions. At a point 0.5 m downstream from the leading edge, the local shear stress at the wall is 282 N/m^2. The gas temperature at the wall is equal to standard sea level temperature. At this point, calculate the velocity gradient at the wall normal to the wall.

1.17 Consider the Space Shuttle during its atmospheric entry at the end of a mission in space. At the altitude where the Shuttle has slowed to Mach 9, the local heat transfer at a given point on the lower surface of the wing is 0.03 MW/m^2. Calculate the normal temperature gradient in the air at this point on the wall, assuming the gas temperature at the wall is equal to the standard sea-level temperature.

1.18 The purpose of this problem is to give you a feel for the magnitude of Reynolds number appropriate to real airplanes in actual flight.

a. Consider the DC-3 shown in Figure 1.1. The wing root chord length (distance from the front to the back of the wing where the wing joins the fuselage) is 14.25 ft. Consider the DC-3 flying at 200 miles per hour at sea level. Calculate the Reynolds number for the flow over the wing root chord. (This is an important number, because as we will see later, it governs the skin-friction drag over that portion of the wing.)

b. Consider the F-22 shown in Figure 1.5, and also gracing the cover of this book. The chord length where the wing joins the center body is 21.5 ft. Consider the airplane making a high-speed pass at a velocity of 1320 ft/s at sea level (Mach 1.2). Calculate the Reynolds number at the wing root.

1.19 For the design of their gliders in 1900 and 1901, the Wright brothers used the Lilienthal Table given in Figure 1.65 for their aerodynamic data. Based on these data, they chose a design angle of attack of 3 degrees, and made all their calculations of size, weight, etc., based on this design angle of attack. Why do you think they chose three degrees?

Hint: From the table, calculate the ratio of lift to drag, *L*/*D*, at 3 degrees angle of attack, and compare this with the lift-to-drag ratio at other angles of attack. You might want to review the design box at the end of Section 1.8, especially Figure 1.36, for the importance of *L*/*D*.